MAGNETO-OPTICAL EFFECTS IN SEMICONDUCTORS

DURDU MEHMET ZENGIN

B.Sc., Ankara/Turkey; M.Sc., London

A Thesis submitted

for the degree of

DOCTOR OF PHILOSOPHY

in the University of London

BEDFORD COLLEGE

LONDON

1976

ABSTRACT

An experimental investigation of magneto-optical effects including free-carrier Faraday rotation, ellipticity and cyclotron resonance in n-type indium antimonide samples with different electron densities has been undertaken in order to measure electron-impurity scattering times in the presence of magnetic fields at cryogenic temperatures.

The experimental apparatus used consisted of a 4 tesla (40 kilogauss) transverse-access optical cryostat in which the temperature of the sample could be held near either liquid nitrogen or liquid helium temperatures. Plane-polarized radiation from a pulsed far-infrared laser which produced a wavelength of 0.337 mm was passed through the sample and detected by means of a Golay cell whose output was gated, integrated, and displayed on a pen recorder.

The results have been analysed with the aid of the classical theory based on the Drude free-electron model and Maxwell's equations for conducting media, taking into account multiple internal reflections in the specimens. The results of calculations for other materials (mercury telluride and gallium arsenide) are also presented. Comparison of the experimental results for n-type indium antimonide with the curves computed from the theoretical expressions yielded scattering times of the order of 10^{-12} sec at liquid helium temperatures for several different samples. These scattering times are in good agreement with earlier measurements of scattering times at these temperatures obtained by other workers from measurements of cyclotron

resonance linewidths and Faraday rotation. There is, however, a considerable discrepancy between electron impurity scattering times obtained by magneto-optical methods and field-dependent d.c. scattering times calculated from d.c. mobility measurements. Discrepancies also exist between the measured and computed values of the ellipticity near cyclotron resonance. Some explanations of the differences between theory and experiment are considered, and further possible lines of investigation are discussed.

CONTENTS

LIST OF ILLUSTRATIONS

LIST OF TABLES

C H A P T E R 1

MAGNETOOPTICAL EFFECTS IN SEMICONDUCTORS

1.1. INTRODUCTION

The investigation of magneto-optical phenomena in semiconductors has proved to be a powerful method of studying the band structure of these materials. These phenomena divide into three principal categories as intraband, interband, and Zeeman effects. The intraband effect will, for our purposes, be discussed in details.

The intraband effect involve only the energy band that contains the carriers, and will be simply referred to as free-carrier effects. These effects are associated with the dispersive phenomena of free carriers, usually in extrinsic material. However the particular phenomena that will be of concern to us at present are the dispersive magneto-optical effects. These will include the magneto-plasma effects, depending on the dispersive properties of free carriers in semiconductors which have been observed in reflection; the Faraday rotation which depends on the differential dispersion of two circularly polarized electromagnetic waves rotating in opposite senses, and which has been observed in transmission and also in the reflection at the plasma frequency (in which case it is known as the Kerr-Magnetooptic effect). Finally the Voigt effect, which involves birefringence in the presence of a magnetic field, has been observed in transmission and also in reflection.

Cyclotron resonance is the simplest basic magneto-optical phenomenon, and it will be discussed first since it can serve as a natural introduction to the Faraday rotation.

1.2. CYCLOTRON RESONANCE

The basic concept involved here is the interaction of electromagnetic radiation with electrons in a magnetic field. The effect was first considered for free electrons in the ionosphere (Appleton, 1925), was theoretically predicted for solids by Dingle (Dingle,952) and subsequently observed in semiconductors by Dresselhaus et al, (Dresselhaus, 1953) and Lax et al. (Lax, 1954a,b). General reviews of the subject have been given by Lax et al (Lax, 1960), Smith (Smith, 1963) and by Palik (Palik, 1970).

More recently a number of experiments on cyclotron resonance using far-infrared laser have been carried out by Apel and Apel et al (Apel,1969; 1970a,b and 1971), Chamberlain and Chamberlain et al (Chamberlain, 1969 and 1970), Poehler (Poehler, 1972), Tuchendler et al (Tuchendler, 1973) and Palmetshofer et al (Palmetshofer,974).

1.3. THEORETICAL ACCOUNT

(i) Classical treatment

In the presence of an external magnetic field B, free carriers such as electrons in the conduction band or holes in the valence band execute cyclotron orbits. Thus a constant magnetic field B_z whose direction is along the z-axis affects motion in the xy plane without affecting motion in the z-direction. Therefore, the equations of motion of an electrons are

$$m^* dv_x/dt = -eB_z v_y$$

$$m^* dv_y/dt = eB_z v_x$$

$$m^* dv_z/dt = 0$$

The solution of these equations is well known. If $v_z = 0$ initially,

a quasi-free electron of scalar mass m^* describes a circular orbit, of radius r and angular frequency w_c in the xy plane. These quantities are related by requirement that the centrifugal force must balance the Lorentz force

$$m^* w_c^2 r = e w_c r B_z / c$$

so that

$$w_c = eB_z/m^* c \qquad (1.1)$$

This angular frequency w_c is known as the cyclotron frequency.

Equation 1.1 defines the cyclotron mass which is a property of an orbit and not of a particular electron state. For a non-isotropic band, the cyclotron mass will vary with the direction of the applied magnetic field B. The motion of the electron is interrupted from time to time by incoherent scattering from lattice defects, phonons, impurity centres and other electrons. It is,however, natural to try and detect this motion by resonance with an applied r.f. field. The condition for the observation of the cyclotron resonance effect is that the electron should complete a sizable fraction of its orbit before it is scattered; we must therefore have $w_c\langle\tau\rangle \gg 1$, where $\langle\tau\rangle$ is an averaged time between collitions and w_c is the orbital frequency defined in eq.1.1.

If a circularly polarized electric field in the plane of the orbits is applied, the force produced from this field, being perpendicular to the direction of the carriers, will accelerate them and enlarge the orbits; the only requirement is that the frequency of the impressed electric field must match the frequency of the carriers; that is, $w = w_c = eB_z/m^* c$. If these conditions are met, the carriers will absorb energy from the electric field. Classically this absorption represents the acceleration of the carriers which results in them acquiring a higher kinetic energy.

(ii) Quantum theory of cyclotron resonance

A quantum-mechanical description of cyclotron resonance follows from a solution of the Schrodinger wave equation for electrons in a magnetic field.

$$H\psi = E\psi$$

$$\text{where} \quad H = \frac{1}{2m^*}\left(\underline{p} + \frac{e}{c}\underline{A} \right)^2 + g\, M_B\, \underline{S}.\underline{B} \qquad (1.2)$$

here, $\underline{p}$ is the momentum operator, $\underline{A}$ is the vector potential, M_B is the Bohr magneton, g is the effective g-factor of the conduction band and m* is the effective mass of the free-electrons; the last term represents spin interaction with the applied magnetic field $\underline{B}$, which is applied along the z-direction. By taking the unsymmetric Landau gauge (0,Bx,0), the solutions are given in the bulk of the material as;

$$\psi = \phi_{nL} \exp(ik_z z)$$

$$E = \hbar w_c (n+\tfrac{1}{2}) + \frac{\hbar^2 k_z^2}{2m^*} \quad , \quad n = 0,1,2,\ldots \text{ etc.} \qquad (1.3)$$

where ϕ_{nL} are the harmonic oscillator wavefunctions and k_z is the electron momentum in the direction of the applied field. Spin effects are neglected in eq.(1.3).

The electron motion is thus seen to be quantised in the xy plane into 'orbits' or permissible energy states. Also the density of state functions in the simplest possible non-degenerate and parabolic conduction band can be represented by the following formula (Blakemore,1962).

$$G(E) = (2\pi^2)^{-1}(2m^*/\hbar^2)^{3/2}\, \hbar w_c \sum_{n=0}^{\infty} \left(E-(n+\tfrac{1}{2})\hbar w_c \pm \tfrac{1}{2}M_B gB \right)^{-\frac{1}{2}}. \qquad (1.3a)$$

where the symbols have their usual meanings. When a large magnetic field is applied the electron energy (in units of $\hbar w_c$) as a function of k_z, and the density of states as the function of the electron energy are represented in fig. 1.1 a and fig. 1.1 b resulting from eqs. (1.3) and (1.3a) respectively (without allowance for spin) by the continuous curve. The dashed curves represent the energy level and density of states G(E) at B=0. The energies corresponding to the infinitely high density of states (Landau levels) are separated by intervals $\hbar w_c$ proportional to the magnetic induction and inversely proportional to the effective mass. The band edge shifts by an amount $\frac{1}{2}\hbar w_c$, which corresponds to an increase in the width of the forbidden band in a magnetic field by an amount $\frac{1}{2}\hbar(w_{ce}+w_{ch})$ where w_{ce} and w_{ch} are the cyclotron frequencies for the conduction and valence bands, respectively.

From the point of view of quantum theory, a finite lifetime $\langle\tau\rangle$ implies an uncertainty ΔE in the energy of each orbital level, where $\Delta E = \hbar/\langle\tau\rangle$. The energy levels will then overlap significantly if $\Delta E > \hbar w_c$, and the condition $\Delta E < \hbar w_c$ again leads to the requirement $w_c\langle\tau\rangle > 1$.

In other words, to observe cyclotron resonance effects, we need high frequencies and long relaxation times. High frequencies imply high fields, and long relaxation times require the use of low temperatures and samples with few imperfections. Consequently cyclotron resonance experiments are nearly always done with high frequency waves, at liquid helium temperature, and with single crystal samples of extreme purity.

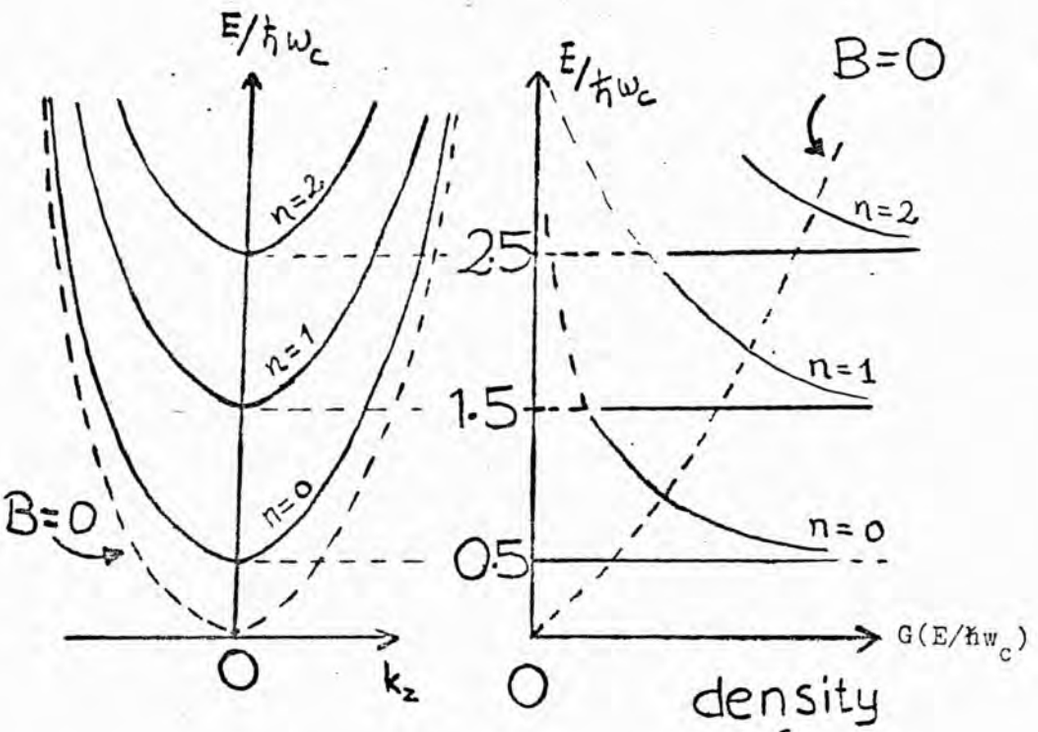

Fig. 1.1a

Fig. 1.1b

1.4. FARADAY ROTATION

Faraday rotation is the earliest observed magneto-optical phenomenon, having been fist seen in 1845. It was discovered by Faraday (1846) who observed a rotation of the plane of polarization of plane-polarized radiation passing through glass in the direction of an applied magnetic field. Physically, this effect, first explained by Lorentz (1906), arises from the differential dispersion of the two circularly polarized components of the plane-polarized wave, in that the left-and right-hand circularly polarized waves interact differently with electrons and holes in the presence of a magnetic field and hence travel with different velocities. Faraday rotation was observed in germanium first at microwave frequencies by Rau and Caspari (Rau,1955) and then at higher frequencies in the near infrared by Mitchell (1955). Some experiments at infrared frequencies were also performed by Von Kimmel (1957) who made measurements in silicon, gallium arsenide, indium phosphide and gallium phosphide in the region from 0.5 to 1.5 microns. However, no quantitative correlation between the experimental results and the electronic band structure of the semiconductors was made until the measurements in n-type InSb by Brown (1958), Brown and Lax (Brown,1959), Moss et al. (Moss,1959) and Smith et al (Smith, 1960).

Further measurements on InSb include work by Smith et al (1959), Pidgeon and Smith (Pidgeon,1964), and Pidgeon et al (1966) on the non-parabolicity on the conduction band as predicted by Kane (1957). The theory of the phenomenon has been considered by Stephen and Liddiard (Stephen,1959) and the temperature dependence of effective mass was studied by Ukhanov and Mal'tsev (Ukhanov,1963); Koteles and Datars (1974).

The theory of the free-carrier effect was given by Donovan and Webster (Donovan,1961,1962,1963), Furdyna and Brodwin (Furdyna,1961), and also the experimental work on n-type InSb was given at microwave frequencies by Mansfield and Mansfield et al (Mansfield,1965,1967). More recently, some experiments on Faraday rotation using far-infrared lasers have been carried out Shimura et al (1970), and Poehler and Wang (Poehler,1972).

The free-carrier Faraday effect provides an excellent method for measuring electron-impurity scattering time at low temperature in a wide range of magnetic fields. Also this effect has been widely used to measure the effective mass of free carriers in many compound semiconductors (Palik,1967).

1.5. THEORETICAL BACKGROUND

(i) Classical case

Consider the propagation, parallel to an applied magnetic induction $\underline{B}$, in the direction oz, of circularly polarized electro-magnetic radiation, given by

$$\underline{E}(z,t) = \underline{E}_0 \exp(i(wt-p_{\pm}z)) \qquad (1.4)$$

where the plus sign denotes that the electric vector is rotating counter-clock wise looking against the direction of propagation (left-handed polarization).

The equation of motion of the carriers may be written as ($\underline{v}$,$\underline{E}$ and $\underline{B}$ are vectors, and the international system (SI) of units is used in this analysis)

$$m^*(d\underline{v}/dt + \underline{v}/\tau) = e(\underline{E}+\underline{v}x\underline{B}) \qquad (1.5)$$

where the carriers have a positive sign, $\underline{E} = \underline{E}_0\exp(iwt)$, $\underline{v}=\underline{v}_0\exp(iwt)$ and τ is the relaxation time. Putting $\underline{B} = \underline{B}_z$ and $w_c = eB_z/m^*$ which is called cyclotron frequency, the components of this equation are

$$(iw + 1/\tau)v_x = \frac{eE_x}{m^*} + v_y w_c$$

$$(iw + 1/\tau)v_y = \frac{eE_y}{m^*} - v_x w_c$$

Solving for v_x and v_y

$$v_x = \frac{eE_x\tau(iw\tau + 1) + ew_c\tau^2 E_y}{m^*((w_c\tau)^2 + (1+iw\tau)^2)}$$

$$v_y = \frac{-eE_x w_c\tau^2 + e\tau(iw\tau+1)E_y}{m^*((w_c\tau)^2 + (1+iw\tau)^2)}$$

and the current density $\underline{J} = Ne\underline{v}$ has components

$$J_x = Nev_x = \frac{Ne^2\tau}{m^*} \frac{(1+iw\tau)E_x + w_c\tau E_y}{(w_c\tau)^2 + (1+iw\tau)^2} = \sigma_{xx}E_x + \sigma_{xy}E_y$$

$$J_y = Nev_y = \frac{Ne^2\tau}{m^*} \frac{-w_c\tau E_x + (1+iw\tau)E_y}{(w_c\tau)^2 + (1+iw\tau)^2} = \sigma_{yx}E_x + \sigma_{yy}E_y \qquad (1.6)$$

Now Maxwell's wave equation for a conducting medium with unit permeability is

$$\nabla^2\underline{E} = \frac{\sigma}{\varepsilon_o c^2} \frac{\partial E}{\partial t} + \frac{\varepsilon_r}{c^2}\frac{\partial^2 E}{\partial t^2}$$

using equation (1.4) and $\underline{J} = \sigma\underline{E}$ then the components are

$$-p^2E_x = \frac{iw}{\varepsilon_o c^2}(\sigma_{xx}E_x + \sigma_{xy}E_y) - \frac{w^2\varepsilon_r}{c^2}E_x$$

$$-p^2E_y = \frac{iw}{\varepsilon_o c^2}(\sigma_{yx}E_x + \sigma_{yy}E_y) - \frac{w^2\varepsilon_r}{c^2}E_y \qquad (1.7)$$

Since equation (1.6) shows $\sigma_{xx} = \sigma_{yy}$ and $\sigma_{xy} = -\sigma_{yx}$ then equation (1.7) gives $E_x = \pm iE_y$, and multiplying the second eq. (1.7) by $\pm i$ gives

$$-p_{\pm}^2(E_x \pm iE_y) = \frac{iw}{\varepsilon_o c^2}\,(E_x(\sigma_{xx} \pm i\sigma_{yx}) + E_y(\sigma_{xy} \pm i\sigma_{yy}))$$

$$- \frac{w^2\varepsilon_r}{c^2}\,(E_x \pm iE_y)$$

using $\sigma_{xx} = \sigma_{yy}$, and $\sigma_{xy} = -\sigma_{yx}$

$$-p_{\pm}^2(E_x \pm iE_y) = \frac{iw}{\varepsilon_o c^2}\,(\sigma_{xx} \mp i\sigma_{xy})(E_x \pm iE_y) - \frac{w^2\varepsilon_r}{c^2}\,(E_x \pm iE_y)$$

putting $E_{\pm} = E_x \pm iE_y$, and $\sigma_{\pm} = \sigma_{xx} \pm i\sigma_{xy}$

$$-p_{\pm}^2 E_{\pm} = -\frac{w^2\varepsilon_r}{c^2}\,E_{\pm} + \frac{iw}{\varepsilon_o c^2}\,\sigma_{\mp}\,E_{\pm} \qquad (1.8)$$

or $$p_{\pm}^2 = \frac{w^2}{c^2}\left(\varepsilon_r - \frac{i\,\sigma_{\mp}}{\varepsilon_o w}\right) \qquad (1.9)$$

So $$\sigma_{\pm} = \sigma_{xx} \pm i\sigma_{xy} = \frac{Ne^2\tau}{m^*}\left(\frac{1+iw\tau}{(1+iw\tau)^2+(w_c\tau)^2} \pm \frac{iw_c\tau}{(1+iw\tau)^2+(w_c\tau)^2}\right)$$

or $$\sigma_{\pm} = \frac{\sigma_o}{(1+iw\tau) \mp iw_c\tau} \qquad (1.10)$$

where $\sigma_o = \frac{Ne^2\tau}{m^*}$ is the dc conductivity. Combining equations (1.10), (1.9) and using the plasma frequency w_p is given by $w_p = (Ne^2/\varepsilon_r\varepsilon_o m^*)^{\frac{1}{2}}$ gives

$$p_{\pm}^2 = \frac{\varepsilon_r w^2}{c^2}\left(1 - \frac{w_p^2\tau^2(w \pm w_c)}{w(1+(w \pm w_c)^2\tau^2)} - i\,\frac{w_p^2\,\tau}{w(1+(w \pm w_c)^2\tau^2)}\right) \qquad (1.11)$$

Also the propagation constant $p_{\pm}$ is given by

$$p_{\pm} = n_{\pm}^* w/c$$

where $n_{\pm}^* = n_{\pm} - ik_{\pm}$ is the complex refractive incex.

so, $$n_{\pm}^{*2} = (n_{\pm}^2 - k_{\pm}^2) - 2in_{\pm}k_{\pm}$$

where $n_{\pm}$ is the real refractive index of the material and $k_{\pm}$ is the extinction coefficient for left- and right-hand circularly polarized radiation respectively. Using eq. (1.11), the complex refractive index squared is

$$n_{\pm}^{*2} = \varepsilon_r\left(1 - \frac{w_p^2\tau^2(w\pm w_c)}{w(1+(w\pm w_c)^2\tau^2)} - i\frac{w_p^2\tau}{w(1+(w\pm w_c)^2\tau^2)}\right)$$

$$\text{let } X_{\pm} = \varepsilon_r\left(1 - \frac{w_p^2\tau^2(w\pm w_c)}{w(1+(w\pm w_c)^2\tau^2)}\right)$$

$$Y_{\pm} = \varepsilon_r\left(\frac{w_p^2\tau}{w(1+(w\pm w_c)^2\tau^2)}\right)$$

$$\text{hence, } X_{\pm} = n_{\pm}^2 - k_{\pm}^2$$

$$Y_{\pm} = 2n_{\pm}k_{\pm} \qquad (1.12)$$

solving $n_{\pm}$, $k_{\pm}$ from equations (1.12)

$$n_{\pm} = ((X_{\pm} + (X_{\pm}^2 + Y_{\pm}^2)^{\frac{1}{2}})/2)^{\frac{1}{2}}$$

$$k_{\pm} = ((-X_{\pm}^2 + (X_{\pm}^2 + Y_{\pm}^2)^{\frac{1}{2}})/2)^{\frac{1}{2}} \qquad (1.13)$$

The rotation of the plane of polarization of a plane-polarized beam arises from the different phase velocities of the two circular components as they propagate through the medium. Over a path length d through the medium, the plane of polarization has undergone a rotation Θ given by (see Clarke (1971))

$$\Theta = \frac{wd}{2c}(n_- - n_+) \qquad (1.14)$$

where w is the angular frequency of the radiation. In addition to this effect, there is a corresponding differential absorption effect depending on $k_{\pm}$. One of the circular modes can be attenuated more

than the other causing the transmitted beam to be elliptically polarized. The ellipticity, which is defined as the ratio of minor to major axis of the ellipse of polarization, is given by (see Donovan (1962))

$$\Delta = \tanh\left(\frac{wd}{2c}\right)(k_- - k_+) \qquad (1.15)$$

Substitution of equation (1.13) into equations (1.14) and (1.15) enables θ and Δ to be written explicitly as

$$\theta = \frac{wd}{2c2^{\frac{1}{2}}}\left((X_- + (X_-^2 + Y_-^2)^{\frac{1}{2}})^{\frac{1}{2}} - (X_+ + (X_+^2 + Y_+^2)^{\frac{1}{2}})^{\frac{1}{2}}\right) \qquad (1.16)$$

and $$\Delta = \tanh\left(\frac{wd}{2c2^{\frac{1}{2}}}\left((-X_- + (X_-^2 + Y_-^2)^{\frac{1}{2}})^{\frac{1}{2}} - (-X_+ + (X_+^2 + Y_+^2)^{\frac{1}{2}})^{\frac{1}{2}}\right)\right) \qquad (1.17)$$

In above calculation it is assumed that there is a single relaxation time τ for all the carriers. This is equivalent to assuming that the relaxation time is independent of the energy of the carriers. The derivation of these equations is given in various texts (Lax,1962), (Moss,1973), but is reproduced here as the classical review of the Faraday effect.

When the conditions $w \gg w_p$ and $\tau|w-w_c| \gg 1$ are satisfied eq. (1.16) simplifies to

$$\theta = \frac{NBe^3 d}{2\varepsilon_r^{\frac{1}{2}} c\, \varepsilon_0 m^{*2} w^2} \quad \text{for } w_c \ll w \text{ (low field case)} \qquad (1.16a)$$

$$\theta = -\frac{eNd}{2\varepsilon_r^{\frac{1}{2}} c\, \varepsilon_0 B} \quad \text{for } w_c \gg w \text{ (high field case)} \qquad (1.16b)$$

The electron density N can be calculated by eq. (1.16b) if the Faraday rotation angle θ is measured for high magnetic fields. In this case, the rotation angle is independent of the momentum relaxation time of electrons τ, therefore, the experimental values

of this angle can be used directly to find the density of free-electrons in the sample at liquid helium temperature. Then, an electron effective mass m^* can be determined with this calculated value of N from eq. (1.16b) if the Faraday rotation angle is measured for low magnetic fields. In both cases, the rotation may be small for samples which have a low electron density. Under these circumtances, the calculated values of m^* and N from eqs. (1.16a) and (1.16b) would depend on the accuracy of the experimental measurements which in turn are limited by the stability of the far-infrared laser output and by the experimental technique used. However, if the Faraday rotation angle θ which is sensitive to impurity scattering time, τ, near w_c is measured through cyclotron resonance where absorption occurs, then the impurity scattering time τ and the effective mass of electrons m^* can be determined by least squares fit of the exact theoretical function (eq. (1.16)) using the carrier concentration of the sample which can be measured at liquid nitrogen temperature by Hall effect experiments to the experimental data, taking these quantities, τ, m^*, as variable parameter, (or even three variable parameters — τ, m^* and N).

The computer curve-fit program developed by Dr. Tom Lake, computing service unit at Bedford College, is a similar sum of squares minimizer to make a least squares fit of a function (non-linear) in certain parameters to data. This program requires a set of data θ_i (rotation angle) which are predicted by certain formula θ (eq. (1.16)) as a function of B (magnetic field) and different parameters (m^*, τ, N). Then the computer calculates the values of the parameters which are best fit to the theoretical expression making the iterative minimization of the sum of squ-

ares of differences between θ_{curve} (calculated) and θ_{data} (measured) values for each given value of magnetic fields. After successful convergence iterations are completed, and then the values of the parameters and the standart deviations for each these parameters are given independantly at the minimum.

(ii) Quantum mechanical case

A quantum-mechanical understanding of Faraday rotation follows from the plasma dielectric tensor and the conduction band energy levels of a semiconductor in a magnetic field. The quantum formulation of these quantities developed earlier for interpreting far-infrared cyclotron resonance measurements can be used to describe this case (Apel et al, 1971)

The dielectric tensor elements are given by

$$\frac{\varepsilon_\pm}{\varepsilon_r} = 1 - \frac{w_p^2}{w^2}\left(1 + \frac{m^* w_c}{4\pi^2 \hbar N} \sum_{n=0}^{\infty} \sum_{s=\pm} (n+\tfrac{1}{2}\pm\tfrac{1}{2}) \int_{-\infty}^{\infty} \frac{\Delta f_o \, dk_z \, w_{n+1,n}}{w_{n+1,n} - w + i/\tau}\right) \qquad (1.18)$$

where n is the initial Landau quantum number, s is the spin index, ε_r is the lattice dielectric constant, τ is the electron-ion collision time, w_p is the plasma frequency and N is the carrier concentration. The cyclotron frequency $w_c = eB/m^*$, where B is magnetic field, m* is the effective electron mass and e is the electronic charge. The resonant denominator of the integral in eq.(1.18) contains the resonant frequency $w_{n+1,n}$ which can be expressed in terms of the conduction-band energy levels as

$$w_{n+1,n} = \frac{1}{\hbar}\left(E(n+1,k_z,s) - E(n,k_z,s)\right) \qquad (1.19)$$

The conduction-band energy levels of n-type InSb which is described by $E(n,k_z,s)$ are given by (Apel et al, 1971)

$$E(n,k_z,s) = \tfrac{1}{2} E_g\left(-1 + \left(1 + \frac{4}{E_g}\left(\frac{\hbar^2 k_z^2}{2m^*} + \hbar w_c\left(n+\tfrac{1}{2}+\tfrac{1}{2}\nu\right)\right)\right)^{\frac{1}{2}}\right) \quad (1.20)$$

in terms of the energy gap E_g and the electron wave-vector component along the magnetic field direction k_z and the electron spin s. where the parameter $\nu = gm^*/2m_o$ relates to the g factor. The electron distribution is considered to be described by the Fermi function $f_o(n,k_z,s)$ with Δf_o defined as

$$\Delta f_o = f_o(n+1,k_z+q_z,s) - f_o(n,k_z,s) \quad (1.21)$$

where $f_o(n,k_z,s) = 1/(1+ \exp(E(n,k_z,s) - \mu)/k_B T)$ is the Fermi function, μ is the chemical potential and $q_z = 1/\lambda$ is a wave number.

In terms of the complex index of refraction, $n^* = n - ik$, the dispersion relations for the Faraday geometry ($\underline{q}//\underline{B}$) are

$$\varepsilon_\pm = n_\pm^{*2} = (n_\pm - ik_\pm)^2 \quad (1.22)$$

Explicitly separating real and imaginary components, one obtains the refractive index squared

$$n_\pm^2 = \tfrac{1}{2}(\mathrm{Re}\,\varepsilon_\pm + ((\mathrm{Re}\,\varepsilon_\pm)^2 + (\mathrm{Im}\,\varepsilon_\pm)^2)^{\frac{1}{2}}) \quad (1.23)$$

the extinction coefficient

$$k_\pm = -(\mathrm{Im}\,\varepsilon_\pm)/2n_\pm \quad (1.24)$$

the absorption constant

$$\alpha_\pm = 2wk_\pm/c \quad (1.25)$$

the reflection coefficient

$$R_\pm = ((n_\pm - 1)^2 + k_\pm^2)/((n_\pm + 1)^2 + k_\pm^2) \quad (1.26)$$

and the transmission coefficient for a sample with rough surfaces and the thickness d in the Faraday geometry ($\underline{q}//\underline{B}$)

$$T_{\pm} = (1-R_{\pm})^2 \exp(-k_{\pm}d)(1+k_{\pm}^2/n_{\pm}^2)/(1-R_{\pm}^2\exp(-2k_{\pm}d)) \qquad (1.27)$$

From the dielectric tensor one can calculate the reflection, absorption and transmission coefficients, R, α and T using eqs. (1.26), (1.25) and (1.27) respectively. To compute Faraday rotation and ellipticity we have to calculate the refractive and absorption indices from equations (1.23) and (1.24) using either equation (1.13) (for the classical case) or (1.18) (for the quantum mechanical case).

1.6. INTERNAL MULTIPLE REFLECTION EFFECTS

The theory of the isotropic free-carrier Faraday effect in semiconductors may be reformulated, taking into account multiple reflections in the specimen. In the usual treatment of these effects, the rotation of the plane of polarization and the ellipticity of the transmitted radiation are derived without taking account of the waves reflected from the surfaces of the sample. But, as in all transmission and reflection experiments, the effect of multiple internal reflections should be taken into account for samples with plane-parallel faces.

So far as the Faraday effect is concerned, the significant of multiple reflections was briefly mentioned by Champlin(1962), with particular reference to guided wave experiments, but quantitutive investigation was not made. Furdyna and Brodwin (1963) made a passing reference to an approximation to take account of reflections, valid in restricted circumtances. Walton and Moss

(1963), and Moss and Ellis (1964) have reported that such reflections can make a substantial contribution to the observed Faraday rotation (in Ge and GaP), and have used a specimen which is slightly wedged to reduce this complication. Only recent papers discuss measurements in the infrared frequency region, (Piller, 1966; Gabriel, 1967 and Palik, 1966). Exact expressions for Faraday rotation and the ellipticity which take multiple reflection into account have been derived by Donovan and Medcalf (Donovan, 1964).

The Faraday rotation θ and ellipticity Δ may be derived from the form of the resultant elliptically polarized wave. These expressions are given by Donovan and Medcalf (1964).

$$\theta = \frac{wd}{2c}(n_- - n_+) - \theta_c/2 \tag{1.28}$$

$$\Delta = \frac{|K_+| \exp(-2wk_+d/c) - |K_-| \exp(-2wk_-d/c)}{|K_+| \exp(-2wk_+d/c) + |K_-| \exp(-2wk_-d/c)} \tag{1.29}$$

θ_c and K_+ are given by

$$\tan\theta_c = \frac{K_+' K_-'' - K_-' K_+''}{K_+' K_-' + K_+'' K_-''} \tag{1.30}$$

$$K_\pm = K_\pm' + iK_\pm'' = (1-R_\pm)/(1-R_\pm \exp(-2ip_\pm d)) \tag{1.31}$$

where d is the thickness of the sample and $p_\pm$ is the complex propagation constant, given by

$$p_\pm = \frac{w}{c} n_\pm^* = \frac{w}{c}(n_\pm - ik_\pm) \tag{1.32}$$

with $n_\pm$ and $k_\pm$ the real and imaginary part of the complex refractive index, and R_+ is the reflection coefficient at normal incidence, given by

$$R_\pm = ((n_\pm - 1)^2 + k_\pm^2)/((n_\pm + 1)^2 + k_\pm^2)$$

The first term in eq. (1.28) is the normal Faraday rotation, and the second term represents the contribution due to multiple internal reflections in terms of the propagation constants for left- and right-hand circularly polarized waves.

Donovan and Medcalf (1964) have reported that the multiple internal reflection is important particularly at low frequencies. Over a wide frequency range (roughly above the microwave region) Faraday rotation and ellipticity are rapidly varying functions of frequency; and exhibit oscillatory behaviour; at sufficiently high frequencies these oscillations are damped out as $K_+ - K_- \rightarrow 0$ and the effect of the reflections will be negligible. The corresponding effect at far-infrared frequencies will be compared the calculated results for the Faraday rotation and ellipticity from eq. (1.13) and eqs. (1.28), (1.29).

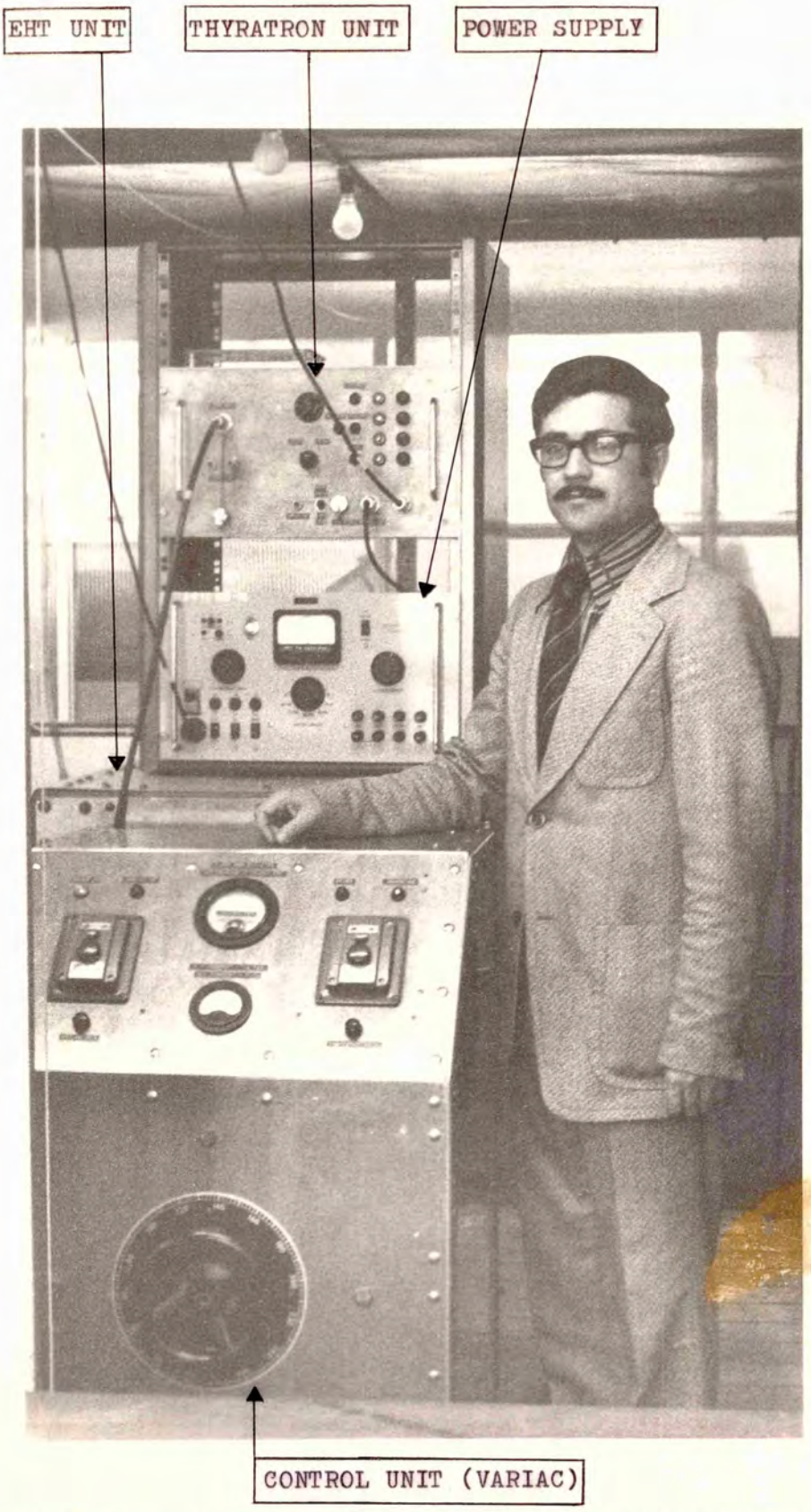

FIG. 2. Power supplies for the 0.337 mm pulsed HCN laser

CHAPTER 2

PULSED 0.337 MM HYDROGEN CYANIDE (HCN) LASER

2.1. INTRODUCTION

Far-infrared-stimulated emission at 0.337 mm involving hydrogen cyanide (HCN) was first reported by Gebbie et al. (1964) with using various organic compounds such as CH_3CN and C_2H_5CN. CW laser action in similar materials was also reported by Muller et al. (1967).

Chantry et al. (1965) and Steffen et al. (1966) reported that the output radiation was associated with transitions between various rotational levels of the v=2 vibrational level of the electronic ground state of the cyanide radical. Broida et al. (1965) commented upon this identification of the transitions and presented a number of arguments to show that this assignment was not correct. Hocker and Javan (Hocker, 1967), and Lida and Maki (Lida, 1967) investigated the possible vibrational-rotational transitions between the (11'0) and ($04^{o}0$) vibrational states of HCN in its ground electronic state.

Mathias et al. (1965) and Stafsudd et al. (1967) reported laser action in several organic materials and concluded that the active species must be of the form H_xCN radical; where x is greater than one.

Operational characteristics of a pulsed HCN laser were described and the variations of output power with gas mixture, pressure, flowrate, discharge voltage and pulse repetition frequency were investigated by Konet et al. (1967), and Robinson and Whitbourn (Robinson, 1971). More recently high power output from HCN laser was reported by Kotthaus (1968), Sharp and Wetherel (Sharp, 1972),

and Jassby et al. (1973).

The present state of understanding of the HCN laser is dispersed in a literature of about one hundred papers. It is desirable, therefore, as a background to our experimental investigation, to summarize some of the most significant features of this knowledge.

2.2. BACKGROUND FEATURES OF CYANIDE LASER

When an electric current is passed through a vapour at low pressure containing hydrogen, carbon and nitrogen, HCN is formed at a low concentration in various excited vibrational levels. Dimethylamine ($(CH_3)_2NH$), methyl cyanide (CH_3CN), ethyl cyanide (C_2H_5CN), ethylenediamine ($C_2H_2(NH_2)_2$), n-propylamine ($C_3H_7NH_2$), and mixtures of methane and ammonia, nitrogen and acetone, nitrogen and methane as well as pure HCN gas have been used to produce 0.337 mm laser radiation.

Lida and Maki (Lida,1967) showed that the line originated from transitions between (11'0) and ($04^0$0) vibrational states of the linear molecule HCN. The transitions are shown schematically in Fig. 2.1a. The levels of (11'0) are shown as doublets in this figure because of the splitting into levels of even and odd parity by the l-type doubling (Wilson,1955; Herzberg,1945; Sugden and Kenney). The rotational levels of ($04^0$0) have even parity for even J and odd parity for odd J. Intense lines must satisfy the selection rules $\Delta J = \pm 1$ and $+ \leftrightarrow -$, and $- \leftrightarrow +$. The two strong laser emissions at 0.311 and 0.337 mm are intersystem transitions made allowed by taking on the character of the pure rotational transitions $J(11) \rightarrow J(10)$ and $J(10) \rightarrow J(9)$ within (11'0). Hocker and Javan (Hocker,1967) made very accurate frequency measurements not only of the

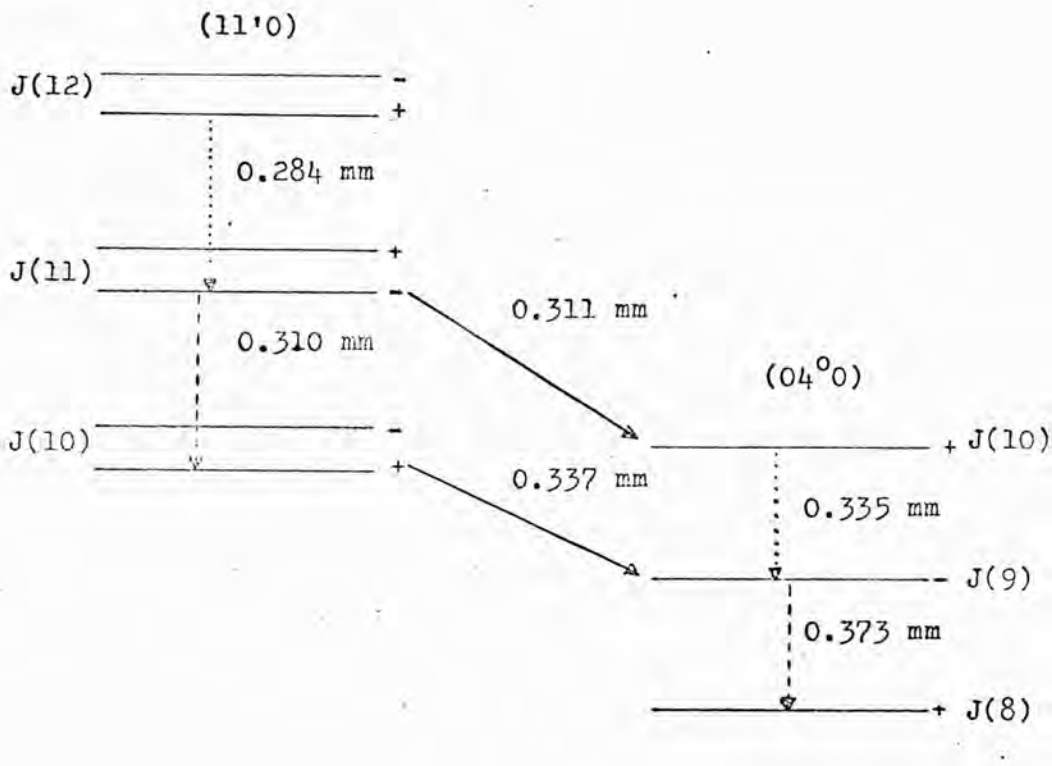

Fig. 2.1a. Rotation-vibration energy levels of HCN near 2900 cm^{-1} and the origin of laser action in HCN vapour. Splitting of the 11'0 lines are due to l-type doubling.

—— pump transitions

---- lines previously seen pulsed

.... new submillimeter transitions; (Hocker, 1967).

0.337 mm radiation but also of several other emissions which could be obtained from the system.

The processes of the electrical discharge dissociate the molecules, partially ionize and provide conditions for the formation of HCN with an excess population of (11'0) vibrons relative to ($04^{0}0$) vibrons. Laser action results because there is an unusually large transition moment between certain rotational levels of those vibrational states. That transition moment arises from a mixing of the two vibrational states which results from a) the near coincidence of the energy levels at a particular value of J and b) a weak coriolis interaction between the states. The necessary conditions for laser action to take place are a) the level must be very close so that the interaction and resultant mixing is large and b) there must be a nonequilibrium population distribution between the two states. The first condition can be tested by calculating the various energy levels.

The origin of the nonequilibrium population distribution among the various energy levels in this laser is not known for certain. Possible mechanisms involve preferred excitation of stretching vibrations or rapid relaxation of bending vibrations or some combination of both (Maki, 1970).

That the function of the applied electric field is to cause breakdown of the gas molecules and, rather than directly excite HCN molecules to the necessary state of inverted population, to create conditions which influence the later formation of excited vibrons is suggested by the observations of time delays between the onset of the current pulse and the beginning of stimulated emission, leads to the suspicion that the CN radical is involved in the mechanism even if it is not the emitter itself. It is pos-

sible that some selective chemical reaction of the type

$$R - H + C N \longrightarrow R' + H C N \qquad (2.1)$$

tends to favour cascade routes to the ground state via (11'0). If this is so then a large fraction of the molecules formed in discharge will pass through the emitting states. Sanders (Sanders , 1959), reported that the population inversion of the energy levels of HCN molecules is achieved by the inelastic impact of electrons accelerated in the applied electric field.

Very shortly after the discovery of stimulated emission at 0.337 mm, it was shown in many laboratories that the system would in fact oscillate at a large number of wavelengths. Some of these are indicated as the primary and cascade processes in Fig.2.1a.

2.3. EXPERIMENTAL ARRANGEMENT

(i) A pulsed 0.337 mm HCN laser

A schematic arrangement of the laser system was shown in Fig. 2.1b.The discharge tube was constructed from Q.V.F glass tube with an internal bore of 10 cm (4 inches) and total length of the system of 315 cm. The Fabry-Perot resonator was formed from two circular aluminized concave glass mirrors of 10 cm (4 inches) diameter and mounted approximately 290 cm apart from each others. One mirror with 1.27 cm ($\frac{1}{2}$ inch) thick and radius of curvature 278 cm was mounted on flexible bellow, which allows independent axial and tilt adjustment; the other with 0.635 cm ($\frac{1}{4}$ inch) thick and the radius of curvature 287 cm was mounted on the spindle of a micrometer, which has a tripod screw adjustments, in order that the cavity length may be adjusted so that the optical axes of these mirrors can be made parallel to one another along the axis of the laser tube, but such a concave geometry was not oversensitive to mirror alignment.

Fig 2.1b: 337 μm FAR INFRARED LASER

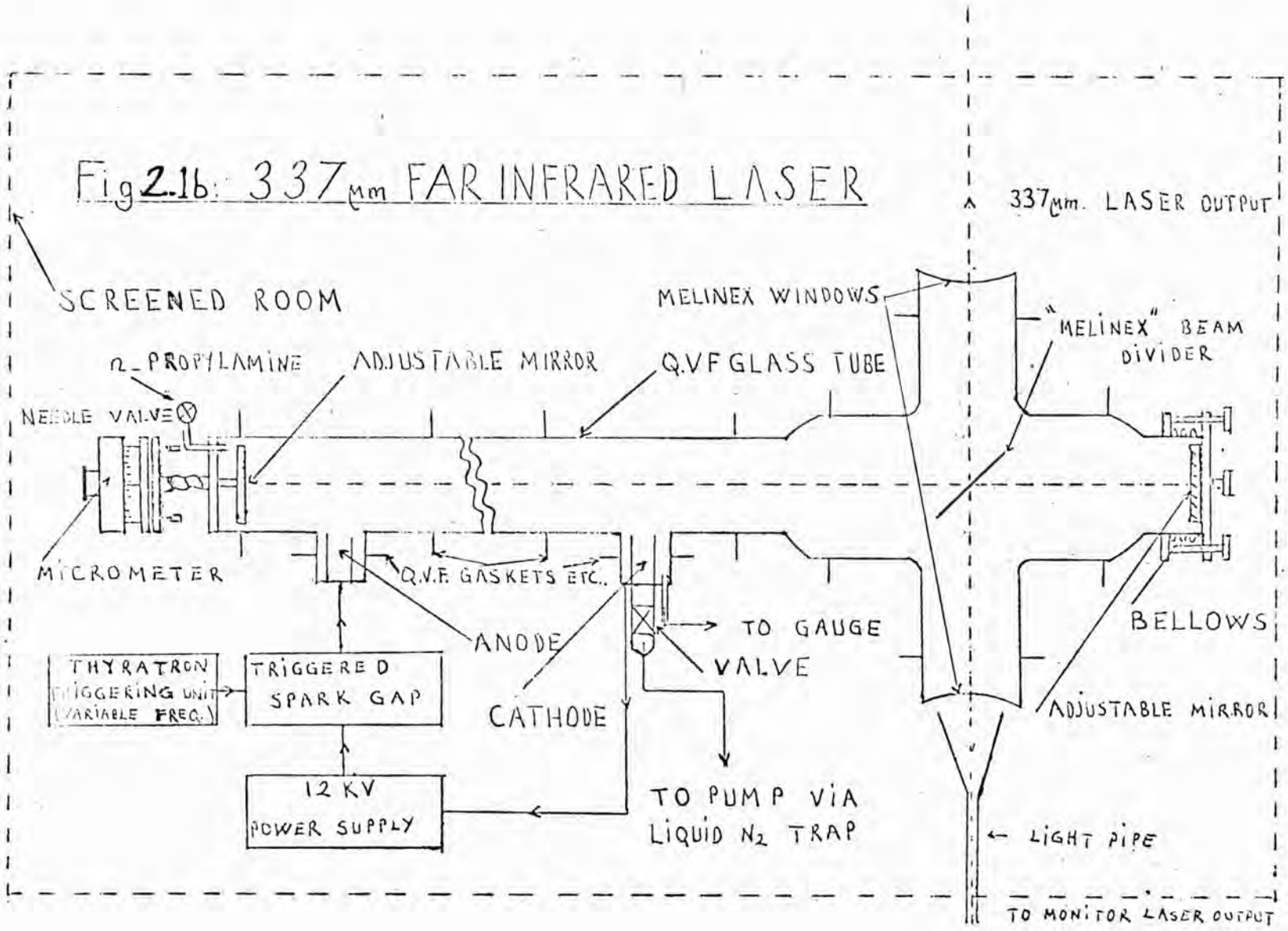

N-propylamine which has 400 mm of Hg vapour pressure at 31.5° centigrade was stored in the small flask and admitted through a needle valve to the high-voltage end of the laser, and continuously pumped at the opposite end with a rotary vacuum pump. A pressure gauge was connected at the low-voltage end of the laser to estimate the operating pressure. The exhausted gas was piped outdoors for safety reasons, since HCN is the active emitter of the 0.337 mm radiation. Also a liquid nitrogen trap was used in between the laser tube and the pump in order to avoid transferring of the active HCN from the laser tube to atmosphere via the rotary vacuum pump.

Breakdown was produced between the brass electrodes with 175 cm apart when a 0.25 microfarad capacitor charged to 8 kV was discharged through a spark gap triggered by a thyratron triggering unit which has a variable frequency control. The voltage pulse applied to the electrodes of the system was chosen on the basis of smoothness of running and power output, but usual operation required 6-10 kV, repeated at about 10 pulses per sec. and operating pressures varied between 0.5-1.0 torr for HCN laser. The flowing of n-propylamine vapour into the laser system were adjusted using both the needle valve at the high-voltage end and the valve at the low-voltage end of the laser till the output power was optimized.

Far-infrared radiation (0.337 mm) was coupled out of the cavity with reflection from a 100 gauge (about 0.025 mm) melinex beam divider which has a low absorption at 0.337 mm, so losses in the beam divider were small. Nevertheless, it was interesting to observe that the radiation coupled out of the cavity was polarized in the plane of Fig. 2.1b. The power outputs from both sides

of the beam divider passed through separate and identical light pipes consisting of 7.5 cm diameter copper cones tapering down to 1 cm diameter brass tube polished internally: one to the cryostat and sample and other to a monitoring detector (Golay cell).

In order to avoid picking up electrical interference from the laser system, the laser and its associated power supplies were enclosed in a screened room, the main input to which was fitted with a filter to reduce mains-borne interference. All the measuring equipments were left outside the screened room.

Both laser outputs were depolarized owing to reflections from the inside walls of the light pipes. Therefore, it was necessary to place a polarizer just before the sample and an analyzer immediatly after the sample for the Faraday rotation and ellipticity experiments.

The laser parameters of most interest to the experimenter are the frequencies and intensities of the radiation which emerges as the cavity is tuned by turning the micrometer knob. It is also important to know the long term stability and short term noise of the system. It is found that the long term stability was not more than ten percent over ten minutes; also it is possible to retune again with turning of the micrometer knob till the optimum output power is obtained.

A rough estimate of the output power of the laser can be obtained by calibrated the Golay cell using a light bulb whose radiation is chopped at 10 Hz. A ordinary tungsten-filament lamp emits a continuous spectrum with a peak at about 1×10^{-3} mm ; since the quartz window of the Golay cell begins to absorb at about 4×10^{-3} mm , most of the energy of the lamp reaches the detecting element of

the Golay cell.

On the assumption that all the energy supplied to the tungsten-filament lamp is radiated isotropically and its total irradiance of about 90% is transmitted by quartz, which was reported by Stair et al. (Stair, 1967), therefore, it is possible to calibrate the Golay cell roughly: such a calibration gives an estimated mean power of 1mW for the pulsed HCN laser.

Our calibration was tested after the Golay cell was calibrated by Cathodeon Ltd. Comparisons showed that it was factor of two between these calibrations.

(ii) The Cryostat

Schematic diagrams of the vertical and top views of the optical cryostat used, and the arrangement of the polarizer, sample holder with an experimental sample, and the analyzer into the transverse aperture of the cryostat are shown in Figs. 2.2b,2.5, and 2.3 respectively.

Several factors influenced the final design of the optical cryostat. These included the limited amount of space available in the 3.0 cm diameter of transverse bore of the 4 tesla (40kG) magnet with superconducting solenoid fitted with superconducting switch and the necessity of keeping the brass light pipe run as short as possible to reduce attenuation of the laser power. The rotating part of the light pipe to which rotates an analyzer was made of a stainless steel tube in order to avoid heat transfer from the outside shielding of the cryostat to near the specimen. The samples were mounted on the pure copper cylindrical holder being inserted into the transverse aperture with the appropriate shield removed where necessary. The sample holder is greased lightly with n-type vacuum grease to make a good thermal contact between the

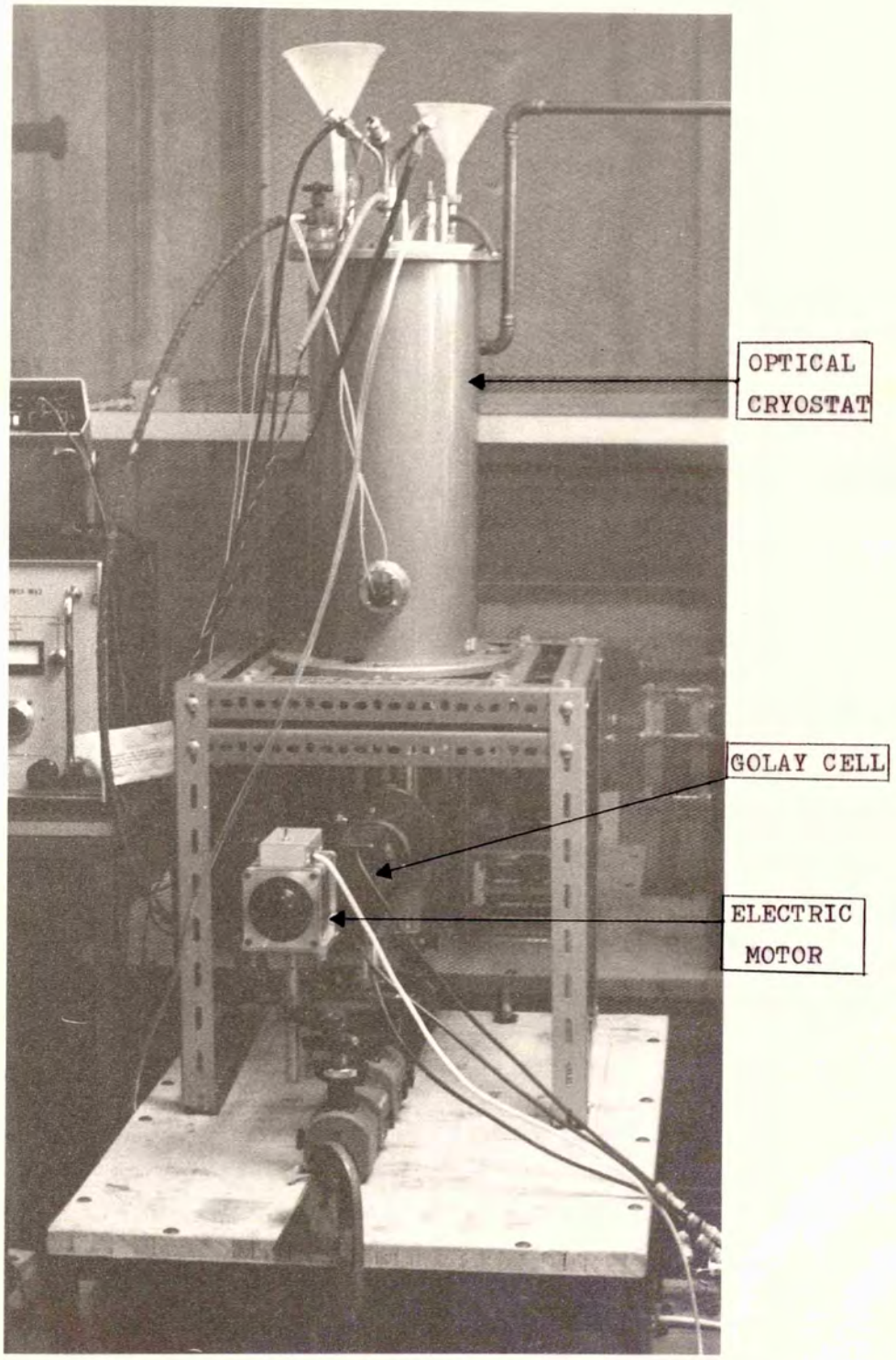

FIG. 2.2a Tranverse access optical cryostat, driving motor for polarizer and Golay cell detector

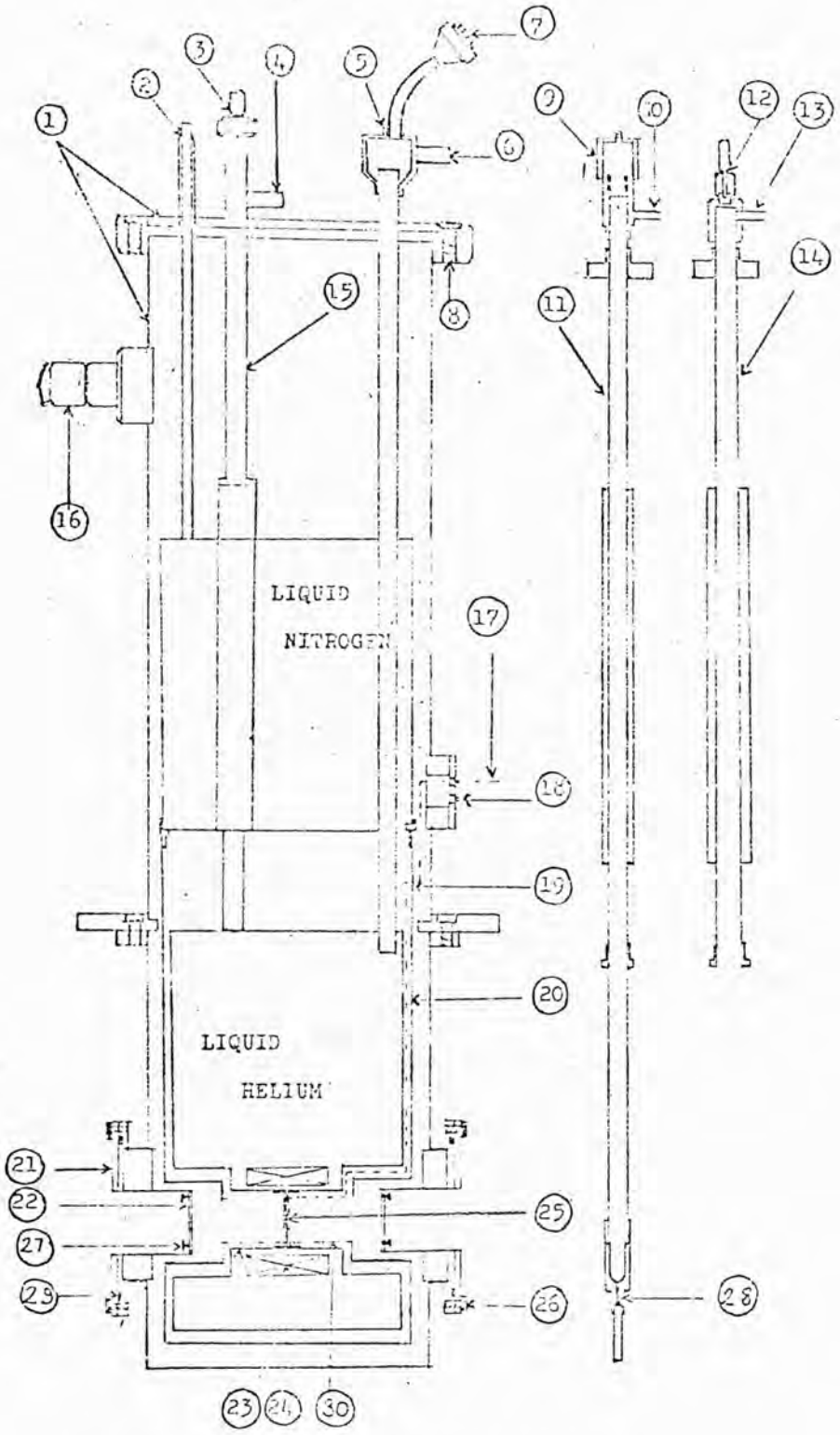

FIG.2.2b. TRANVERSE-ACCESS OPTICAL CRYOSTAT

Numbers in the open circles in Fig. 2.2b represent following meanings:

1- The stainless steel outer shield

2- Nitrogen fill and vent tube

3- Syphon entry

4- Helium recovery tube

5- Terminals (magnet and magnet common)

6- Helium recovery tube

7- Superconducting switch

8- Screws

9- Needle valve

10- Liquid nitrogen pre-cooling outlet

11- Liquid nitrogen pre-cooling and vent tube

12- Liquid helium level indicator entry

13- Helium recovery tube

14- Liquid helium level indicator tube

15- Syphon entry tube

16- Valve

17- Thermocouple wire

18- Glass-metal laed-through for thermocouples

19- 0.25 inch wide slot in pure copper radiation shield

20- Pure copper radiation shield

21- Outer flanges

22- Window and window holder

23- Helium can tube

24- Superconducting magnet

25- Pure copper sample holder and sample

26- Screws for the outer flanges

27- Screws for the windows

28- Needle ; 29- 'O-ring'

30- Tubular radiation shield

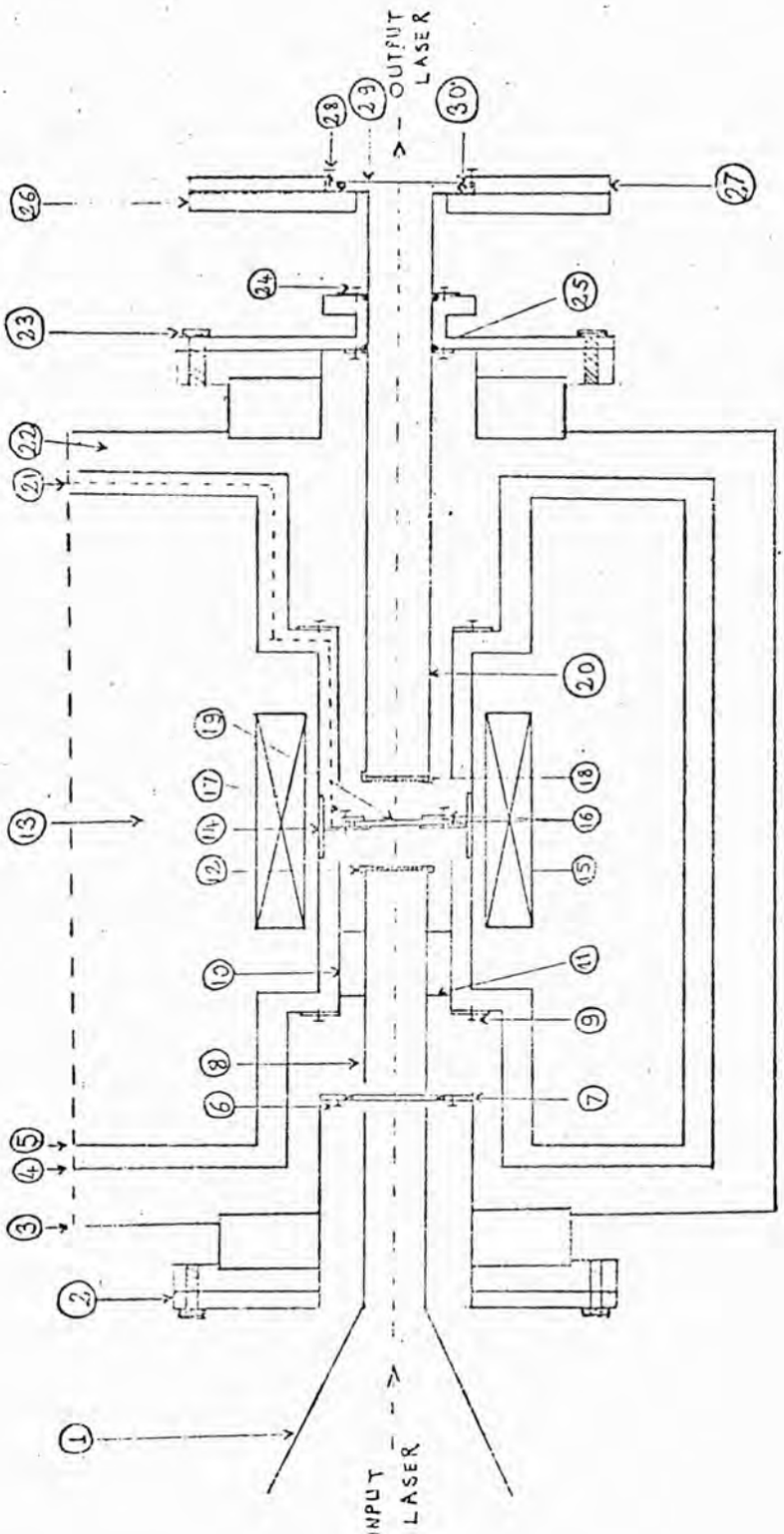

FIG. 2.3: Schematic diagram of the transmission laser light through the access cryostat.

Numbers in the open circles in Fig. 2.3 represent following meanings:

1- Light cone

2- Outer flange of the cryostat

3- The stainless steel shield of the cryostat

4- The pure copper liquid nitrogen radiation shield

5- Liquid helium dewar

6- Screws for the TPX window

7- TPX window

8- Brass light pipe

9- Screws for the tubular radiation shield

10- The tubular radiation shield

11- Support for the light pipe

12- POLARIZER (fixed)

13- Liquid helium

14- The pure copper sample holder

15- Superconducting magnet

16- Pure copper 'O-ring' support for sample

17- Screws for the pure copper 'O-ring' support

18- ANALYZER (rotating)

19- SAMPLE

20- Rotating stainless steel tube

21- Thermocouple wire

22- Pressure 10^{-5} torr

23- Screws for outer flange

24- Screws

25- 'O-ring' seal

26- Fixed base

27- Rotating base

28- Screws ; 29- TPX window

30- 'O-ring' seal

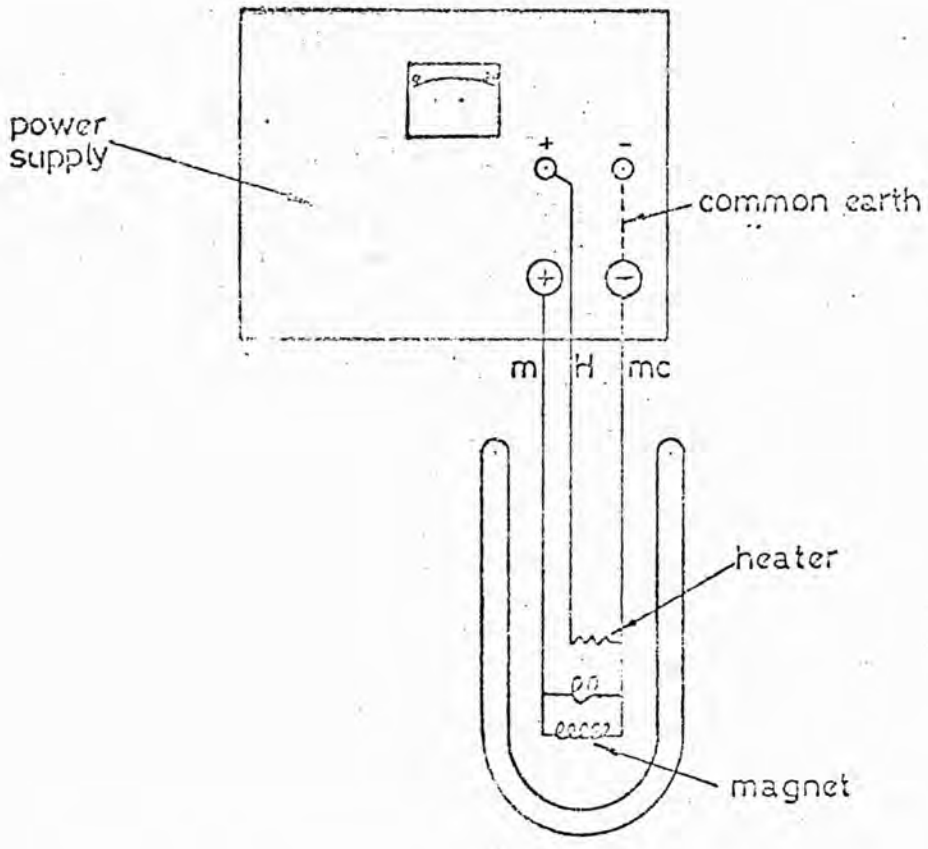

Measured Resistances Across Terminals

m - H	105 — 107 ohms
mc - H	100 ohms
m - mc	5 — 7 ohms

Fig.2.4. CRYOSTAT-CONNECTIONS TO POWER SUPPLY

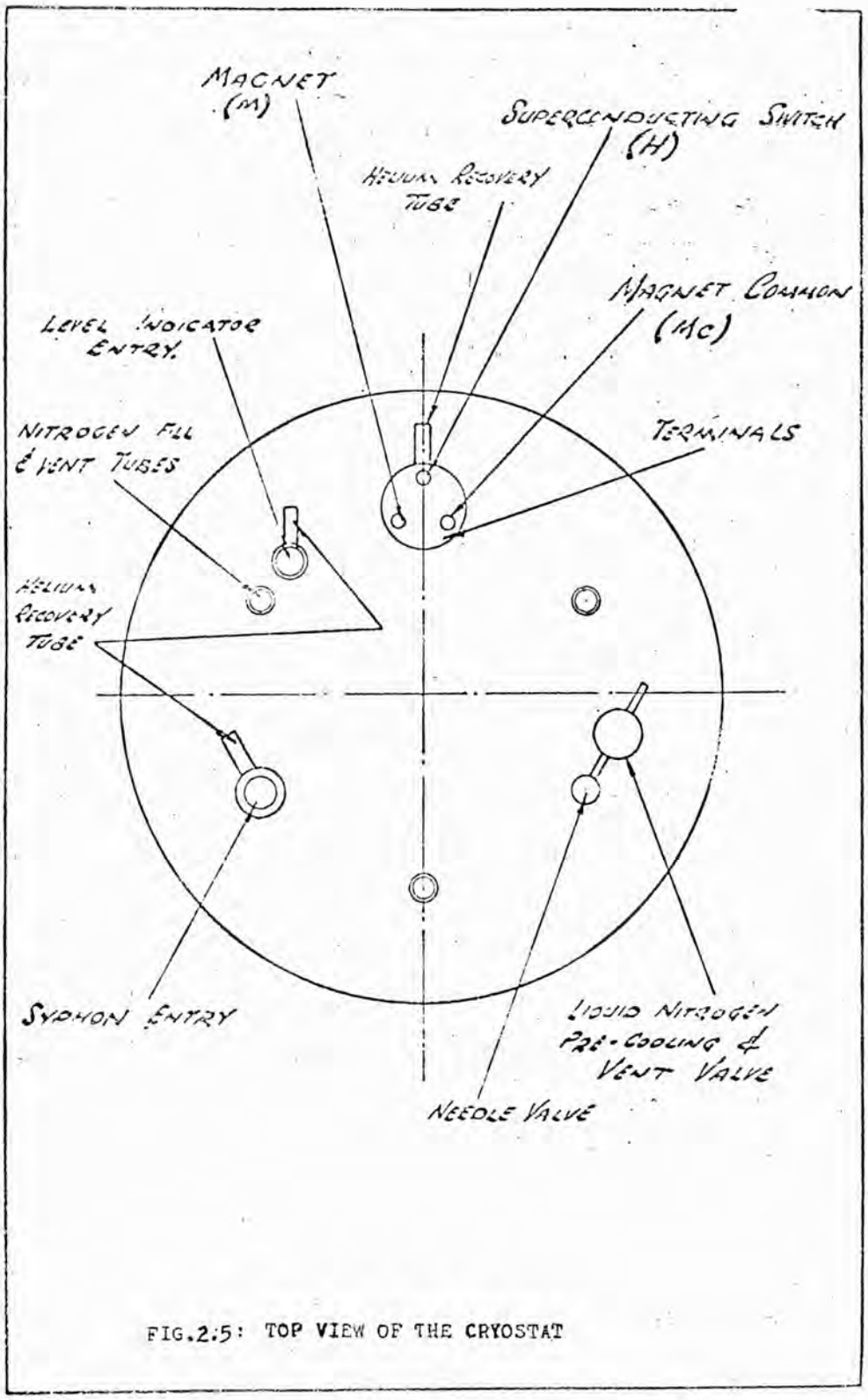

FIG.2.5: TOP VIEW OF THE CRYOSTAT

Xcms	Y gauss/amp	Xcms	Ygauss/amp	Xcms	Ygauss/amp	Xcm	Ygauss/amp
0.0	1101.[illegible]	1.0	[illegible]	2.0	[illegible]	3.0	592.94124
0.1	1101.07062	1.1	1034.65301	2.1	841.68359	3.1	564.63403
0.2	1099.47820	1.2	1021.46934	2.2	819.02439	3.2	536.87978
0.3	1096.78814	1.3	1007.00315	2.3	795.[illegible]	3.3	509.81431
0.4	1093.01838	1.4	991.23473	2.4	765.03089	3.4	483.55314
0.5	1088.14805	1.5	974.15232	2.5	736.97638	3.5	458.19031
0.6	1082.15324	1.6	955.75174	2.6	708.43195	3.6	433.79853
0.7	1075.02744	1.7	936.03911	2.7	679.57304	3.7	410.42997
0.8	1066.77[illegible]	1.8	915.03807	2.8	650.55060	3.8	388.11703
0.9	1057.28033	1.9	892.76812	2.9	621.64758	3.9	366.87844

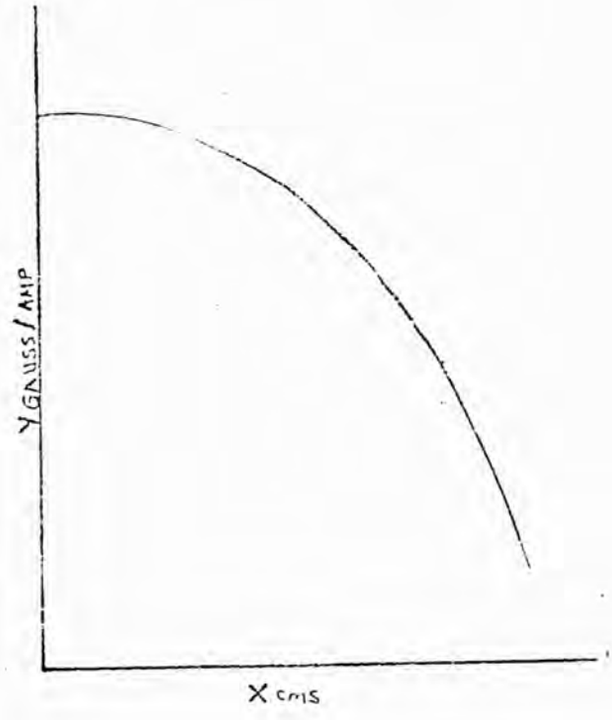

FIG.2.6: MAGNET CALIBRATION FOR THE ACCESS CRYOSTAT

specimen and the helium bath.

It was, of cause, important to transfer the laser beam to the sample with the minimum loss of power. The laser system and the cryostat were therefore supported on tables whose heights could be adjusted so that the beam from the laser passed straight through the bore of the cryostat.

A far-infrared polarizer of evaporated gold grating with lines spaced approximately 0.050mm apart was used to polarize the incident radiation, and was cemented with a bostik 7 (two- components quick setting epoxy resin) to the end of the light pipe just before the sample. The same kind of polarizer was used to measure the Faraday rotation as an analyzer, and was rotated by a motor-driven gear. The degree of polarization after transmitting through the polarizer and the analyzer was obtained to be 90 % at 0.337 mm, because the polarized beam was slightly depolarized by reflection between the polarizer and the analyzer. If there was no space between them the degree of polarization was approximately 96 % at wavelenth of interest and for these polarizers.

The transmitted light was received by a Golay cell which is still the most widely used detector for far-infrared studies. The detected signal was amplified and analyzed by two linear gates which were used in single-point mode and then recorded on a X-Y recorder as a function of the rotating angle of the analyzer. This signal processing and recording technique will be discussed in detail later in next section.

The temperature of the sample was monitored by a gold-iron vs chromel thermocouple with its reference on the liquid helium dewar (4.2K) and temperature junction on the sample holder as near as the sample.

R.L. Rosenbaum's data (Rosenbaum, 1968) on the gold-iron vs chromel thermocouple were used for the calibration. It was found that the thermocouple reading was not satisfactory due to bad thermal contact to the helium and nitrogen dewars for the thermocouple junction. Nevertheless, it gave an indication of the sample temperature.

In designing the optical components of the cryostat it had to be borne in mind that the laser output was at best no more than 1 mW for 0.337 mm radiation. Thus it might be seen that efficient guiding of the radiation onto the sample was required. In actual tests of the transmission of the external copper condensing cone and the brass light pipe it was found that use of the light cone increased the signal by a factor of three and that the light pipe with 25 cm total length transmitted about 65 % of the radiation entering it. Transmission of a brass straight light pipe with 1.1 cm diameter as a function of its length was investigated by Ohlmann et al. (Ohlmann, 1958) at 0.070 and 0.140 mm for radiation of f/1.5. They reported that such pipes was quite efficient for infrared radiation; but comparison between their calculation and our experimental values couldn't be done due to different wavelength and geometry used. Approximately 60 % of the beam was lost at each of the far-infrared polarizers and 10 % was lost at each of the TPX windows, some was lost by absorption at the sample itself, and some was diffracted out of the light path at each of the discontinuities in the system.

Chantry (Chantry, 1969) has examined the transmission properties of TPX window and found 2 mm thick window to be have 60 % transmission for incident radiation of 0.337 mm wavelength. Losses

in stainless steel and brass light pipes have also been investigated by Harris et al. (Harris, 1966) for trasmitting radiation of wavelength 0.337 mm. They reported that the losses in such pipes were very high, amounting to 85 % approximately. Experimentally, the net loss of signal when only the polarizers were present (no sample in the cryostat) was about 50 % - 60 %.

It was clearly an undesirable feature of the design that the cryostat light-pipe should so strongly attenuate the radiation passing through it. Better transmission would, of course, be obtained in a larger diameter tube. Such a tube couldn't be used since the bore of the cryostat was too small.

(iii) Description of the experimental technique

The main difficulty in making measurements of Faraday rotation and cyclotron resonance in semiconductors was the fact that the laser beam was strongly attenuated by the sample when the magnetic field was close to that required to give cyclotron resonance and the signal from the far-infrared detector which was a Golay cell in our experiments was seen of the same size as the random noise in the system. Another difficulty in measuring Faraday rotation and ellipticity was that the plane polarized radiation became elliptical as a resuld of absorption and scattering by the sample when the magnetic field was increased. As shown in figs. 2.8 and 2.9 the eccentricity of the ellipse decreased (i.e. the radiation became more nearly circularly polarized). At the cyclotron resonance field the maxima and minima became nearly equal and it was hard to differentiate between them on the screen of the oscilloscope. This made measurement of the Faraday rotation difficuld.

In order to extract this signal from the noise and to determine its amplitude more accurately, as shown in fig. 2.7b, the

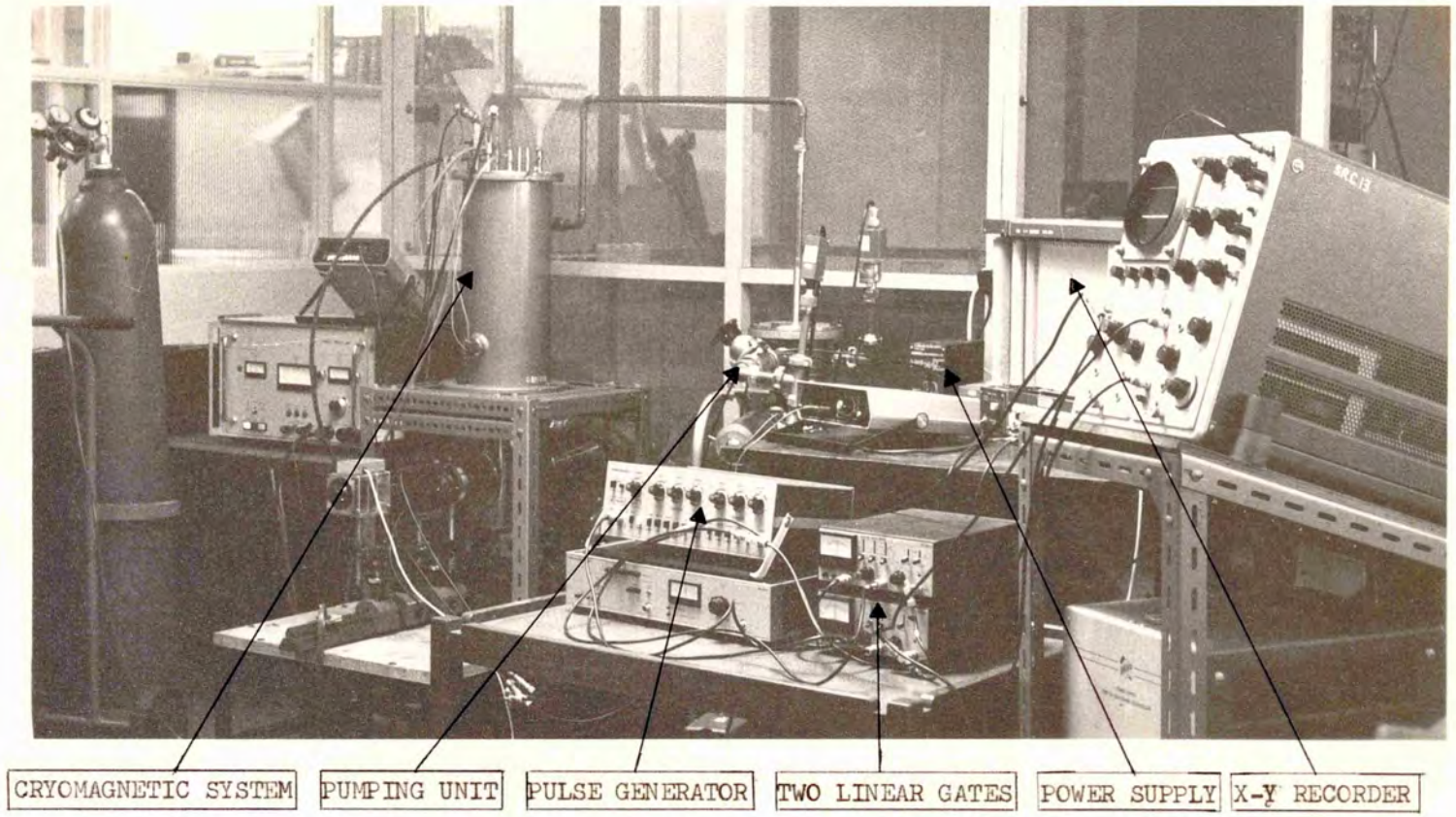

FIG. 2.7a General view of experimental apparatus used for Faraday rotation and ellipticity measurements

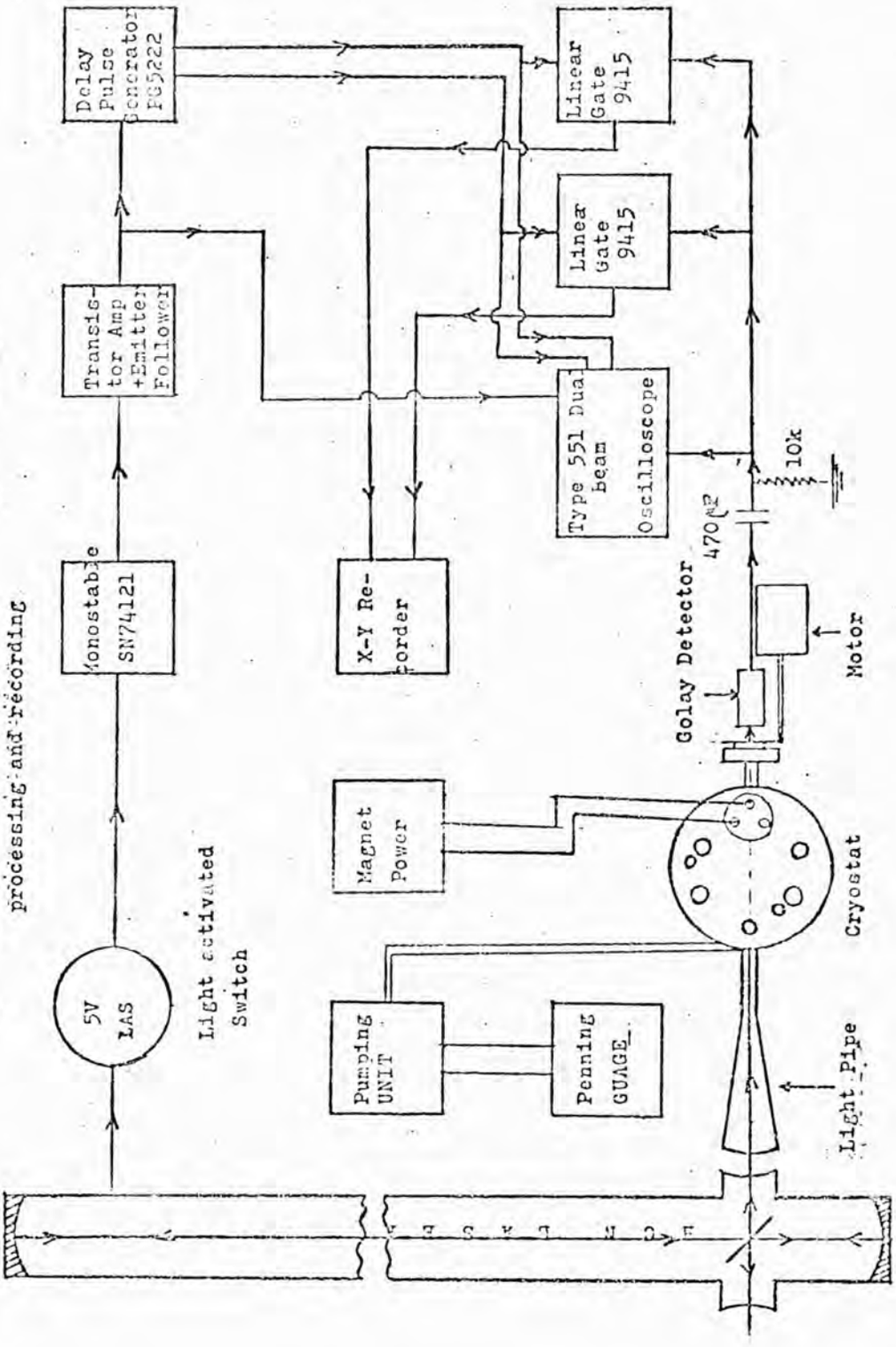

Fig. 2.7b Block diagram of experimental apparatus, signal processing and recording

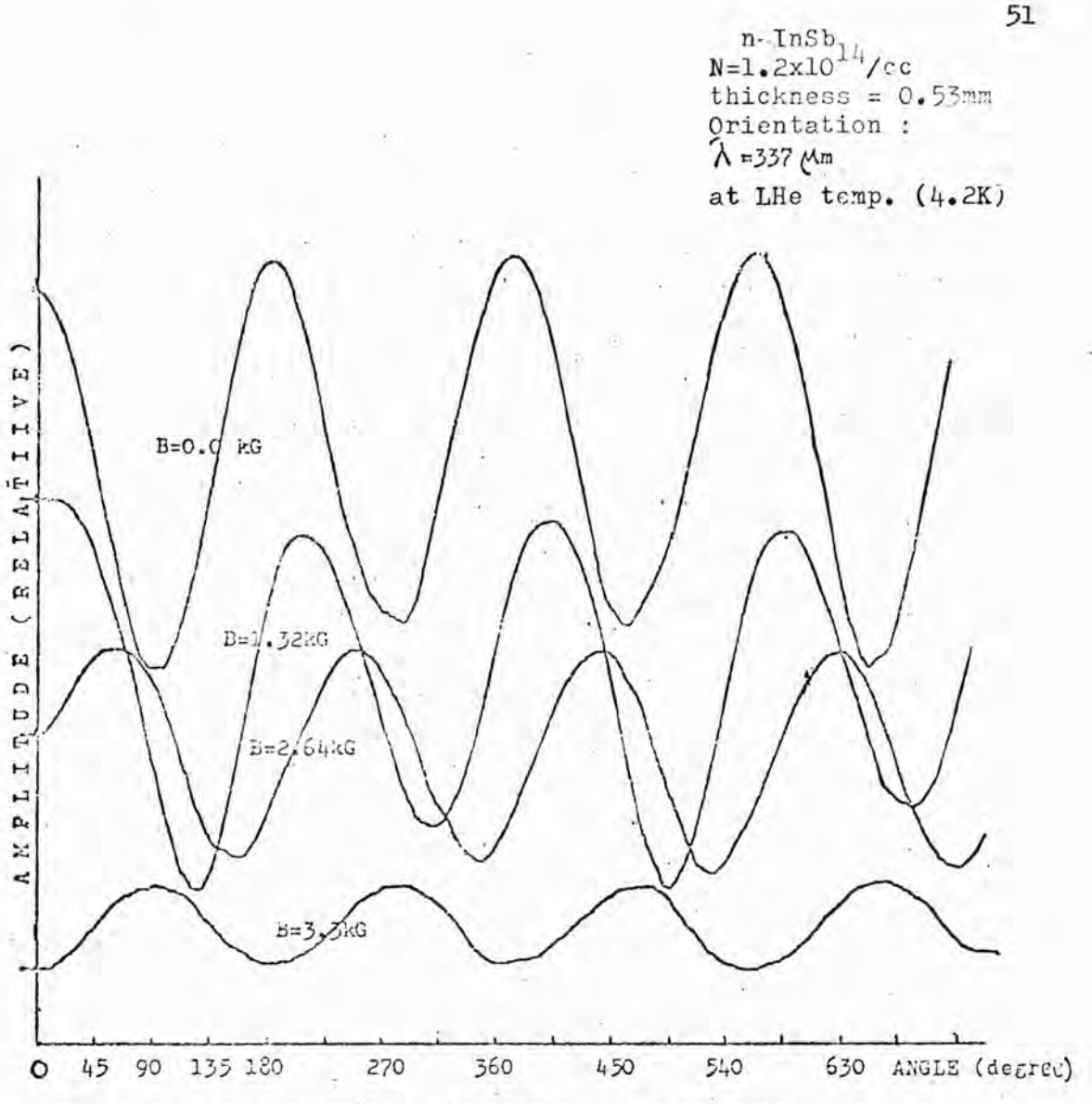

FIG.2.8 Infrared transmission of InSb specimen as function of angle between polarizer and analyzer for several values of magnetic field. The progressive rotation and increase in ellipticity is clearly illustrated. (N.B after each one of the run in same magnetic field the pen of the X-Y recorder was shifted downwards by hand to make illustration clear.)

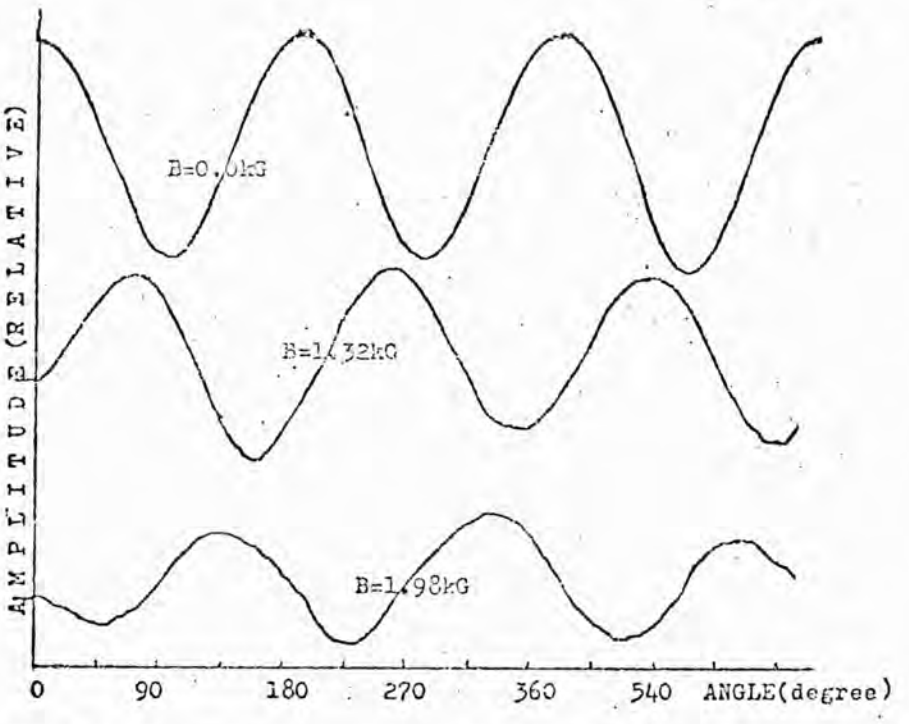

FIG.2.9 Infrared transmission of InSb specimen as function of angle between polarizer and analyzer for several values of magnetic field. The progressive rotation and increase in ellipticity is clearly illustrated. (N.B after each one of the run in same magnetic field the pen of the X-Y recorder was shifted downwards by hand to make illustration clear.)

output from the detector was fed into two linear gates which were triggered by a coherent reference trigger input with the signal of interest via a light activated switch, a monostable, a transister amplifier and a double pulse generator which has delay facilities. These linear gates were used in 'single-point' mode: one to look at the position of the peak of the signal and the other to look at the base-line of the signal. The linear gates averaged-out the noise and gave d.c. levels at their outputs which were proportional to the height of the input signal from the detector. One of these linear gates recorded the average d.c. level, and other recorded the average height of the detector signal+d.c. level. The signals from these linear gates were then subtracted using a differential amplifier which was part of the pen recorder, and the resultant signal, which was proportional to the detector signal alone, was displaced on a pen recorder. It was impossible to obtain meaningful results by using only one gate, owing to the fluctuations in the d.c. level of the detector output. Hence the need for a differential amplifier which would eliminate these fluctuations.

In Faraday rotation experiments, the magnetic field applied to the experimental sample was changed step by step. At each fixed magnetic field applied to the sample, the motor-driven gear which rotated the analyzer and the time base of the pen recorder were started at the same time, then the transmitted radiation through the polarizer, sample and analyzer were recorded automatically as a function of the rotating angle of the analyzer. As shown in figs. 2.8. and 2.9. the traces of the pen recorder were sinusoidal. With an applied magnetic field the sample also rotated the plane of polarization of the beam producing a phase shift with respect to zero

magnetic field. The shift in the minima or in the maxima was proportional to the Faraday rotation angle. After each run in fixed magnetic field the transmitted beam from the sample was cut off simply by putting an iron plate in front of the detector and then the zero d.c. level was recorded by the pen recorder. Thus the relative pulse heights I_a, I_b at the minima and the maxima points were obtained and these were used to calculate the ellipticity which was given by $\Delta^2 = a^2/b^2 = I_a/I_b$, where a and b were the semi-minor and the semi-major axes of the ellipse respectively. A more complex case occurred when the two identical polarizers were not perfect and the minima were not negligible in zero field (Palik, 1963). In this case the ellipticity was given by the expression $\Delta^2 = (M-X)/(MX-1)$, where M is the intensity ratio of minimum to maximum in zero field and X is the same ratio in a magnetic field B.

(iv) Measurement of the wavelength of the pulsed HCN laser

The block diagram of experimental set-up for measuring the laser wavelength was shown in fig. 2.10. Radiation from the laser system was collected by a light pipe (such light pipes were widely used for condensing and transmitting far-infrared radiation and were discussed in detail elsewhere, (Poehler, 1970; Ohlmann, 1958; Williamson, 1952; Harris, 1966, and Loewenstein, 1969)). The beam was then divided by a 'melinex' beam splitter with 0.025 mm thickness and was subsequently recombined after reflection from the two plane Michelson mirrors. One of these mirrors was driven by an electric motor with a speed of 0.0135 mm per second and the signal at the detector varied between a maximum and zero values as the mirror was moved along.

The detected signal was amplified and processed by two linear

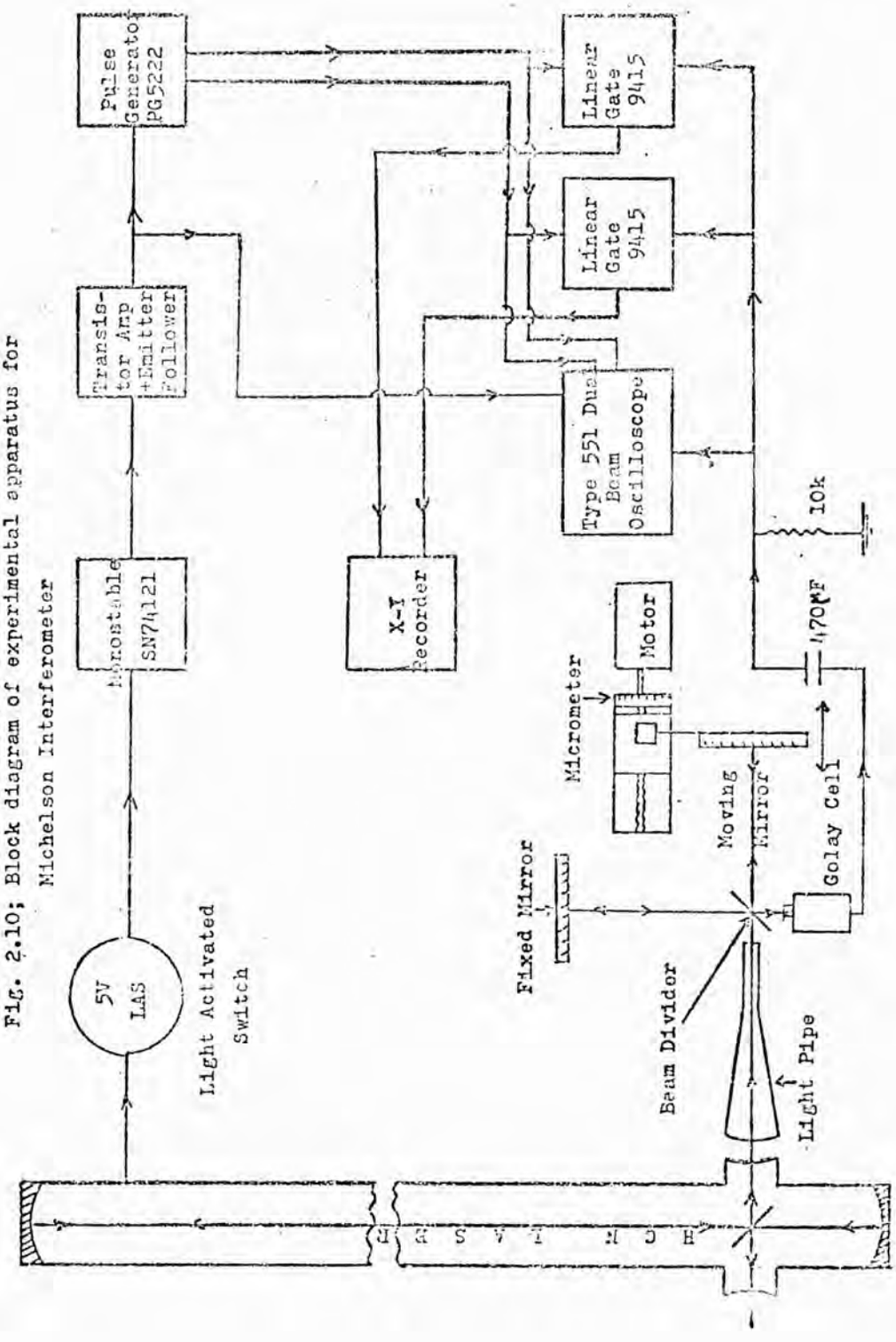

Fig. 2.10; Block diagram of experimental apparatus for Michelson Interferometer

gates in the manner discussed in detail in the previous section, and recorded by a pen recorder with a paper speed of 600 mm per hour or 10 mm per minute.

When the mirror was driven by the motor, the pen recorder was drawing a sinusoidal curve. The mirror displacement was measured by a micrometer with ±1 micron accuracy. It was seen that the relative amplitude of the interfering wave which was recorded by the pen recorder was modulated about 10 % due to 0.311 mm and other wavelength emission. However, accurate frequency measurements have been made elsewhere (Hocker, 1967; Lide, 1967) not only for the 0.337 mm radiation but also for the other wavelengths which can be obtained from cw HCN laser. It was found that the 0.337 mm emission was much more stronger than the 0.311 mm and the other emissions. The reason for checking the wavelength emitted by the HCN laser was to make sure which wavelength is being emitted here and to obtain meaningful results from the other experimental investigations. The experimental measurements of the wavelength emitted by the laser in the experiments described in this thesis were given in the following table.

TABLE 2.1

mirror positins start (cm)	stop (cm)	d displacement (μm)	number of maxima (m)	wavelength measured(μm) λ=2d/m	observed values (μm)
18.0000	14.3200	36800±1	218±0.1	337.615±0.309	336.6±0.3
13.3000	10.2000	31000±1	184±0.1	336.956±0.366	(Steffen,966)
9.0000	14.1900	51900±	308.25±0.1	336.740±0.218	336.5578
					(Hocker,967b)
			mean value:	337.1±0.3	336.564
			weighted mean value: ($\bar{\lambda}=\Sigma\lambda m/\Sigma m$)	337.06±0.30	(Hocker,967a)

CHAPTER 3

SAMPLES

3.1. INTRODUCTION

Undoped n-type indium antimonide specimens with different carrier concentrations were used for the Faraday rotation and ellipticity experiments at 0.337 mm wavelength, since at this wavelength, InSb has a low absorption coefficient and this makes easy to observe transmission experiments in a reasonable degree of accuracy. But, if other semiconductors are used for measurement of the Faraday rotation at this wavelength it will be needed very thin samples owing to their large absorption coefficients even at low temperatures. If the thickness of these semiconductors is reduced in order to increase the transmission of the radiation, then the Faraday rotation which is proportional to this thickness will be small (as an amount of the experimental error) and difficult to measure with any degree of accuracy. Also the small effective mass of the electrons in InSb, magnetic fields produce large effects. For example, the Landau splitting ($Be\hbar/m^*$) is almost seventy times larger than for an electron mass.

This small effective mass is mainly responsible for the high mobility of electrons in indium antimonide - 7×10^4 $cm^2/V\text{-sec}$ at room temperature - which is some 20 times higher than in germanium.

Indium antimonide crystallizes in the zinc-blende structure, with the interatomic spacing as 0.648 nm. The coefficient of linear expansion was studied by Gibbons (1958) in the temperature range from 300K to 10K and it was given as 5.04×10^{-6} per degree kelvin at room temperature. An interesting feature of the thermal

expansion coefficient is that it drops to zero at 56K and becomes negative for temperatures below this.

3.2. PROPERTIES OF INDIUM ANTIMONIDE

Many of the interesting properties of InSb can be explained from the energy band structure which has been calculated in detail by Kane (1957) using the Kronig-Penney perturbation approach. There have also been several publications dealing with the band structure of InSb in a magnetic field, (Luttinger,1955; Bovers, 1959; Lax, 1961 and Apel, 1970). Usually the results are given in the form of numerical solutions to high-order matrix equations and yield energies $E_b(\underline{k})$ for the conduction band and the three valence bands under specific numerical assumptions. The relevant energy bands in InSb at zero magnetic field are shown in fig.3.1.

There have been several papers in the literature on the electric and galvanomagnetic properties of InSb at low temperatures (Sladek, 1958 and 1959).

Probably the most important galvanomagnetic effect arising out of the interaction of electric and magnetic field is the Hall effect which is a particularly fruitful mean of investigating semiconductor properties. In all Hall effect investigations, care must be taken to avoid spurious voltages arising from bad contacts and from the mixing of magnetoresistance components due to contact misalignment and sample inhomegeneity.

Hall data taken at high and low magnetic fields may lead to different values for the carrier concentration through a dependence of the Hall coefficient factor 'r' on the magnetic field via the scattering time τ, as will now be explained.

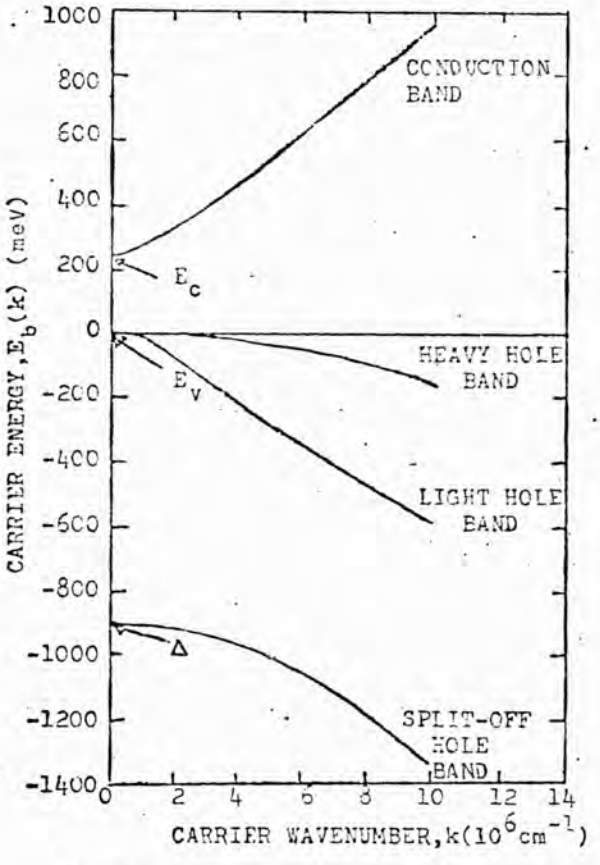

Fig.3-1 Band structure in InSb at zero magnetic field.

The transport theory on n-type semiconductor in a magnetic field yields the following expression for the Hall constant (Beer, 1963).

$$R_H = -\left(\left\langle \frac{\tau^2}{1+w_c^2\tau^2} \right\rangle\right) \Big/ \left(Ne\left(\left\langle \frac{\tau}{1+w_c^2\tau^2} \right\rangle^2 + w_c^2 \left\langle \frac{\tau^2}{1+w_c^2\tau^2} \right\rangle^2\right)\right) \qquad (3.1)$$

where R_H is the Hall constant; N and e are, respectively, the electron density and the electron charge; τ is the scattering time; $w_c = eB/m^*$ is the cyclotron frequency; B is the magnetic induction and m* is the effective mass of an electron.

The angular brackets $\langle \ldots \rangle$ represents a suitable average over Boltzmann statistics, of the type usually applied transport theory.

When the conditions $w_c\tau \ll 1$ and $w_c\tau \gg 1$, for weak and strong magnetic fields respectively, are satisfied eq. (3.1) simplifies to

$$R_H(0) = \lim_{B \to 0} R_H = -\frac{1}{Ne} \frac{\langle \tau^2 \rangle}{\langle \tau \rangle^2} \qquad (w_c\tau \ll 1) \qquad (3.2)$$

and $$R_H(\infty) = \lim_{B \to \infty} R_H = -\frac{1}{Ne} \qquad (w_c\tau \gg 1) \qquad (3.2)$$

The quantity $r = \frac{\langle \tau^2 \rangle}{\langle \tau \rangle^2}$ from eq. (3.2) is called the Hall coefficient factor and depends on the magnetic field and the various types of scattering mechanism.

The product $R_H(0) \times \sigma(0)$ is defined as the Hall mobility

$$\mu_H(0) = R_H(0) \times \sigma(0) = -\frac{e}{m^*} \cdot \frac{\langle \tau^2 \rangle}{\langle \tau \rangle} \qquad (3.3)$$

where $\sigma(0)$ is the conductivity in zero magnetic field. It is to be distinguished from the drift mobility which is given by

$$\mu_D(0) = -\frac{e}{m^*} \langle \tau \rangle \qquad (3.4)$$

so that

$$r = \mu_H(0)/\mu_D(0) = R_H(0)/R_H(\infty) \tag{3.5}$$

therefore

$$\mu_D(0) = R_H(\infty)x\sigma(0) \tag{3.6}$$

If it is possible to satisfy the condition $w_c\tau \gg 1$ experimently by using strong magnetic fields, then eq. (3.2) is an extremely useful relation which can be used to find the number of electrons in the conduction band (at liquid nitrogen temperature) without being specially concerned about the scattering mechanism.

3.3. IMPURITY LEVELS

Impurity states in semiconductors have been studied in detail by many workers as using a hydrogen-like model approximation. In this hydrogenic model the ground and excited impurity states n = 1,2,3,... etc. are directly associated with the hydrogenic wavefunctions 1s, 2p, 2s, ...etc. The discrete energy levels and the effective Bohr radii of the system are thus given as;

$$E_I = E_{HI} \frac{m^*}{m_o} \frac{1}{\varepsilon_r^2 n^2}, \quad n = 1, 2, 3, \ldots \text{ etc.} \tag{3.7}$$

$$a_n = a_H \left(\frac{m_o}{m^*} \right) \varepsilon_r \tag{3.8}$$

where E_{HI} and a_H are the hydrogenic donor ionization energy (13.6 eV) and Bohr radius (0.053 nm) respectively, and ε_r is the static dielectric constant. For n-type InSb, $m^*/m_o = 0.014$, and $\varepsilon_r = 17.9$, so that $E_I \cong 0.6$ meV below the conduction band edge and $a \cong 67.8$ nm for the ground state (n=1) at zero magnetic field. Therefore, in even the purest n-type InSb available, donor energy levels are merged with the conduction band and the electron orbit extends

over the order of a hundred lattice cells under ordinary circumtances. In momentum space, the impurity levels are localised in the region $k_z = 0$.

The hydrogenic model is, of cause, an approximation. The Coulomb potential used in the evaluation of the energy states will be incorrect because the ionized donor is not simply a proton, but it is a heavy nucleus surrounded by valence electrons. In addition, the impurity atom will distort its surroundinds leading to a local warping of the bands. As a result of these effects ("central cell corrects") the ionization energy will differ from the simple hydrogenic value by an amount dependent on the particular element constituting the impurity. A recent calculation (Larsen, 1968) for donor impurities in InSb included conduction-band non-parabolicity and showed that this should lead to observable discrepancies between the earlier theories and experiments.

The donor ionization energy in a magnetic field is defined as the energy difference between the donor ground state and the $n = 0$ Landau level at $k_z = 0$. This ionization energy in a magnetic field are discussed in terms of the parameter $\gamma = \frac{1}{2}\hbar w_c / E_I(0)$ by Yafet et al(1956) and Wallis et al (1958). Where $E_I(0)$ is the ionization energy of the ground state at zero magnetic field. Recently these donor energy levels in InSb have been studied by Kaplan (1969) at higher magnetic fields ($\gamma \gg 1$) and reported that the most important impurity transition for left-hand circularly polarized radiation is between the ground state (000) and one of higher orbital angular momentum state (010) lying below the $n = 1_+$ continuum.

The approximate impurity energy levels, $E_i(n,M,\lambda)$, are identified by the quantum number set $(nM\lambda)$ respectively. Where n is the Landau number, M is the value of orbital angular momentum, and λ is a variable parameter which goes over into k_z for electrons in the Landau continuum.

The ionization energy increases when the magnetic field is increased. Therefore, at temperatures below about 10K, some of the conduction electrons drop into the impurity band (freeze-out effect). This has been studied by Sladek (1958 and 1959) for n-type InSb samples which have different carrier concentration (N_D-N_A) by measuring the Hall constant at low temperatures (from 77K to 1.5K), using magnetic field strength up to 2.8 T (28 kG).

The important thing is that in an experiment, both the free-electron and the impurity transitions are observed, their amplitudes depending on the proportion of free to frozen carriers. Thus the importance of the impurity line depends on the temperature and magnetic field strength.

Approximate conduction electron energy levels $E(n,k_z,s)$ which are calculated from eq.(1.20) and discrete impurity levels $E_i(n,M,\lambda)$ which are estimated from Kaplan's experimental results (Kaplan, 1969) are shown in fig. 3.2. as curved and straight lines respectively for a particular value of the magnetic field (10 kG). The nearly vertical transitions ΔE and ΔE_i represent free-electron transitions between the lowest Landau levels with spin parallel to the magnetic field ($n = 0_+(\uparrow)$ $n = 1_+(\uparrow)$) and a predominant impurity transitions between the impurity ground states below these Landau levels ($E_i(000) \longrightarrow E_i(010)$) respectively. The energy difference $\Delta E_i = E_i(010) - E_i(000)$ is somewhat larger than the free-elec-

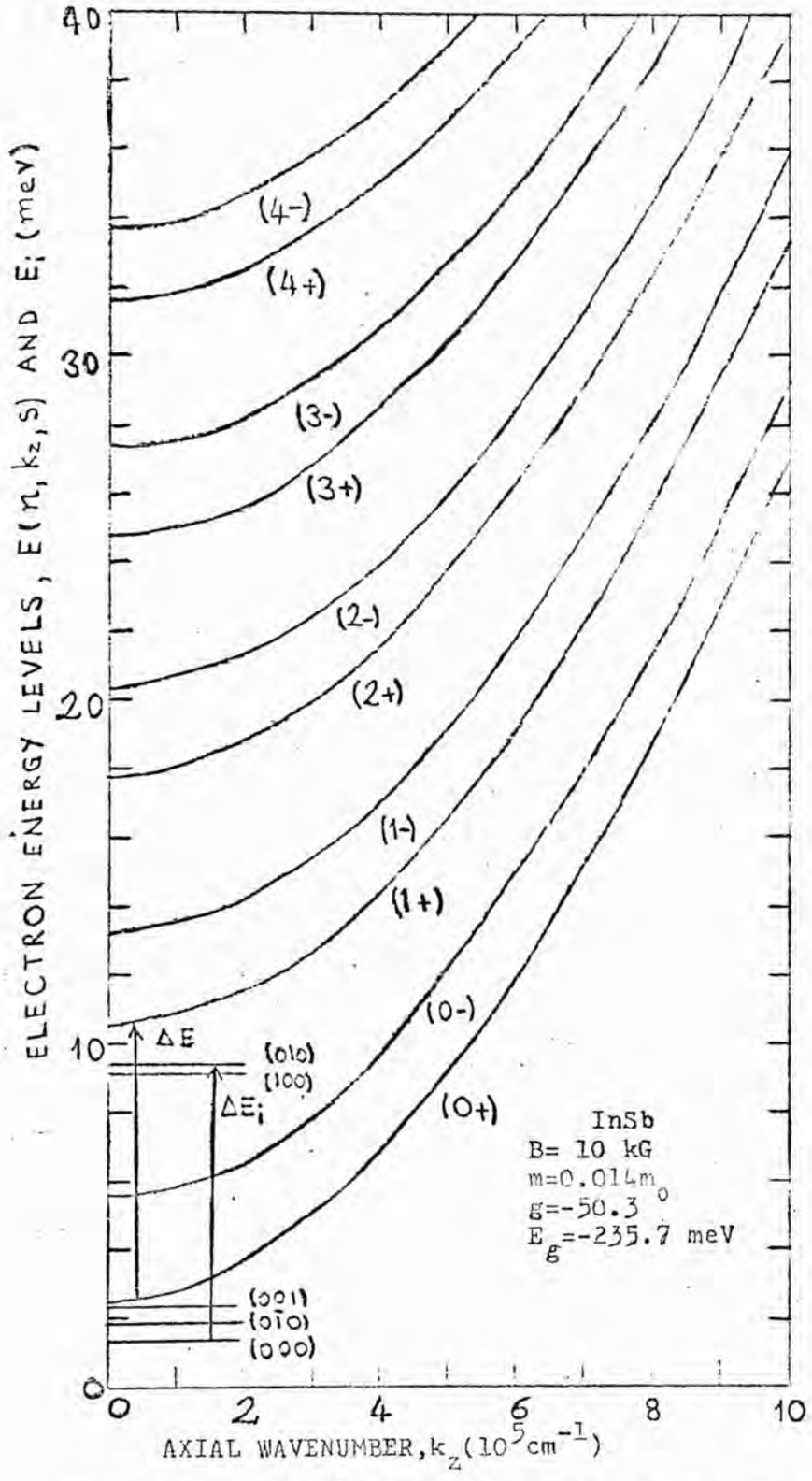

Fig.3-2 Conduction electron levels $E(n,k_z,s)$, and impurity levels E_i in a 10 kG field, as calculated from eq. (1.20).

tron cyclotron resonance transition energy ΔE and much larger than the ionization potential. At liquid helium temperature the lower-energy spin up ($\uparrow$) states are much more populated than the spin down ($\downarrow$) states and,therefore, all of these transitions are between these spin up states according to the spin conservation.

3.4. SAMPLE PREPARATION FOR D.C. AND A.C. MEASUREMENTS

The sample used have been prepared from single crystal n-type indium antimonide made by Malvern Electronic Material Unit (MEM) and MCP Electronics Limited (MCP). Two different shapes of samples were used for the Faraday rotation and ellipticity measurements. The samples supplied by MEM were cut as circular discs 14 mm in diameter and with various thickness; the other samples supplied by MCP were cut as square plates with 13 mm sides (again with various thickness). Also, bars, approximately 1x1x10 mm^3 in size, were cut as near to the corresponding circular disc or square plate as possible to avoid any error arising inhomegeneity of the samples. These were used for Hall constant and conductivity measurements in order to find the carrier concentration and d.c. scattering time at liquid nitrogen temperatures.

The Hall bars were fixed on an electrically insulated PTFE sample holder with two current and four potential leads of thin platinum wire. The current leads were soldered to the sample with indium, and the potential leads were attached to the sample by spot welding. After the Hall bar had been replaced on the sample holder, it was immersed in a liquid nitrogen dewar which was in a magnetic field. The field was measured with a gauss-meter which was calibrated with a known magnetic field. Specimen current and

potentials were measured by means of Keithley digital multi-meters (types 168 and 160B).

The measured electrical properties of the specimens at liquid nitrogen temperature (77K) are given in table 3.1.

The schematic diagram of the experimental set-up for the measurement of the far-infrared Faraday effect was shown and discussed in detail in chapter 2. It should be noted that the Faraday rotation and ellipticity measurements are a transmission type of experiment which has the advantage of using a sample which is free of pertubations caused by soldered leads. However, it suffers from the disadvantage that the signal decreases at resonance, and if linear rather than circular polarization is used, the maximum absorption never exceeds 50 %.

The circular or square samples were mounted in an aperture in a cylindrical pure copper sample holder shown in detail in fig. 3.3. After the specimens had replaced and fixed into this sample holder with apiezon 'N' type high vacuum grease then it was gently inserted into the transverse aperture of the optical cryostat until it reached to the optimum magnetic field position, (see fig 2.3 and fig 2.6 in chapter 2). The plane of the sample was arranged normal to the direction of propagation, so that the polarized radiation propagated ,in the Faraday configuration, parallel to the magnetic field direction which was along the axis of the transverse bore of the optical cryostat.

TABLE 5.1

Sample properties at 77K

N-InSb sample	thickness (mm)	Hall mobility (cm^2/V-sec) at zero field	d.c. conductivity $(Ohm.cm)^{-1}$ at zero field	N_D-N_A (cm^{-3})	d.c scattering time(second) at zero field
		x10^5		x10^{13}	x10^{-12}
MCP-1	2.00	2.8±0.5	0.087±0.009	0.36±0.04	1.2 ±0.2
MEM-1	0.50	5.5±1.0	4.1 ±0.3	4.6 ±0.3	4.4 ±0.5
MEM-2	0.50	7.4±0.8	5.7 ±0.5	5.6 ±0.4	5.1 ±0.6
MEM-3	0.53	6.9±1.7	11.3 ±0.9	12.1 ±0.9	4.7 ±0.5
MEM-4	2.00	4.8±0.9	10.8 ±0.9	14.0 ±0.9	3.8 ±0.4
MCP-2	0.63	5.9±1.3	27.6 ±3.2	36.7 ±3.1	3.8 ±0.5

Note that the sample letters given in this table or other tables stand for the source of the materials as follows:

MEM: Malvern Electronic Material Unit

MCP: MCP Electronics Limited.

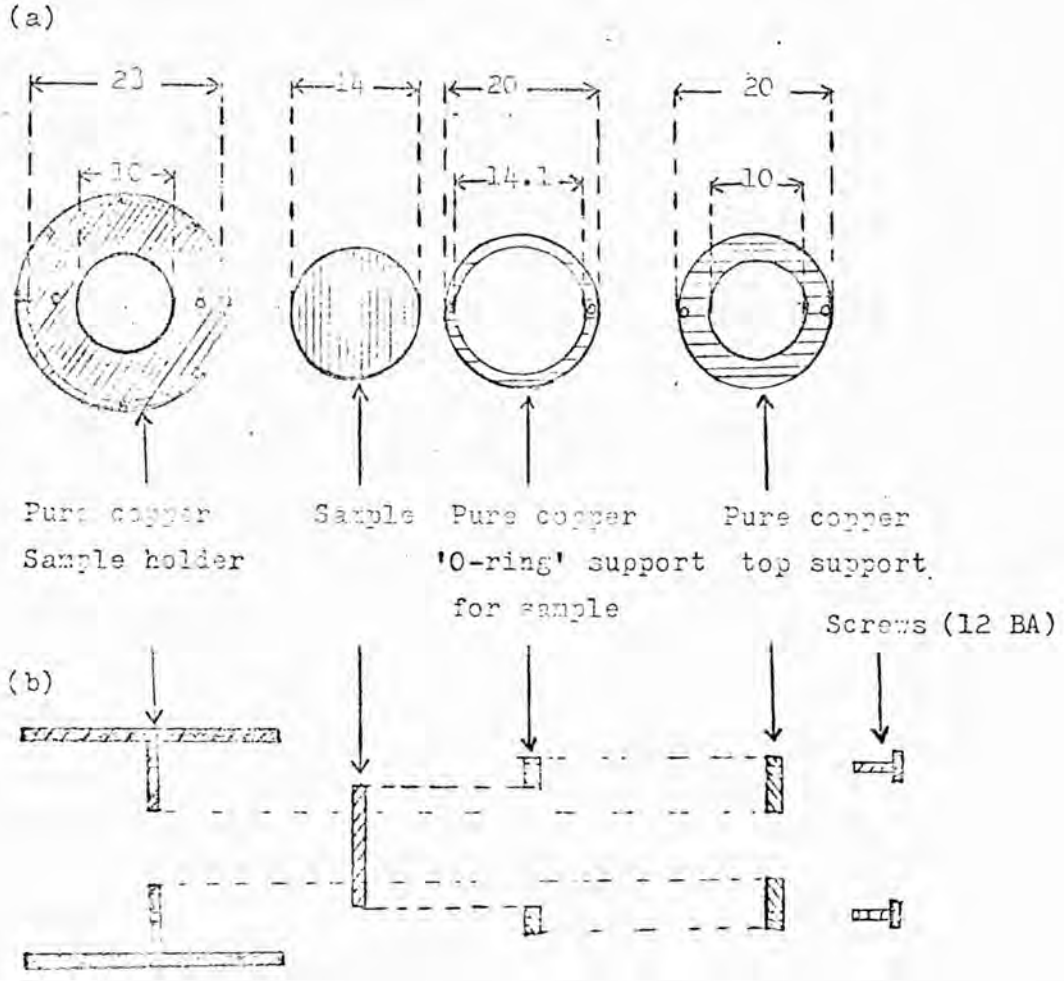

(a): Top view of the sample holder
(b)and (c): Longitudinal aspect of the sample holder and other bits before and after the replacement respectively.

Note: all dimensions are written in millimeters (mm)

Fig. 3-3 Schematic diagram of the method of mounting the specimen on the pure copper sample holder

C H A P T E R 4

EXPERIMENTAL RESULTS AND DISCUSSION

4.1 INTRODUCTION

The theory and the experimental method for measuring the Faraday rotation and ellipticity, and the properties and preparation of the samples used were given and explained in the previous three chapters. The experimental techniques required for studying the Faraday effect in semiconductors at far-infrared frequencies are in many ways similar to those for magneto-absorption. The principal difference is that one measures the intensity of plane polarized radiation transmitted by the sample, not to determine absorption, but to determine the angle through which the plane of polarization has been rotated by the sample in the magnetic field. In addition, the direction of propagation of the radiation must be parallel to the magnetic field (Faraday configuration) so that the differential dispersion of the right- and left-hand circularly polarized components will produce a rotation of the incident plane polarized wave.

The free-carrier Faraday effect provides an opportunity to obtain information concerning the detailed nature of the low-temperature scattering mechanism. Measurements of low-temperature electron-impurity scattering times in n-type InSb using infrared cyclotron linewidths have yielded scattering times greatly in excess of those determined by d.c. mobility measurements (Apel, 1970b; Apel and Poehler 1970a)

More recently, Kaplan et al.,(Kaplan, 1973) have obtained low-energy scattering times in thin samples of higher quality n-InSb using far infrared cyclotron resonance linewidths in magnetic fields in the range 8-25 kG. They reported that the experimental data gave maximum scattering time near r/a = 0.5; where r is the magnetic length ($r=(\hbar c/eB)^{\frac{1}{2}}$), a is the screening length ($a = (\hbar/4m^*w_p)^{\frac{1}{2}}$), m^* is the carrier effective mass and w_p is the plasma frequency ($w_p=(4\pi Ne^2/m^*\varepsilon_r)^{\frac{1}{2}}$), and the other symbols have their usual meanings. Their experimental results showed that the magnetic fields below this maximum (r/a = 0.5), the linewidth decreased with increasing field, while at fields above this maximum the width increased with increasing field. However, the experiments of Apel (1970b) and Apel et al. (1971) gave linewidths that narrowed as the magnetic field was increased from 4 to 20 kG. Therefore, there is a discrepancy between these two experimental results. Also the lowest frequency data of Apel's experiment (Apel, 1970b) using radiation of 0.337 mm wavelength were complicated by an impurity absorption line that overlapped the free carrier cyclotron resonance. So it thus appeared that some further experimental work on the low-frequency region of the far infrared (corresponding the magnetic fields less than the 8 kG. used by Kaplan) was required to determine scattering times which were not obtain in Kaplan et al's experiments (Kaplan, 1973) and to overcome the difficulties which arose in the cyclotron resonance linewidth measurements of Apel (1970b) due to overlapping of the impurity line and the free-carrier absorption line in InSb at this wavelength. Therefore, Faraday rotation experiments at liquid helium temperatures to determine the low-frequency scattering times in n-type InSb using an HCN laser of

wavelength 0.337 mm and are described in the rest of this chapter.

4.2 EXPERIMENTAL RESULTS

(i) Faraday rotation and ellipticity

The experimental technique used was explained and discussed in detail in chapter 2. The far-infrared pulsed HCN laser beam transmitted through the polarizer, experimental sample and analyzer varies periodically as a function of the rotation of the analyzer (as illustrated in Figs. 2.8 and 2.9 for different values of magnetic field strength). The shift of the maximum or the minimum of the signal due to the magnetic field gives the Faraday rotation angle, and the intensity ratio between the minimum and maximum gives the square of the ellipticity Δ. When the plane-polarized radiation becomes elliptical as a result of scattering, this ratio between maxima and minima becomes smaller. The ellipticity Δ is then given by the expression (Palik, 1963)

$$\Delta^2 = (M-X)/(MX-1) \qquad (4.1)$$

where M is the intensity ratio of minimum to maximum in zero field and X is the same ratio in the magnetic field.

Analysis of data for the indium antimonide samples with different electron densities lead to the measurements of the Faraday rotation angle and ellipticity at 0.337 mm wavelength as a function of magnetic field shown in Figs. 4.1 to 4.22. The observed Faraday rotation angle increases with magnetic field up to the resonant field strength where there is a sign reversal, followed by a decrease in rotation angle. Near the cyclotron resonance field, both rotation and ellipticity exhibit drastic changes, but the experimentally observed ellipticity is much lower than the values predicted by computation.

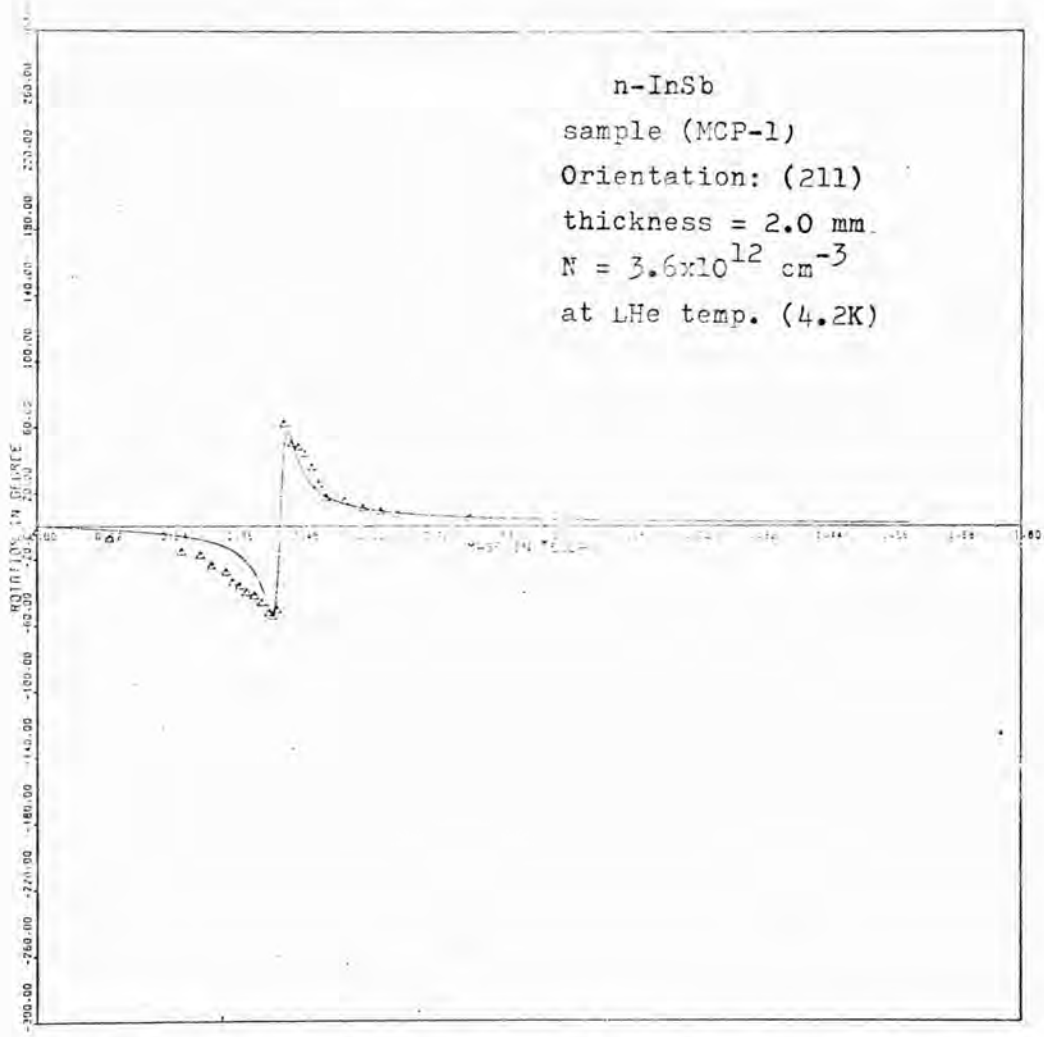

Fig. 4.1. Measured Faraday rotation angle shown as triangles versus magnetic field with 0.337 mm incident pulsed HCN laser radiation. Solid line is computed from eq. (1.16) with dielectric constant = 17.9, and the parameters calculated by least squares fit of the Faraday rotation function to experimental data, m^*/m_o=0.0139 and scattering time = 6.06×10^{-12} seconds.

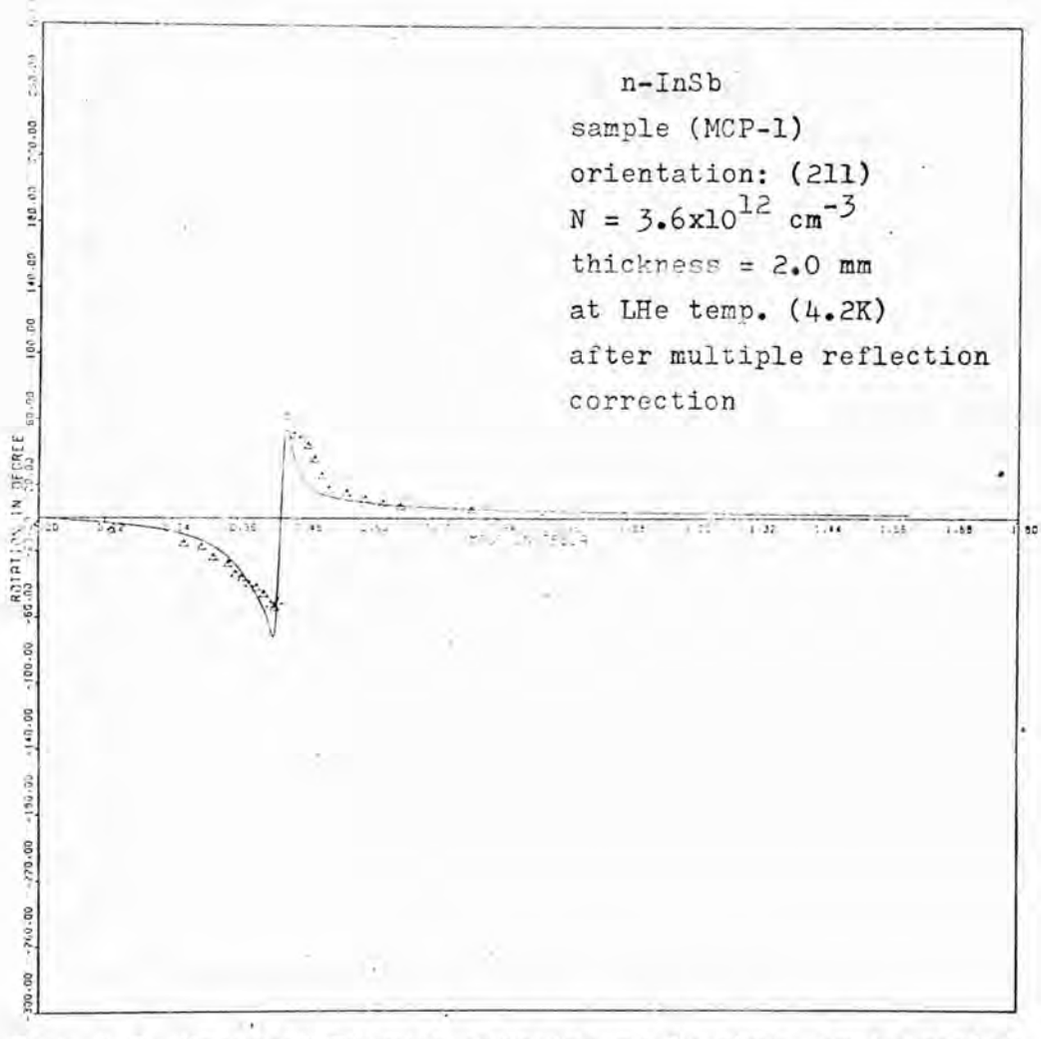

Fig. 4.2. Measured Faraday rotation angle shown as triangles versus magnetic field with 0.337 mm incident pulsed HCN laser radiation. Solid line is computed from eq. (1.28) with dielectric constant = 17.9, and the parameters calculated by least squares fit of the Faraday rotation function to experimental data, $m^* = 0.0138 m_o$ and scattering time = 6.84×10^{-12} seconds.

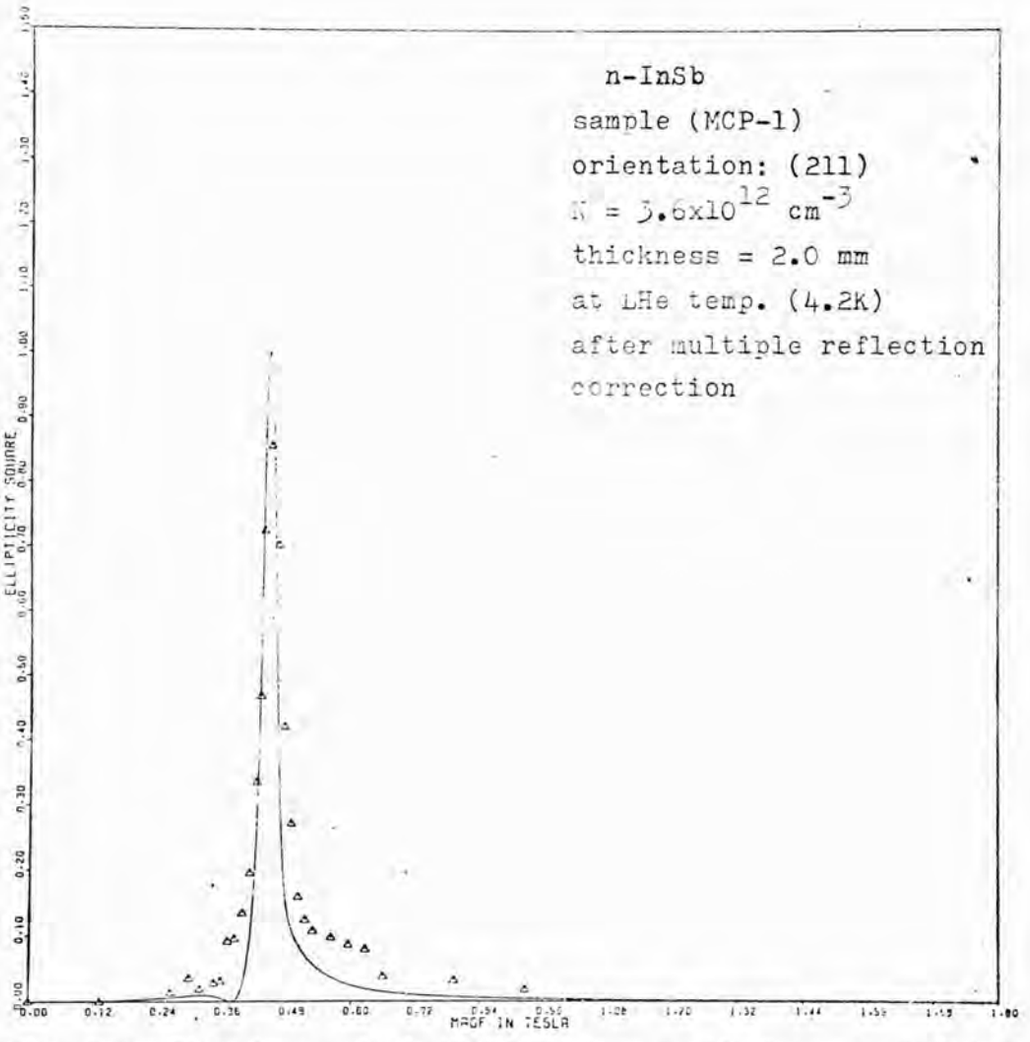

Fig. 4.3. The observed ellipticity (squared) shown as triangles versus magnetic field with 0.337 mm incident pulsed HCN laser radiation. Solid line is computed from eq. (1.29) with dielectric constant = 17.9, and the parameters calculated by least squares fit of the function of ellipticity to experimental data, $m^* = 0.0140 m_o$ and scattering time = 6.8×10^{-12} seconds.

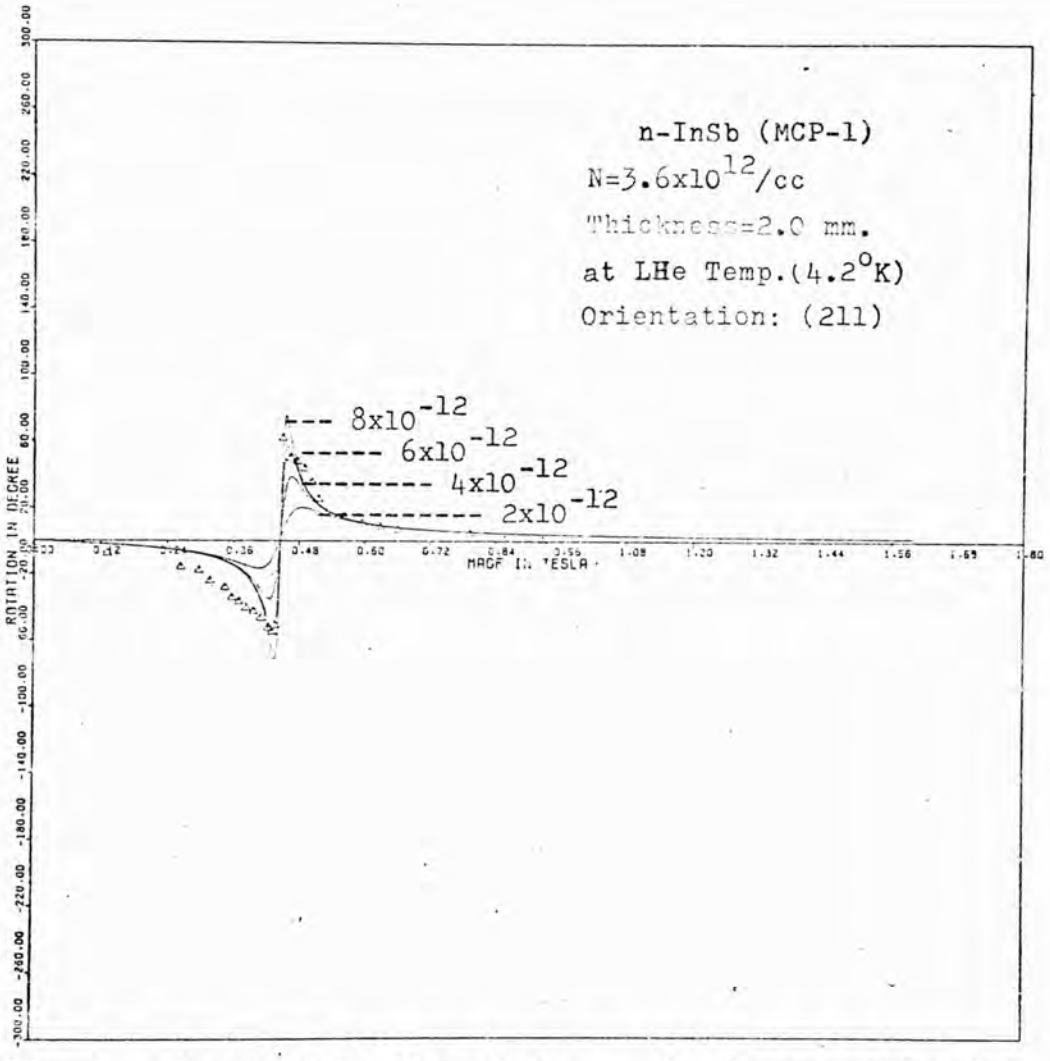

Fig. 4.4. Measured Faraday rotation angle shown as triangles versus magnetic field with 0.337 mm pulsed incident HCN laser radiation. Solid lines are computed from eqs.(1.13) and (1.14) with parameters dielectric const. =17.9, and $m^* = 0.014 m_o$ for different values of scattering time (in seconds).

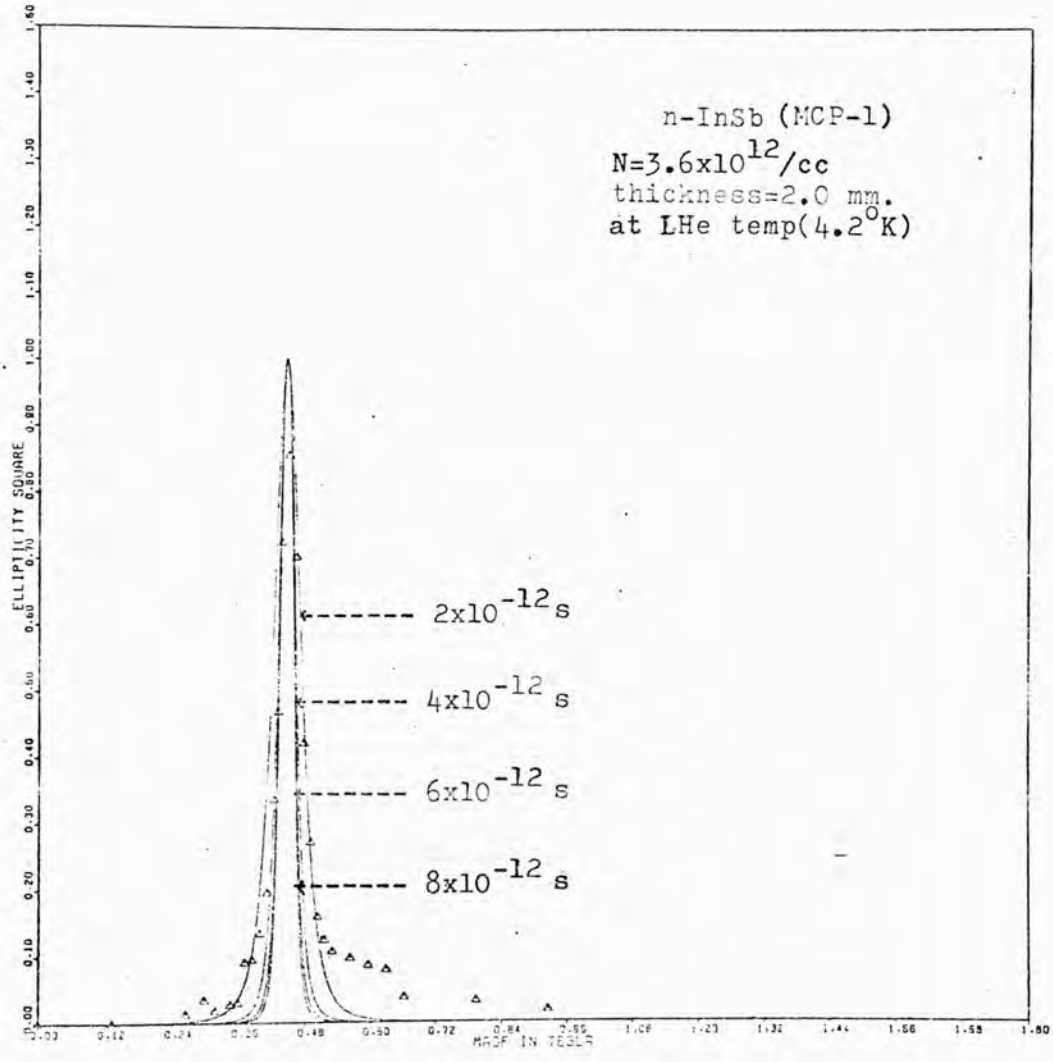

Fig. 4.5. Measured ellipticity (squared) versus magnetic field with 0.337 mm. pulsed HCN laser radiation. Solid lines are computed from eq. (1.17) for different values of scattering time. Experimental data shown as open triangles.

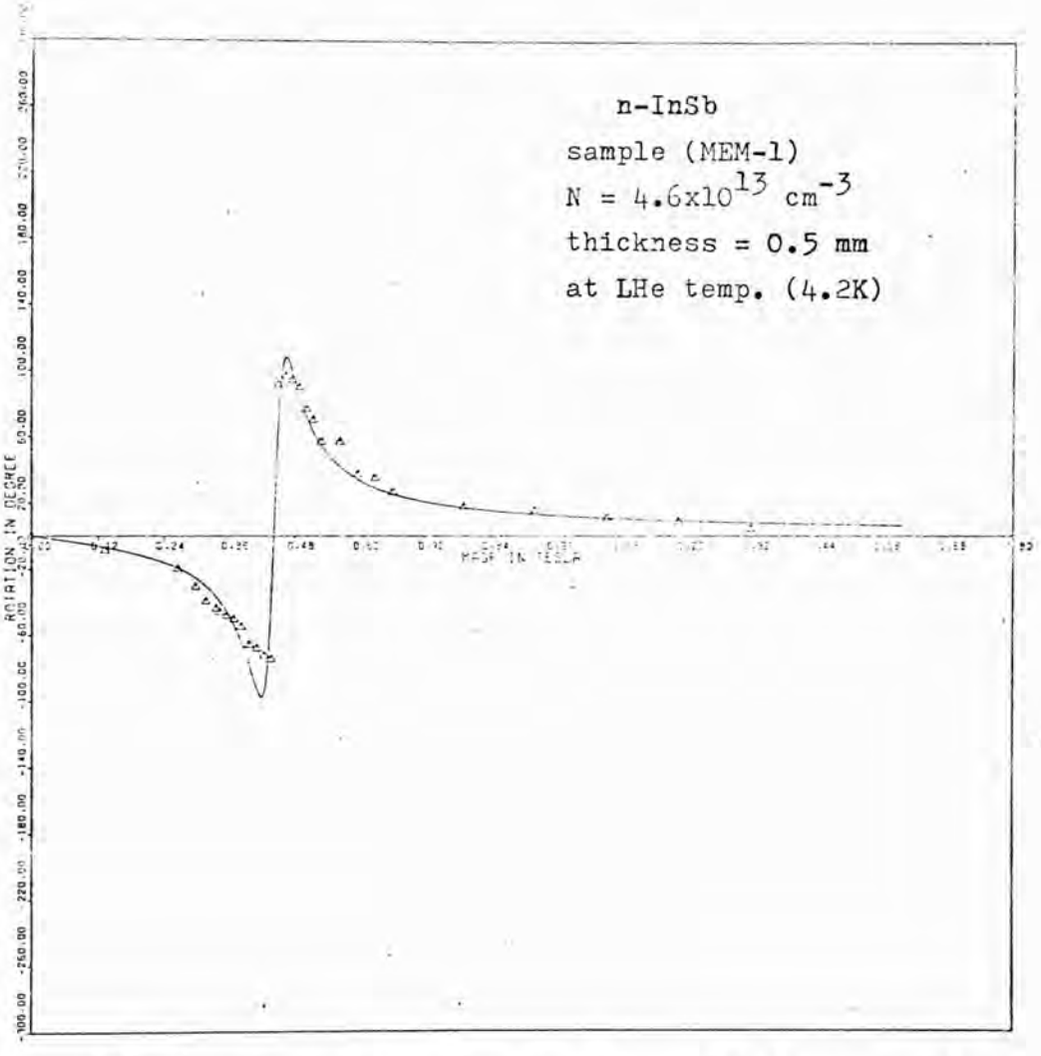

Fig. 4.6. The observed Faraday rotation angle shown as triangles versus magnetic field with 0.337 mm incident pulsed HCN laser radiation. Solid line is computed from eq. (1.16) with dielectric constant = 17.9, and the parameters calculated by least squares fit of the Faraday rotation function to experimental data, $m^* = 0.0139 m_o$ and scattering time = 3.46×10^{-12} seconds.

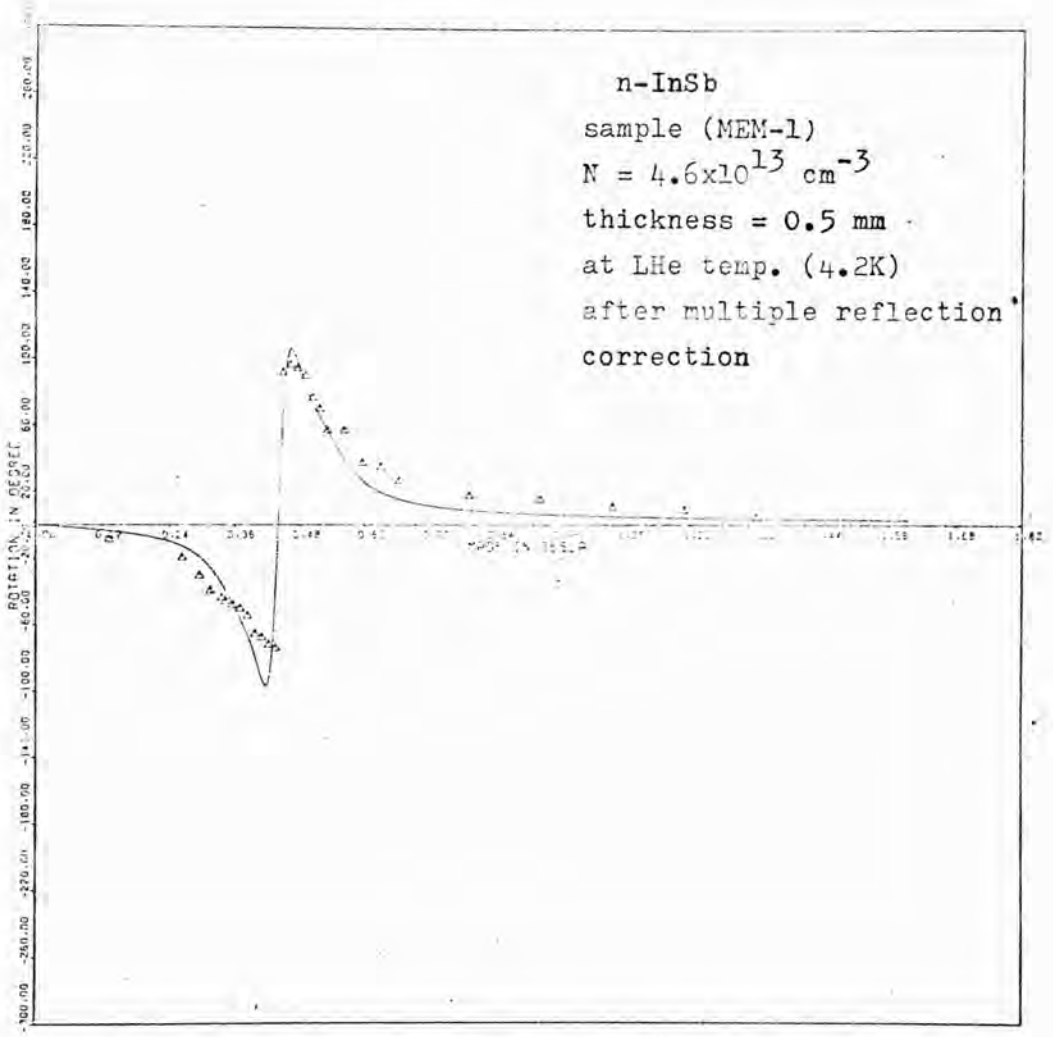

Fig. 4.7 The observed Faraday rotation angle shown as triangles versus magnetic field with 0.337 mm incident pulsed HCN laser radiation. Solid line is computed from eq. (1.28) with dielectric constant = 17.9, and the parameters calculated by least squares fit of the Faraday rotation function to experimental data, $m^* = 0.0139 m_o$ and scattering time = 3.46×10^{-12} seconds.

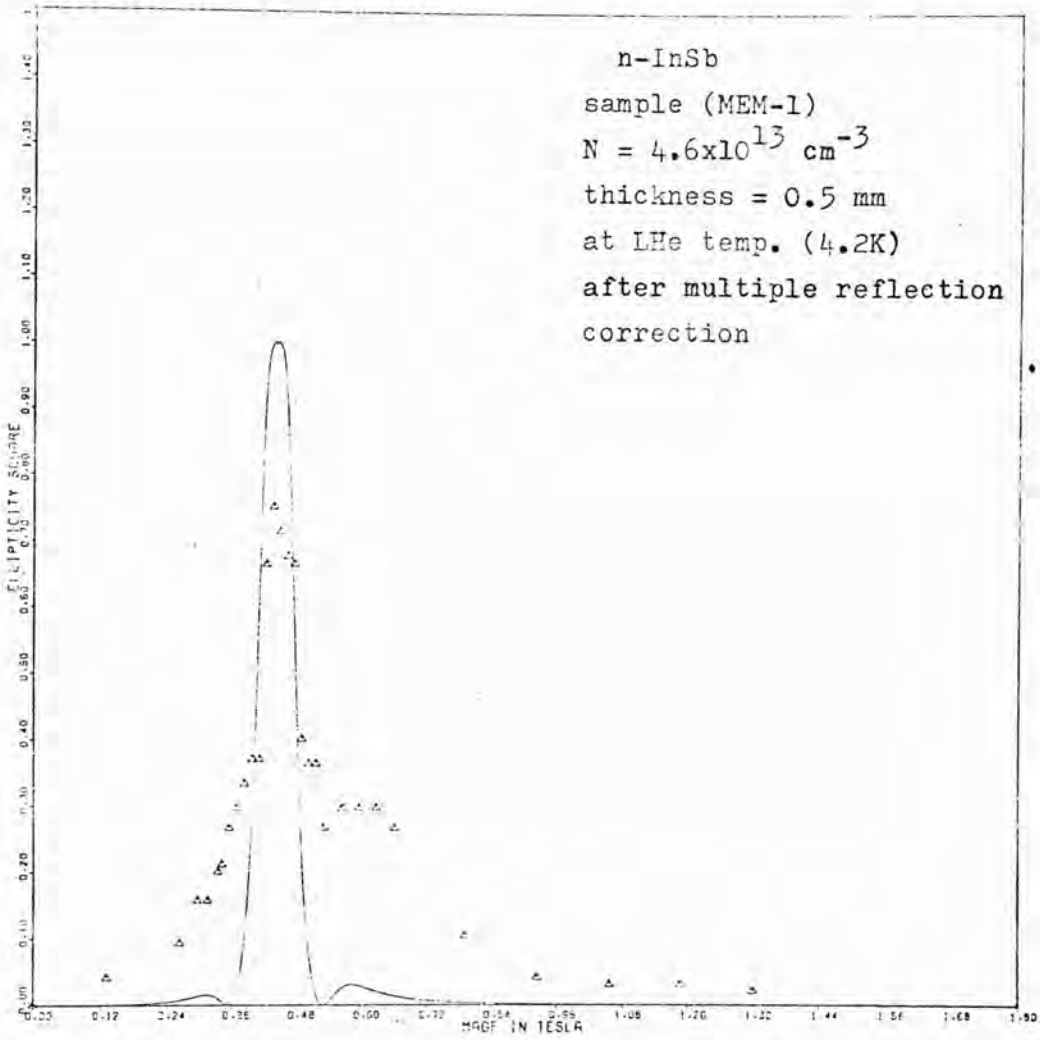

Fig. 4.8. The observed ellipticity (squared) shown as triangles versus magnetic field with 0.337 mm incident pulsed HCN laser radiation. Solid line is computed from eq. (1.29) with dielectric constant = 17.9, and the parameters calculated by least squares fit of the function of ellipticity to experimental data, $m^* = 0.0139 m_o$ and scattering time = 3.46×10^{-12} seconds.

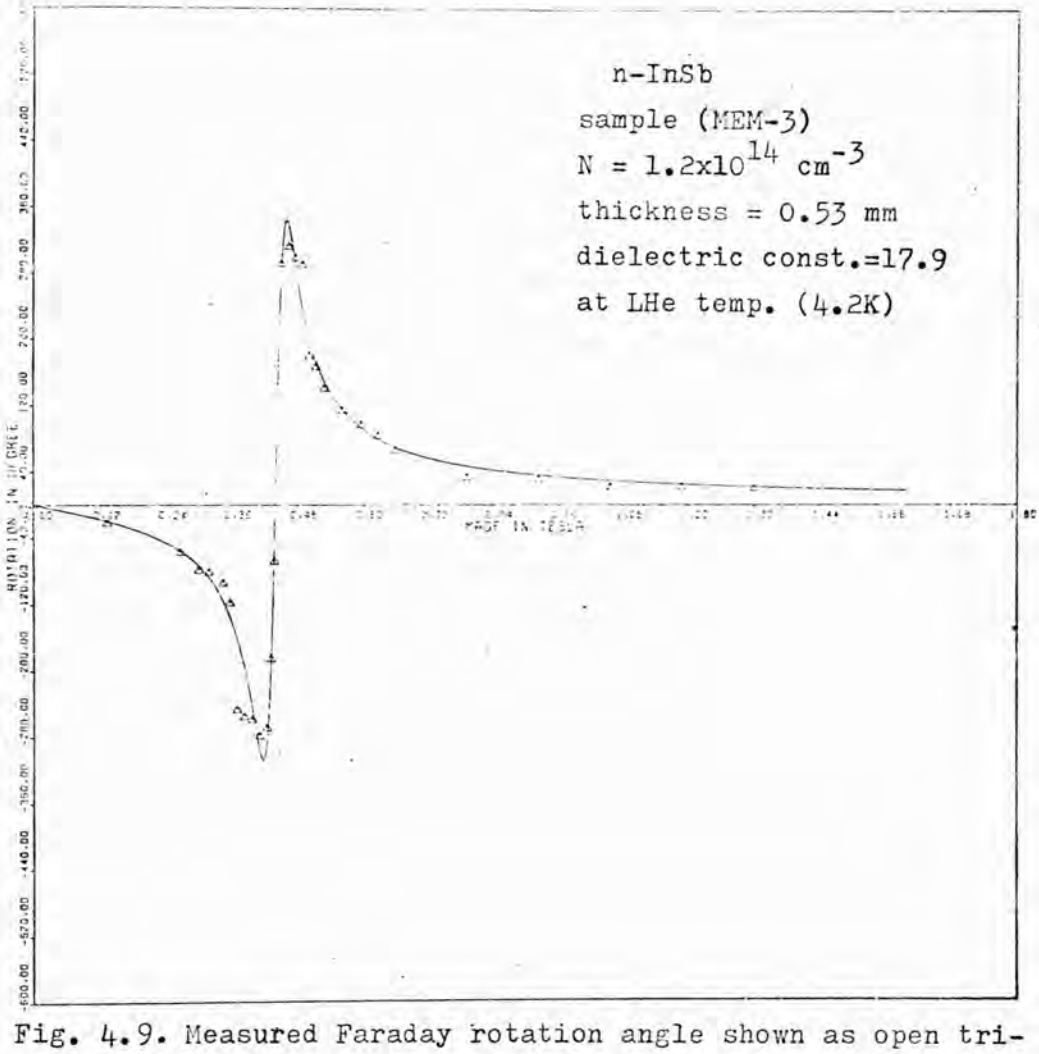

Fig. 4.9. Measured Faraday rotation angle shown as open triangles versus magnetic field with 0.337mm incident pulsed HCN laser radiation. Solid line is computed from eq. (1.16) with the parameters calculated by least squares fit of the Faraday rotation function to experimental data, $m^* = 0.0139 m_o$ and scattering time = 4.15×10^{-12} seconds.

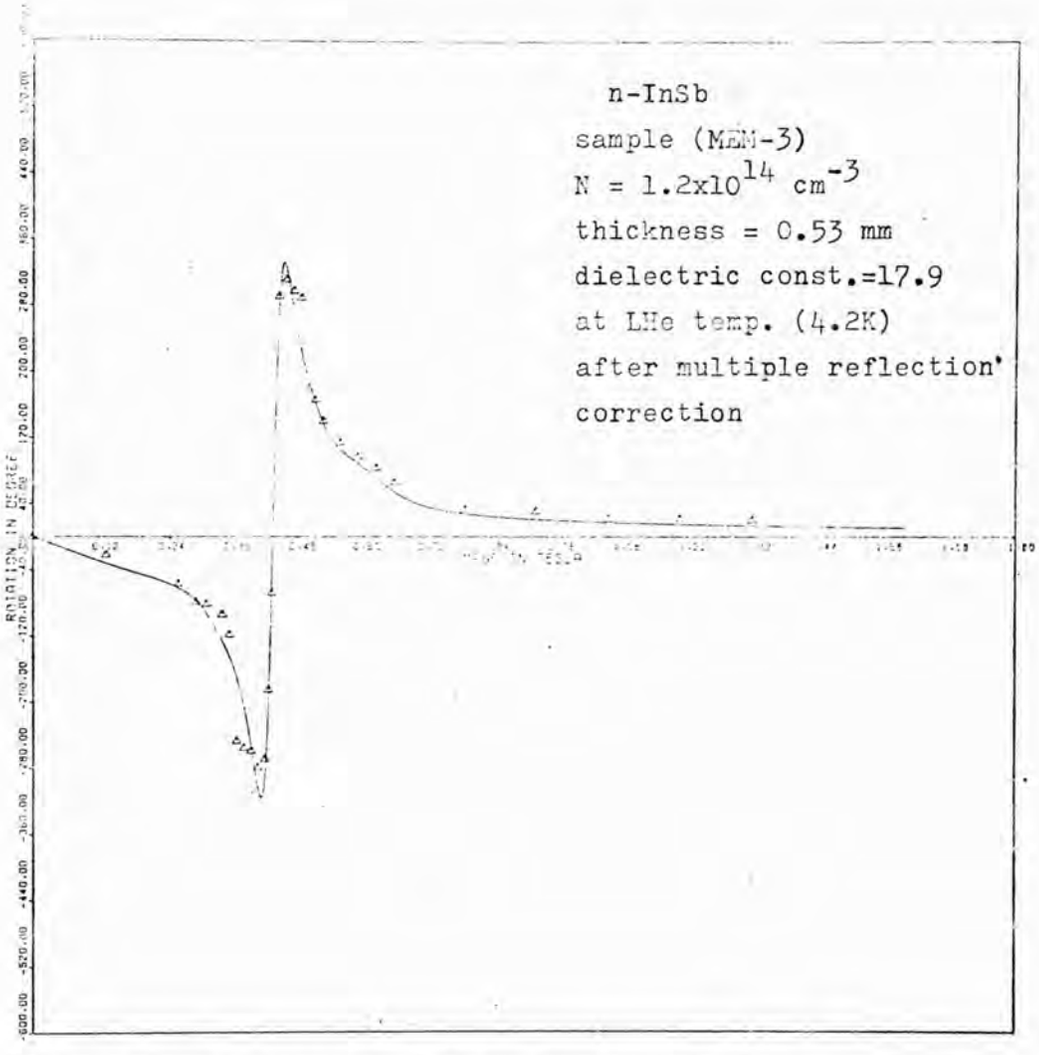

Fig. 4.10. Measured Faraday rotation angle shown as open triangles versus magnetic field with 0.337 mm incident pulsed HCN laser radiation. Solid line is computed from eq. (1.28) with the parameters calculated by least squares fit of the Faraday rotation function to experimental data $m^* = 0.0139m_o$ and scattering time $=4.15\times10^{-12}$ seconds.

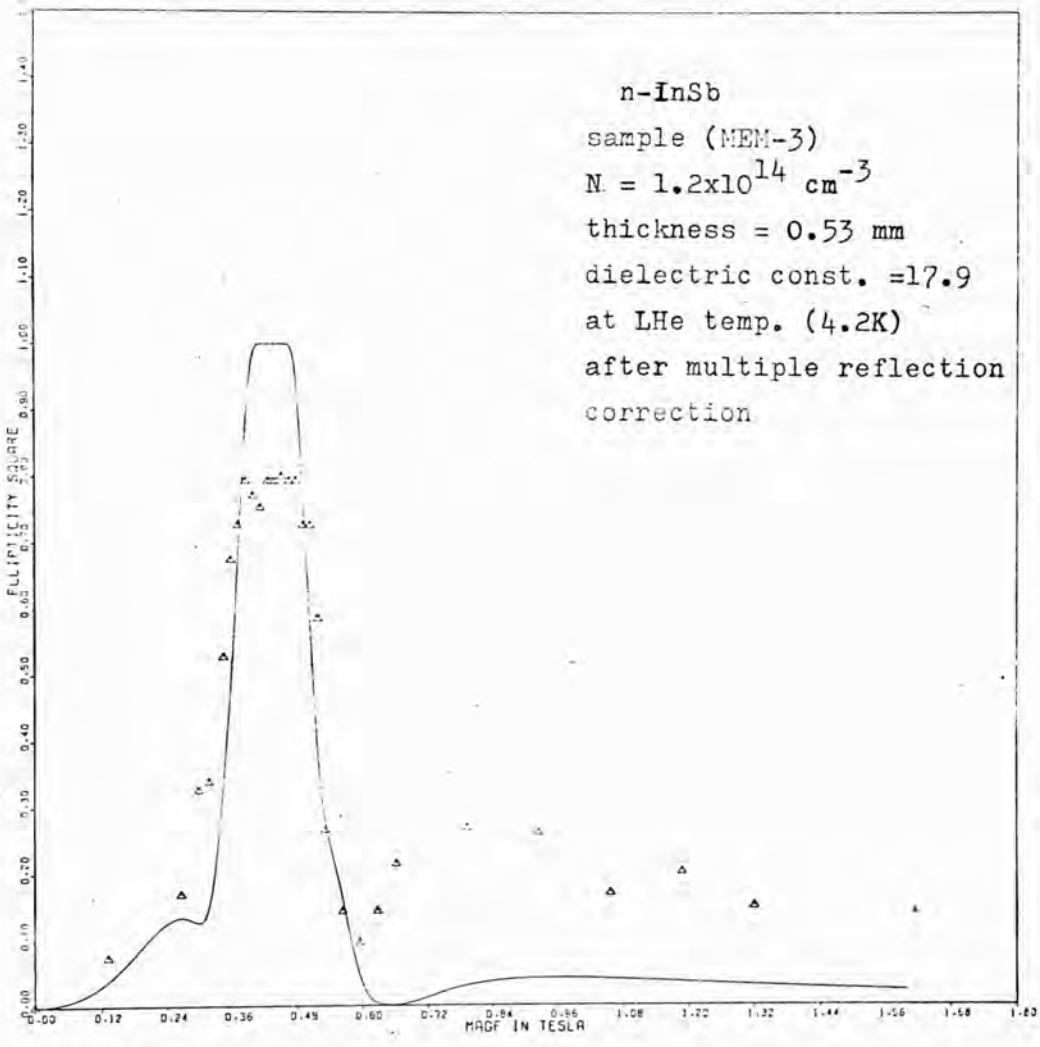

Fig. 4.11. Measured ellipticity (squared) shown as open triangles versus magnetic field with 0.337 mm incident pulsed HCN laser radiation. Solid line is computed from eq. (1.29) with the parameters calculated by least squares fit of the function of ellipticity to experimental data, $m^* = 0.0137m_o$ and scattering time = 4.0×10^{-12} seconds.

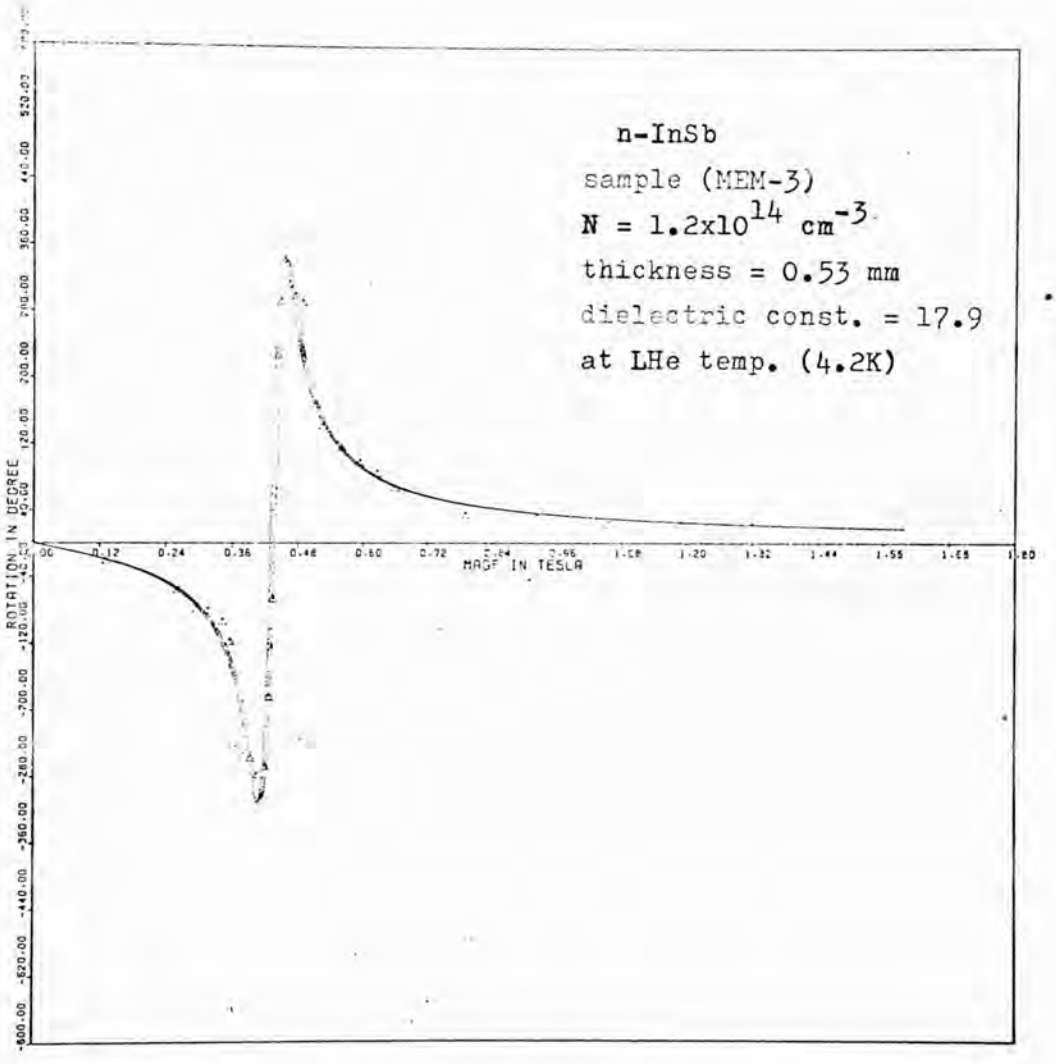

Fig. 4.12. The observed Faraday rotation angle shown as open triangles versus magnetic field with 0.337 mm incident pulsed HCN laser radiation. Solid lines are computed from eq. (1.16) with scattering time = 4.15×10^{-12} seconds for different values of effective mass ratio: m^*/m_o = 0.0137, 0.0138, 0.0139, 0.0140.

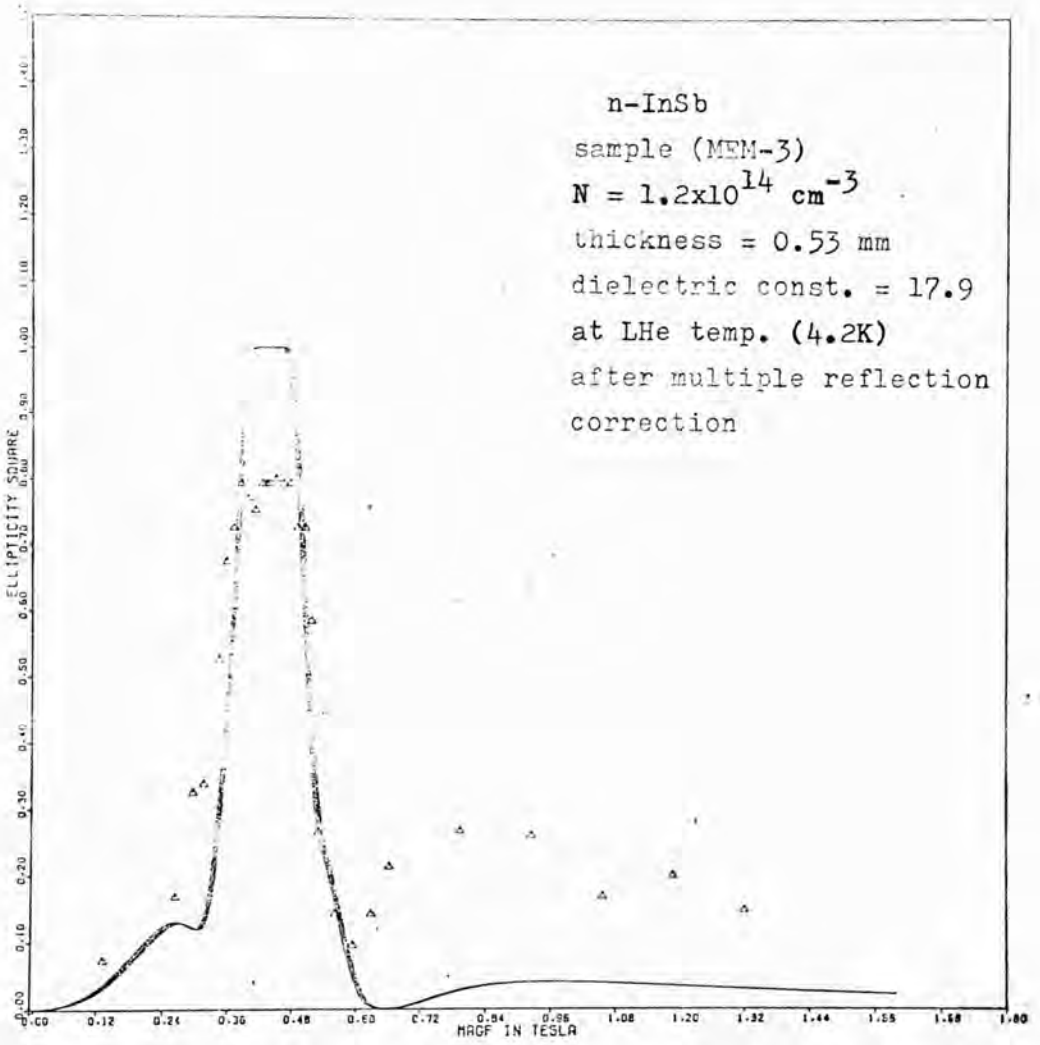

Fig. 4.13. The observed ellipticity (squared) shown as open triangles versus magnetic field with 0.337 mm incident pulsed HCN laser radiation. Solid lines are computed from eq. (1.29) with scattering time = 4.15×10^{-12} seconds for different values of effective mass ratio: m^*/m_o = 0.0137, 0.0138, 0.0139, 0.0140.

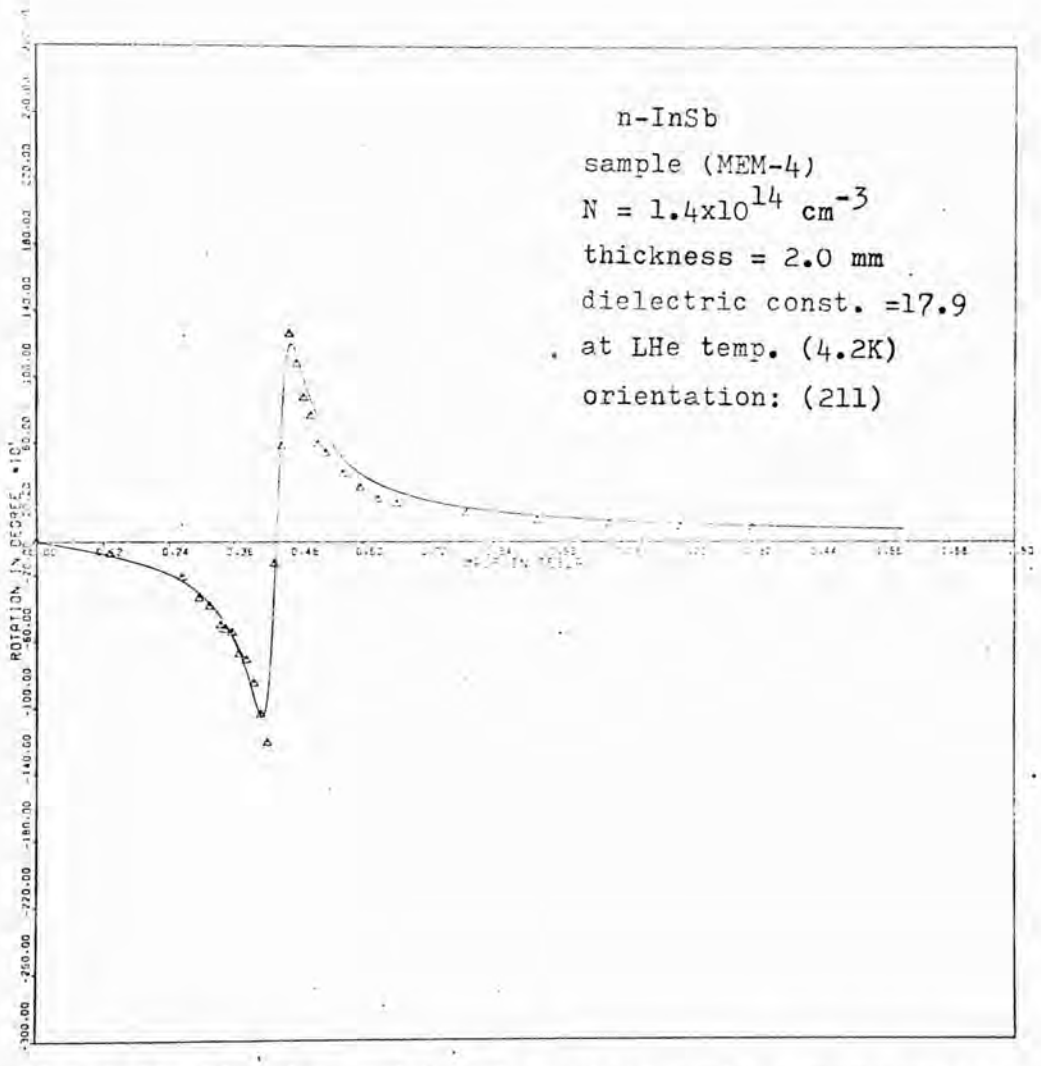

Fig. 4.14. The observed Faraday rotation shown as open triangles versus magnetic field with 0.337 mm incident pulsed HCN laser radiation. Solid line is computed from eq. (1.16) with the parameters calculated by least squares fit of the Faraday rotation function to experimental data, $m^* = 0.0140 m_o$ and scattering time $= 3.26 \times 10^{-12}$ seconds.

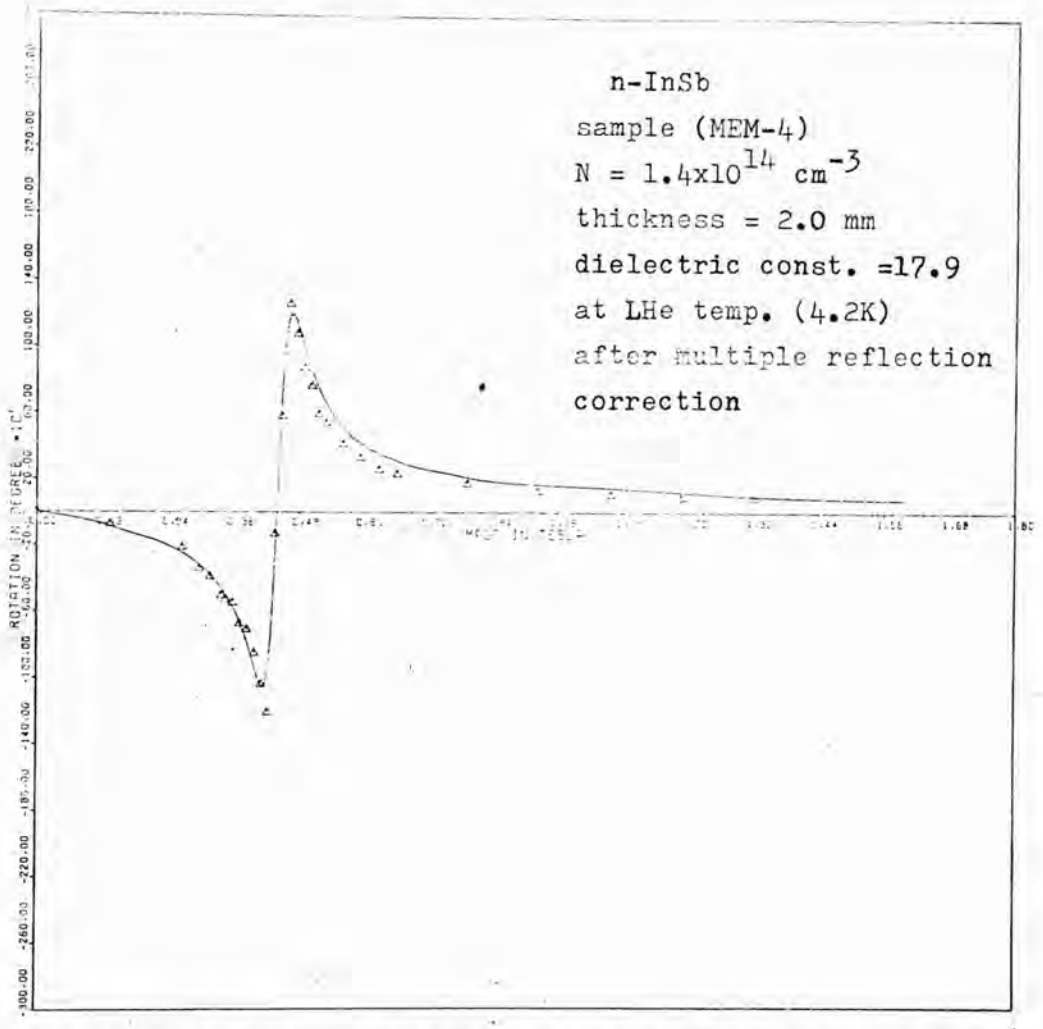

Fig. 4.15. The observed Faraday rotation shown as open triangles versus magnetic field with 0.337 mm incident pulsed HCN laser radiation. Solid line is computed from eq. (1.28) with the parameters calculated by least squares fit of the Faraday rotation function to experimental data , $m^* = 0.0140 m_o$ and scattering time = 3.26×10^{-12} seconds.

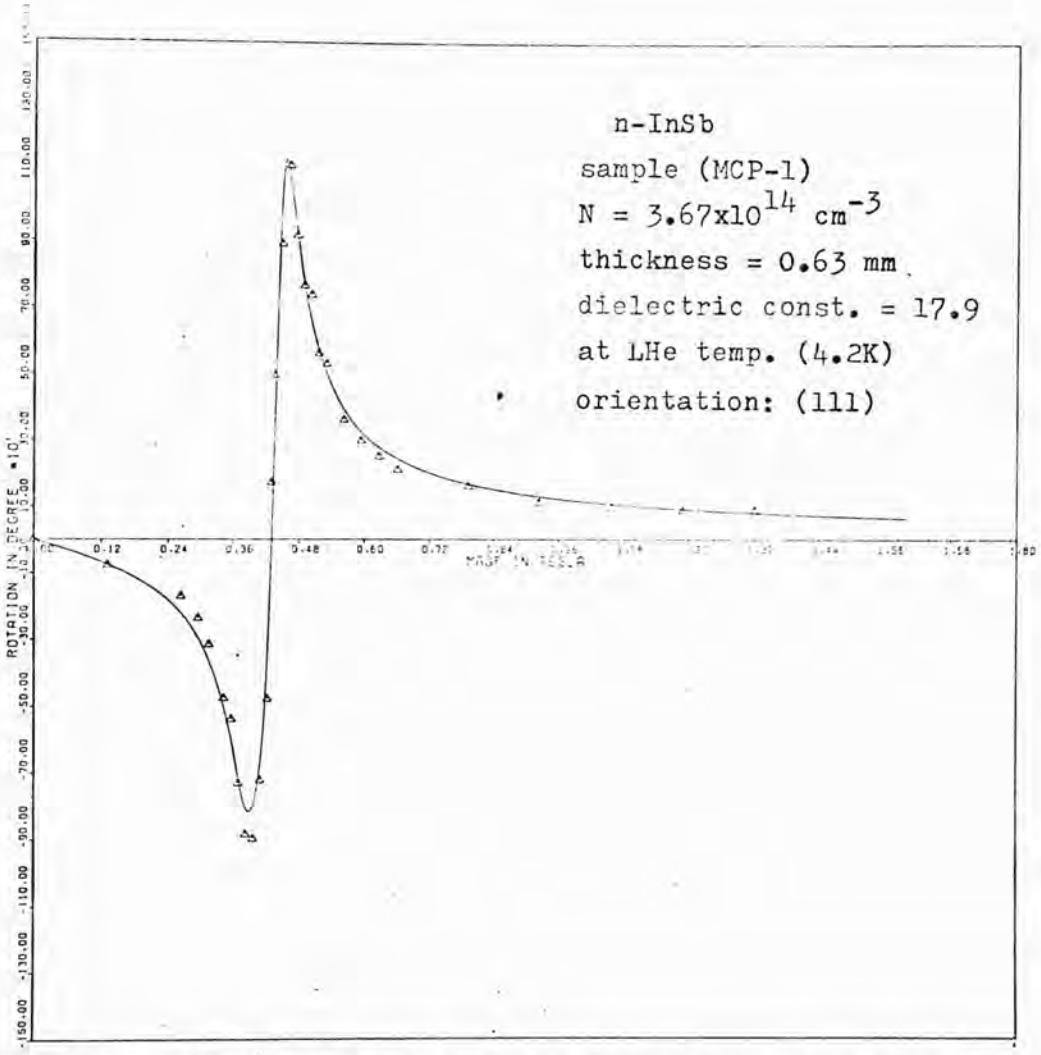

Fig. 4.16. Measured Faraday rotation angle shown as open triangles versus magnetic field with 0.337 mm incident pulsed HCN laser radiation. Solid line is computed from eq. (1.16) with the parameters calculated by least squares fit of the Faraday rotation function to experimental data, $m^* = 0.0139m_o$ and scattering time = 4.25×10^{-12} seconds.

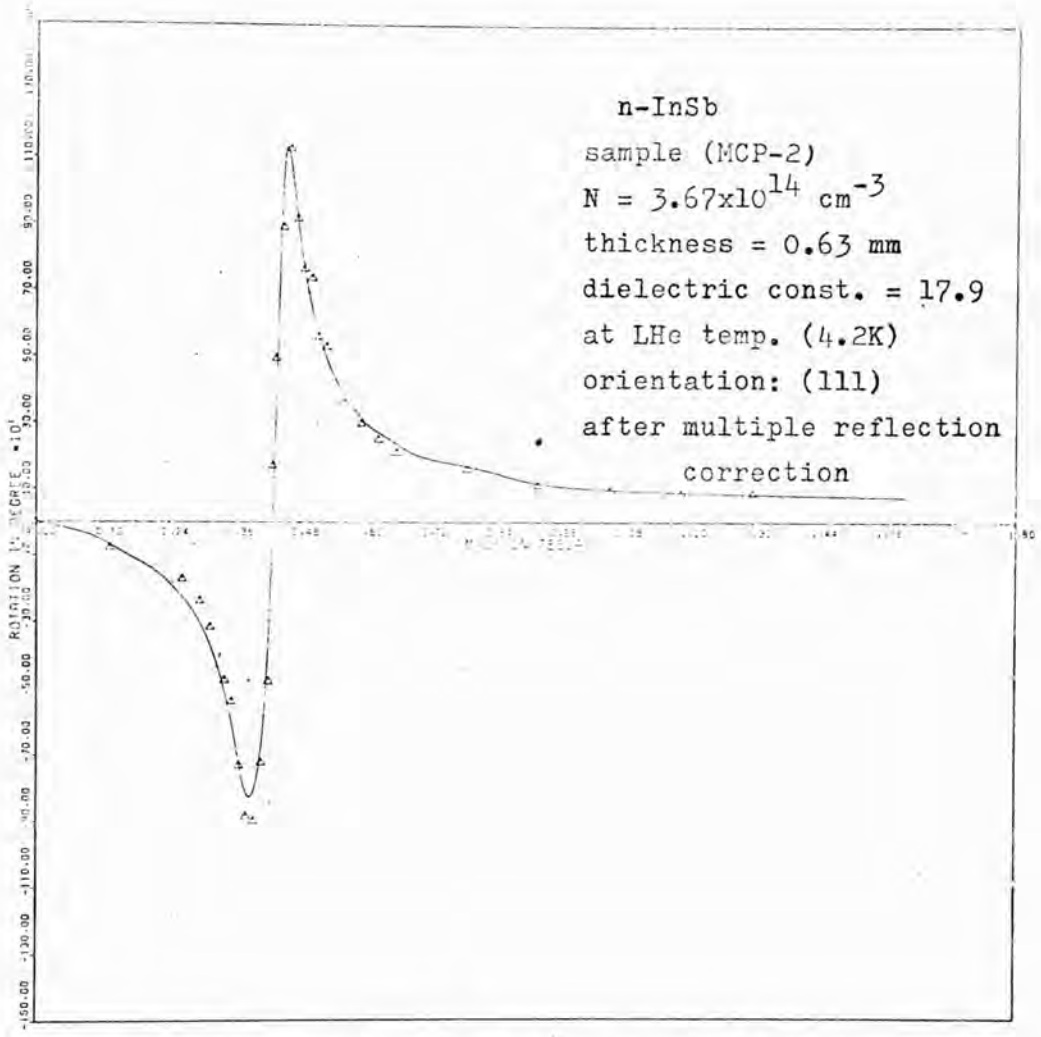

Fig. 4.17. Measured Faraday rotation angle shown as open triangles versus magnetic field with 0.337 mm incident pulsed HCN laser radiation. Solid line is computed from eq. (1.16) with the parameters calculated by least squares fit of the Faraday rotation function to experimental data, $m^* = 0.0139 m_o$ and scattering time = 4.25×10^{-12} seconds.

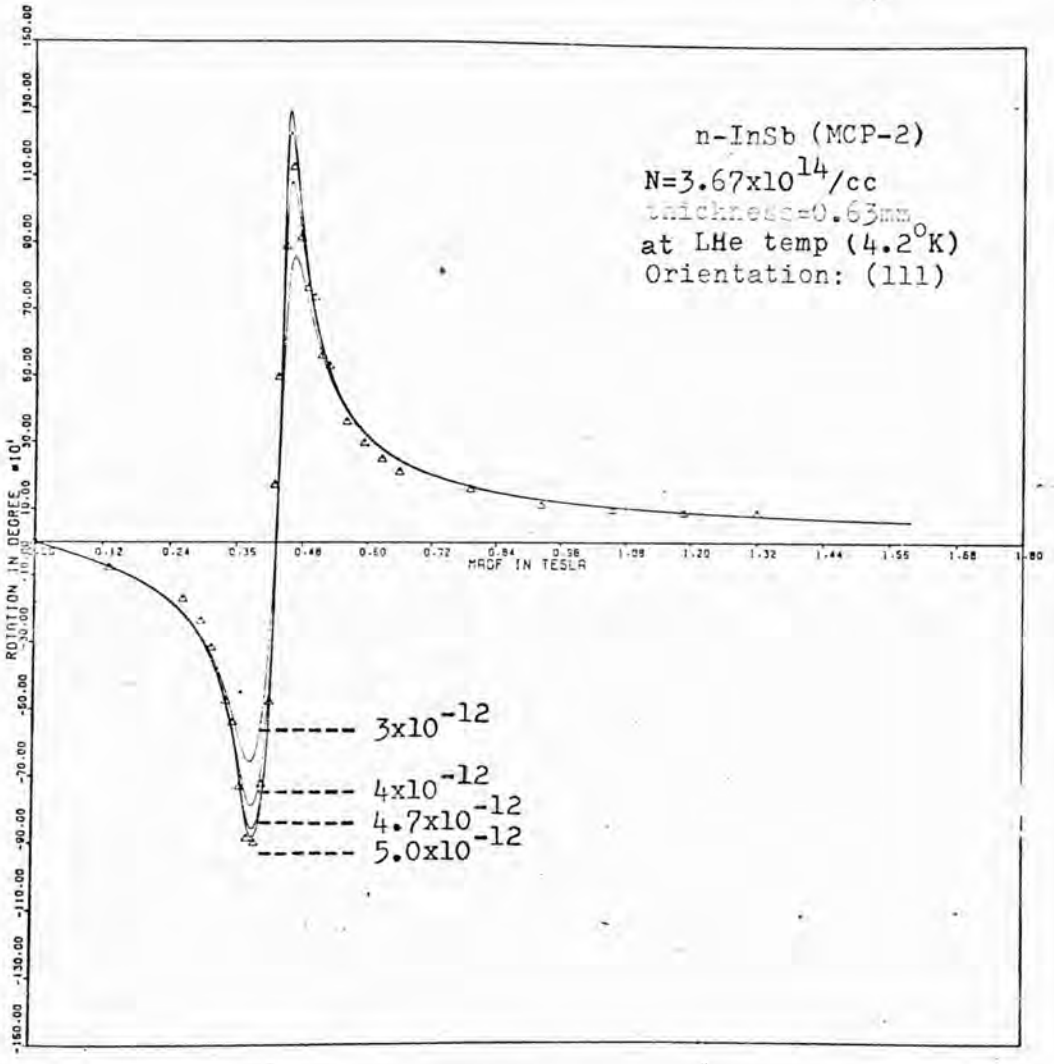

Fig.4.18. Measured Faraday rotation angle shown as open triangles versus magnetic field with 0.337mm HCN laser radiation. Solid lines are computed from eq.(1.16) with dielectric const.=17.9 and effective mass ratio =0.014 for different values of scattering time (in seconds).

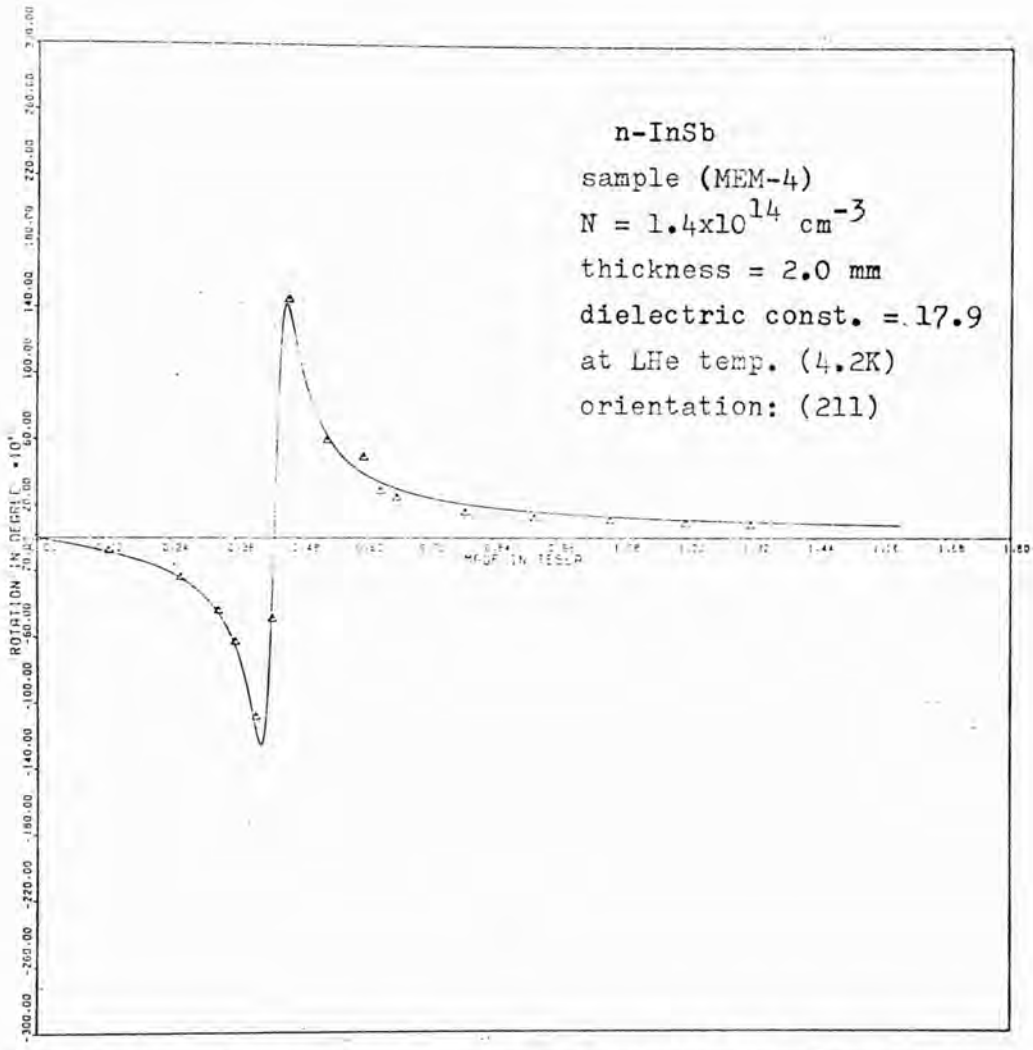

Fig. 4.19. The observed Faraday rotation angle shown as open triangles versus magnetic field at 0.337 mm. Solid line is computed from eq. (1.16) with the parameters calculated by least squares fit of the Faraday rotation function to experimental data, $m^* = 0.0139m_o$ and scattering time $= 3.88 \times 10^{-12}$ seconds.

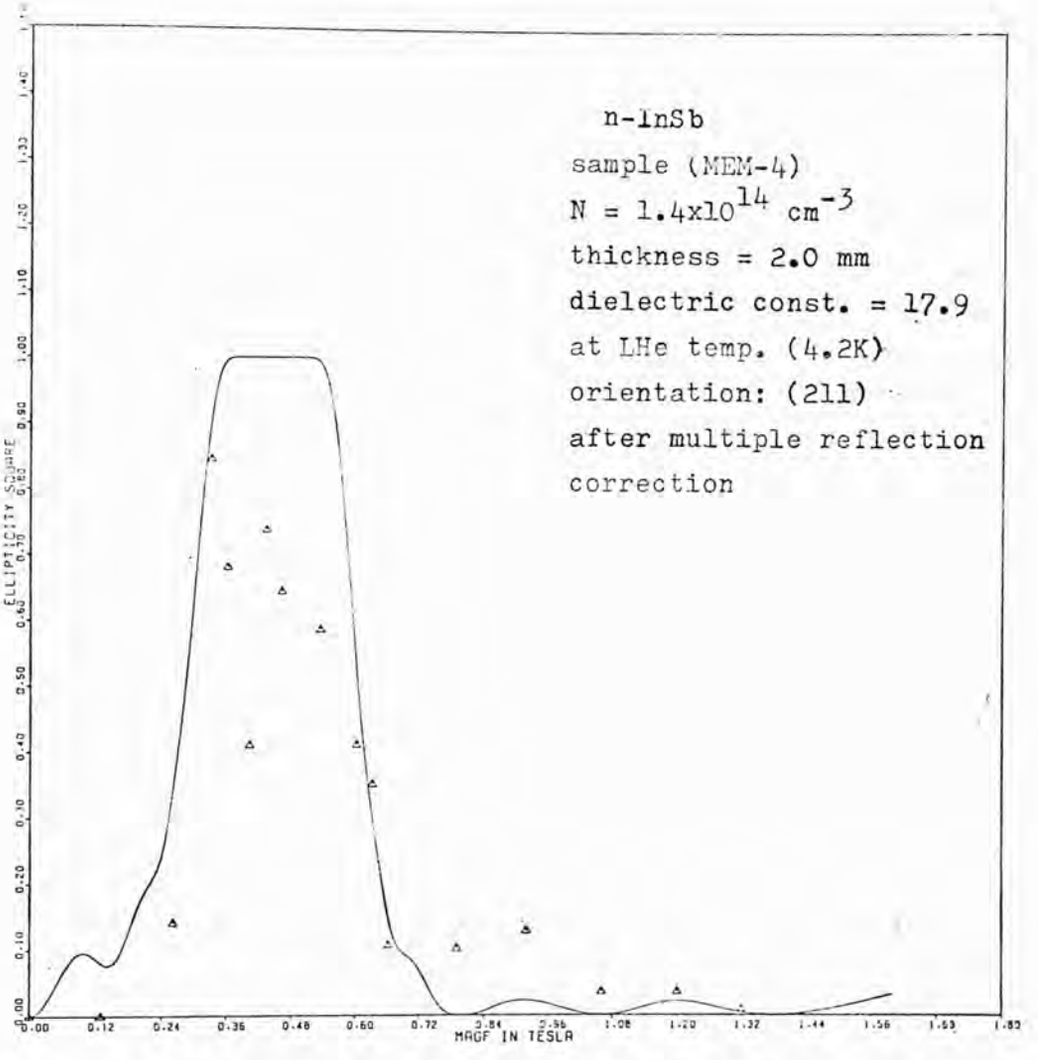

Fig. 4.20. The observed ellipticity (squared) shown as open triangles versus magnetic field at 0.337 mm. Solid line is computed from eq. (1.29) with the parameters calculated by least squares fit of the function of ellipticity to experimental data, $m^* = 0.0141m_o$ and scattering time $= 3.0 \times 10^{-12}$ seconds.

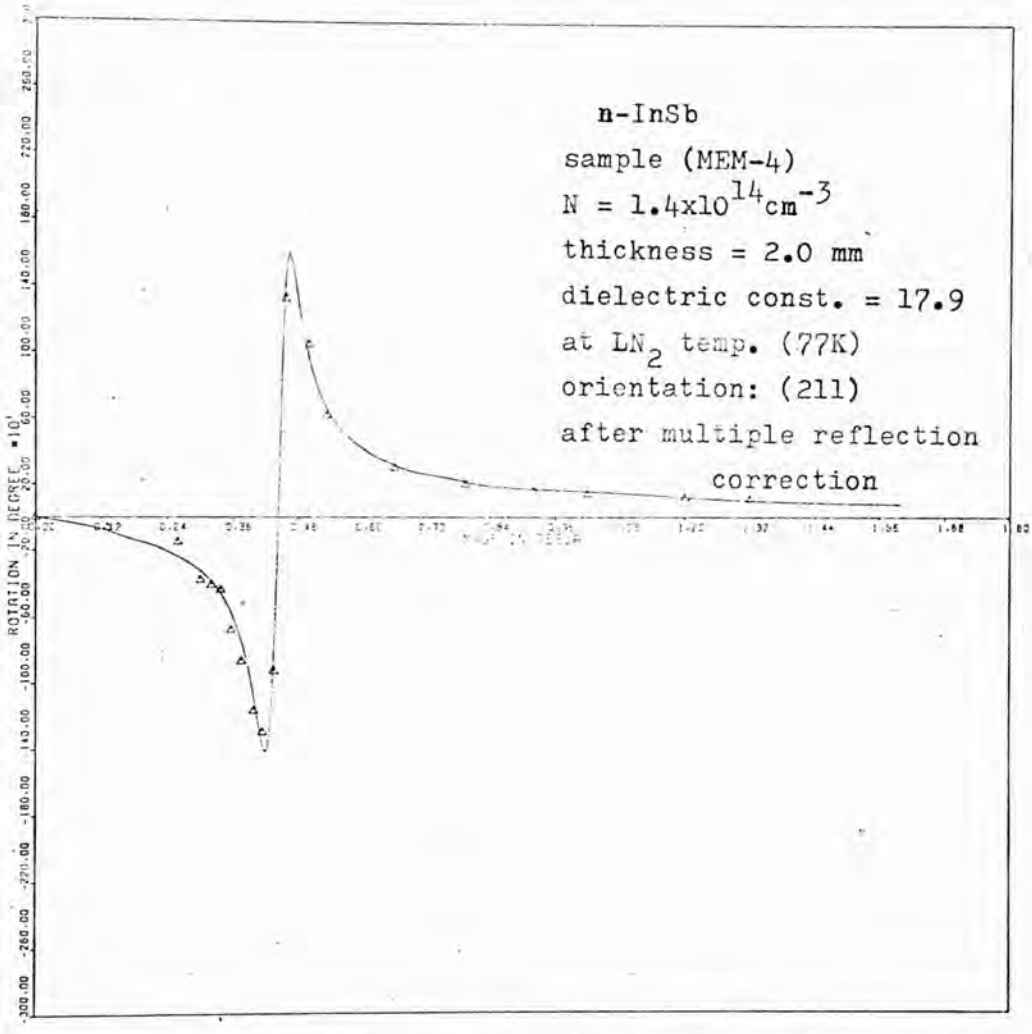

Fig. 4.21. Measured Faraday rotation angle shown as open triangles versus magnetic field at 0.337 mm. Solid line is computed from eq. (1.28) with parameters calculated by least squares fit of the Faraday rotation function to experimental data, $m^* = 0.0141m_o$ and scattering time = 4.5×10^{-12} seconds.

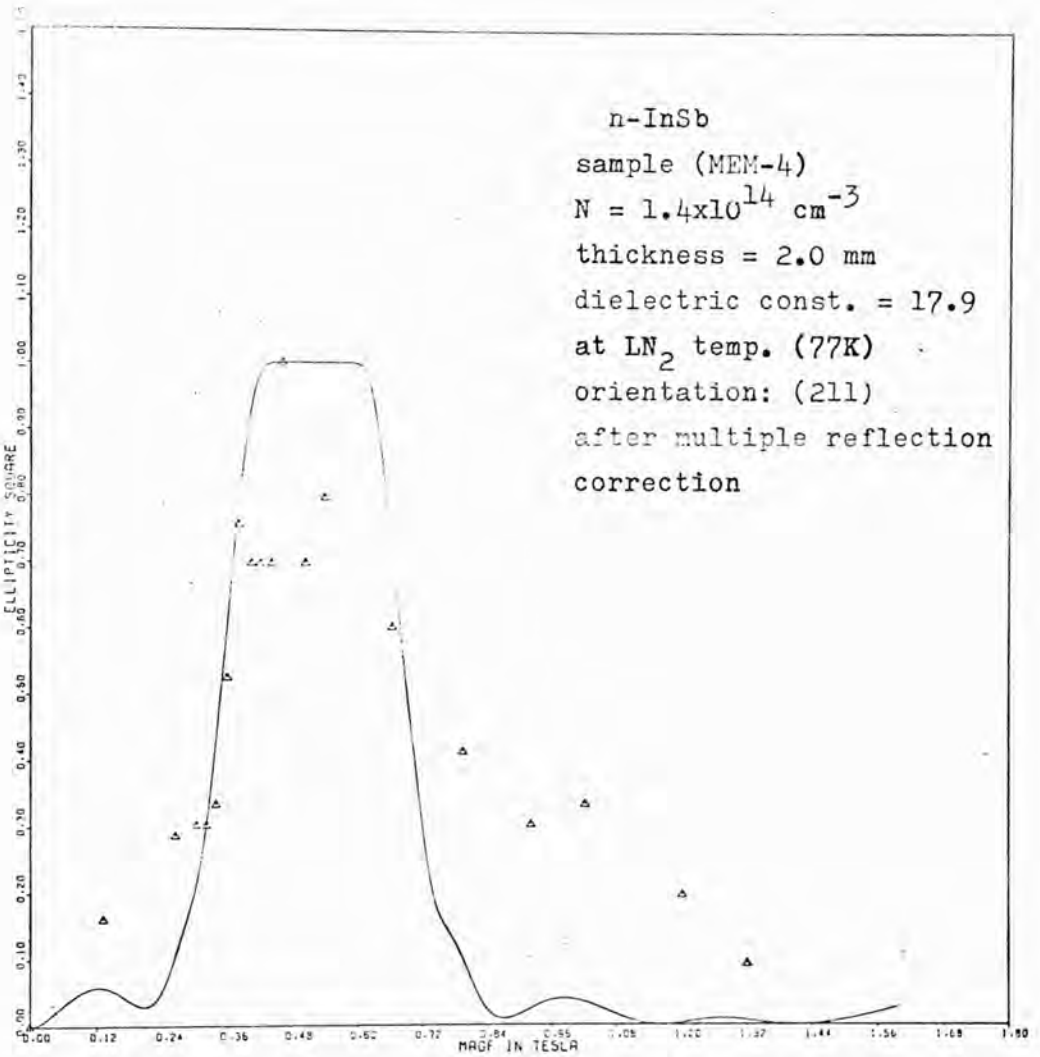

Fig. 4.22. Measured ellipticity (squared) shown as open triangles versus magnetic field at 0.337 mm. Solid line is computed from eq. (1.29) with the parameters calculated by least squares fit of the function of ellipticity to experimental data, $m^* = 0.0163m_o$ and scattering time = 3.0×10^{-12} seconds.

The effective mass ratio (m^*/m_o) and the impurity scattering time of electrons were determined by a least squares fit of the theoretical function including a correction for internal multiple reflection, eqs. (1.16) and (1.28) for Faraday rotation; and (1.17) and (1.29) for ellipticity to experimental data taking these quantities as variable parameters. All the calculated quantities are tabulated in table 4.1 and 4.2 for n-InSb samples with different electron densities. The theoretical curves computed from eqs. (1.16), (1.17), (1.28) and (1.29) using the appropriate values of effective mass ratio and scattering time are shown in Figs. 4.1 to 4.22 as solid lines.

The effect of using different values for the scattering time τ on the theoretical curves for Faraday rotation and ellipticity is shown on a few of the graphs (see Figs. 4.4, 4.5, and 4.18): Figs. 4.12 and 4.13 shown the effect of slight changes in the effective mass ratio on the theoretical values for Faraday rotation and ellipticity (the scattering time τ being kept constant).

The electron density of the samples were also calculated by a least squares fit of the same theoretical function using three variable parameters (carrier density, effective mass ratio and impurity scattering time) to the experimental data. All these calculated quantities and the carrier density measured by the Hall effect measurement at 77K are given in table 4.3. These calculated electron densities are in good agreement (within experimental error) with the electron densities measured by the Hall effect method except for the higher compensated sample (MCP-1).

TABLE 4.1

n-InSb sample	scattering time(second)	scattering time(second) after MRC.	temp. (K)	experiment performed
	$x10^{-12}$	$x10^{-12}$		
MCP-1	6.06±0.36	6.84±0.03	4.2	FR
MCP-1	5.95±0.03	6.80±0.03	4.2	EL
MEM-1	3.50±0.13	3.46±0.15	4.2	FR
MEM-1	3.40±0.40	3.46±0.40	4.2	EL
MEM-3	4.15±0.10	4.13±0.10	4.2	FR
MEM-3	2.28±0.34	3.99±0.18	4.2	EL
MEM-4	3.26±0.08	3.26±0.08	4.2	FR
MEM-4	4.18±0.30	3.00±0.28	4.2	EL
MCP-2	4.25±0.12	4.25±0.12	4.2	FR
MEM-2	5		4.2	CR
MEM-2	6.86±1.53	6.9 ±1.2	4.2	FR
MEM-2	3.98±0.47	7.0 ±0.9	4.2	EL
MEM-4	3.88±0.08	3.87±0.09	4.2	FR
MEM-4	4.18±0.30	3.00±0.83	4.2	EL
MEM-4	4.50±0.08	4.50±0.08	77	FR
MEM-4	3.09±0.17	3.00±0.83	77	EL

MRC = MULTIPLE REFLECTION CORRECTION

FR = FARADAY ROTATION

EL = ELLIPTICITY

CR = CYCLOTRON RESONANCE

Note: see explanation given in footnote on the table 4-2.

TABLE 4.2

n-InSb sample	effective mass ratio (m^*/m_o)	effective mass ratio (m^*/m_o) after MRC.	temp. (K)	experiment performed
MCP-1	0.01387±0.00003	0.01384±0.00004	4.2	FR
MCP-1	0.01408±0.00004	0.01400±0.00003	4.2	EL
MEM-1	0.01395±0.00002	0.01395±0.00003	4.2	FR
MEM-1	0.01405±0.00012	0.01390±0.00013	4.2	EL
MEM-3	0.01392±0.00001	0.01391±0.00001	4.2	FR
MEM-3	0.01364±0.00013	0.01374±0.00013	4.2	EL
MEM-4	0.01402±0.00002	0.01402±0.00002	4.2	FR
MEM-4	0.01408±0.00085	0.01409±0.00037	4.2	EL
MCP-2	0.01389±0.00002	0.01389±0.00002	4.2	FR
MEM-2	0.01439±0.00004	0.01439±0.00003	4.2	FR
MEM-2	0.01331±0.0005	0.01384±0.00021	4.2	EL
MEM-4	0.01386±0.00001	0.01386±0.00001	4.2	FR
MEM-4	0.01408±0.00085	0.01409±0.00037	4.2	EL
MEM-4	0.01414±0.00001	0.01414±0.00001	77	FR
MEM-4	0.01710±0.0004	0.0163 ±0.0005	77	EL

MRC = MULTIPLE REFLECTION CORRECTION

FR = FARADAY ROTATION

EL = ELLIPTICITY

Note that the calculated quantities given below the broken lines in tables 4-1 and 4-2 are not accurate because the experimental data from which the values of effective mass ratio and scattering time were calculated were obtained by a simple technique using only an oscilloscope.

TABLE 4.3

The data in this table are determined by least squares fitting of the curve computed from the theoretical expressions in three parameters, carrier density, effective mass ratio, and impurity scattering time to experimental data at liquid helium temperature.

FARADAY ROTATION

n-InSb sample	$(N_D-N_A)_{Hall}$ (cm^{-3})	$(N_D-N_A)_{Curfit}$ (cm^{-3})	effective mass ratio (m^*/m_o) after MRC.	Impurity scattering time(second) after MRC.
	$x10^{13}$	$x10^{13}$		$x10^{-12}$
MCP-1	0.36±0.04	0.51±0.02	0.01386±0.00003	5.04±0.04
MEM-1	4.6 ±0.3	4.8 ±0.3	0.01395±0.00003	3.28±0.25
MEM-3	12.1 ±0.9	13.0 ±0.4	0.01393±0.00002	3.83±0.13
MEM-4	14.0 ±0.9	12.6 ±0.3	0.01399±0.00002	3.62±0.12
MCP-2	36.7 ±3.1	35.8 ±0.9	0.01388±0.00002	4.35±0.16
		ELLIPTICITY		
MCP-1	0.36±0.04	0.45±0.09	0.01412±0.00002	6.42±0.02
MEM-1	4.6±0.3	4.6 ±0.5	0.01417±0.00011	3.38±0.32
MEM-3	12.1±0.9	14.0 ±0.3	0.01380±0.00012	4.00±0.92
MEM-4	14.0±1.0	10.2 ±5.0	0.01375±0.00126	3.21±0.28

MRC = MULTIPLE REFLECTION CORRECTION

It should be noted that the observed Faraday rotation and ellipticity shown in Figs. 4.19, 4.20, 4.21 and 4.22 were not accurately measured because the experimental data were obtained by a simple technique in which the pulse height of the signal from the laser was measured directly from the screen of an oscilloscope, the data for the other figures (Figs. 4.1 to 4.18) was obtained using a box-car detector.

(ii) Cyclotron resonance

The shapes of the cyclotron resonance absorption lines at 4.2K of the sample MEM-2 having carrier concentration $N=5.6\times10^{13}$ cm^{-3} are presented in Figs. 4.23 and 4.24 as a function of magnetic field using polarized and unpolarized 0.337 mm HCN laser radiation. Solid lines in each figure were computed from eq.(1.27) using the following values: dielectric constant, $\varepsilon_r = 17.9$, effective mass, $m^* = 0.014m_o$ and scattering time, $\tau = 5\times10^{-12}$ second. The power transmission coefficient (transmission ratio) was normalized to low values of magnetic field. Both the observed and calculated transmission ratios became larger than unity at $B > B_c$, which may arise from the Fabry-Perot resonance effects. Because the sample thickness used (0.50 mm) was greater than the critical thickness above which these effects are seen (given by $d = \lambda_o/2n(B)$) where λ_o is the free-space wavelength and n(B) is the sample refractive index at a magnetic field. For n-InSb sample with 0.337 mm, $d \cong 0.04$ mm. The other effect which may give rise to spurious resonance spectra in thick sample arises from the interference of right and left circularly polarized components of the radiation passing through the specimen.

It should be noticed that the observed transmission ratio with plane-polarized radiation is in better agreement with the

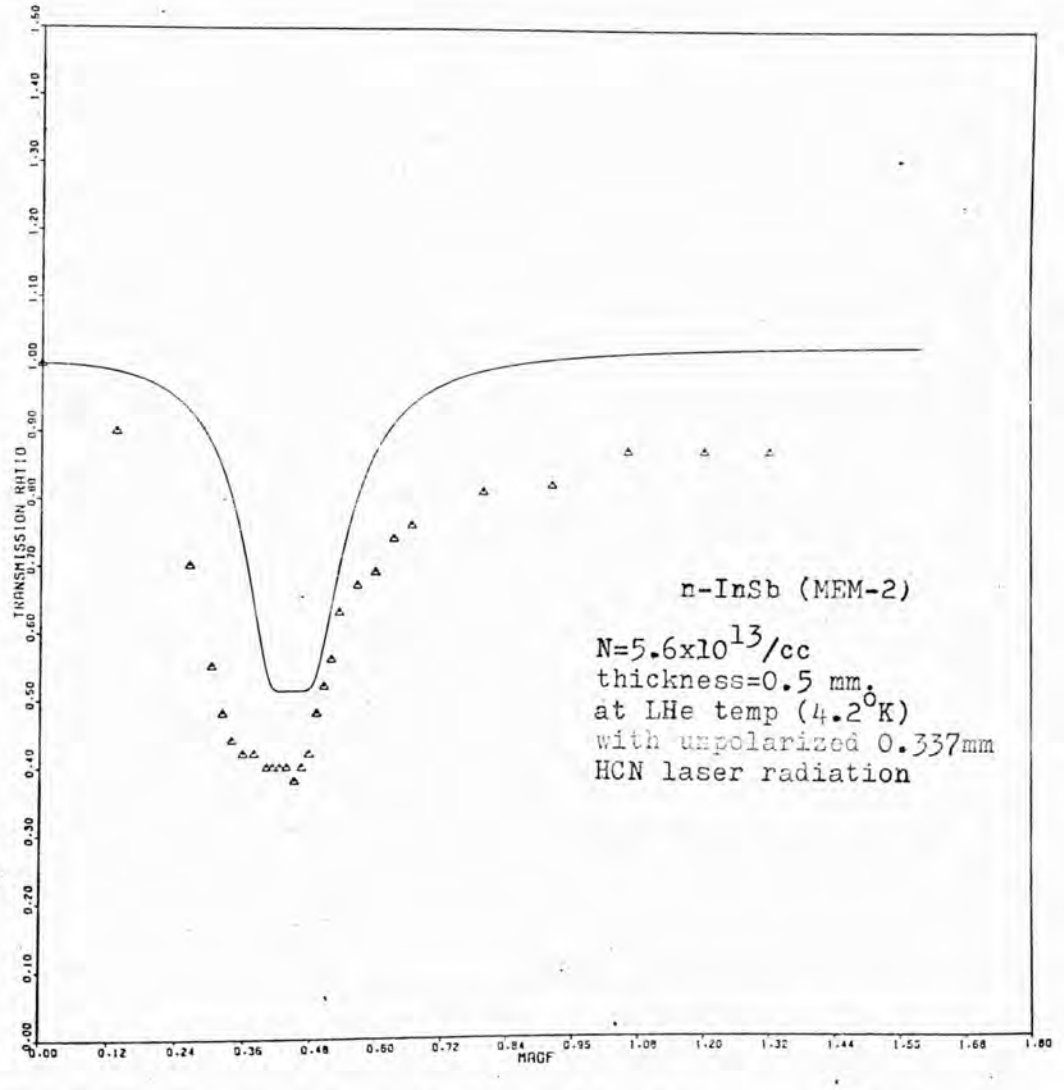

Fig.4.23. Measured transmission ratio shown as open triangles versus magnetic field. Solid line is computed from eq. (1.27) with dielectric const.=17.9 and effective mass ratio =0.014 for scattering time =5×10^{-12} secs.

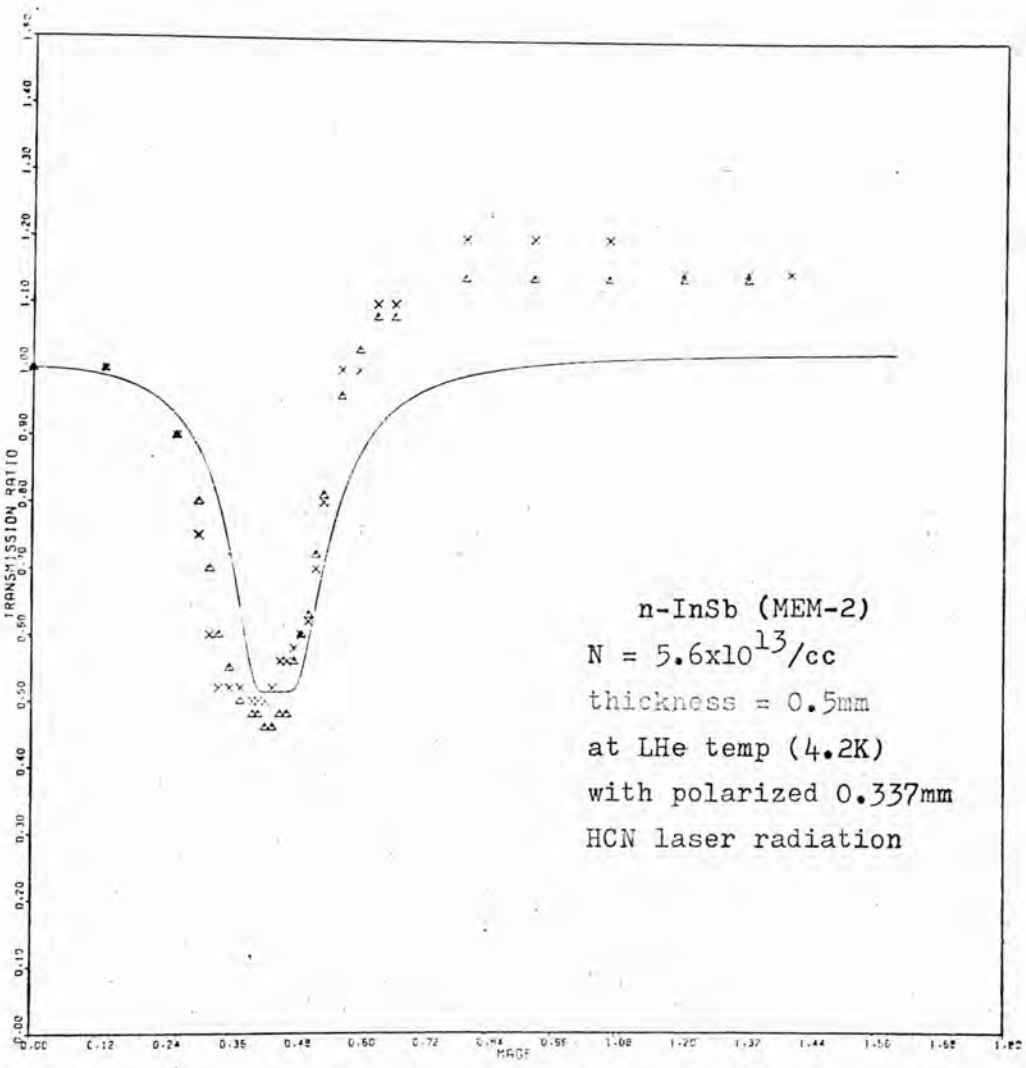

Fig. 4.24. The observed transmission lines of same sample shown as open triangles and crosses for two experimental runs versus magnetic field. Solid line is computed from eq.(1.27) with dielectric const. =17.9. and $m^* = 0.014 m_o$ for scattering time = 5×10^{-12} seconds.

theoretical expression, which was obtained from two circular counter-rotating components of the plane-polarized radiation, than the transmission ratio which was observed by an unpolarized radiation.

The linewidth is usually used to characterize the cyclotron resonance absorption line. Since the linewidth depends sensitively on the scattering mechanisms. For a spherical parabolic energy band the low energy impurity scattering time is given by $\tau = 1/\Delta w_{\frac{1}{2}}$, where $\Delta w_{\frac{1}{2}}$ is the equivalent angular frequency half-width at half-maximum absorption (Apel, 1970b; Kaplan et al., 1973).

The magnitude of the linewidth is influenced by several factors. Due to conduction band non-parabolicity, cyclotron transitions from different low-lying electron levels do not have the same resonant fields at fixed wavelength, thus asymmetrically 'broadening' the line. The fact that the sample is several absorption lengths thick makes it difficult to measure the linewidth precisely owing to the exponential nature of the absorption and to spurious interferences of geometrical origin.

All of these spurious effects can be removed by using thinner specimens, and the resultant spectrum displays only the simple cyclotron resonance absorption. However, another difficulty in precise linewidth measurements at low temperatures is that the free-carrier cyclotron resonance is accompanied by impurity transitions at lower field. At 0.337 mm the impurity line overlaps the free-carrier cyclotron resonance and accurate linewidth measurement becomes impractical. These doubled lines are seen in Figs. 2.23 and 2.24; the low field minimum is due to the impurity transitions ΔE_i, and high field minimum is the cyclotron resonance line.

Such a doubled line in n-type InSb sample with 0.080 mm thickness was observed by Apel (1970b) at 0.337 mm, and its doubled components were analyzed in order to determine the free-carrier electron cyclotron resonance linewidth.

For more precise cyclotron resonance linewidth measurements, the doubled components must be sufficiently well resolved to allow reliable determination of the impurity scattering time at 4.2 K. Therefore, for this reason, no attempts were made the perform cyclotron resonance experiments for thinner n-InSb samples with different electron density at 4.2K using the 0.337 mm wavelength HCN laser radiation.

4.3 DISCUSSION

(i) Effective masses

In order to predict or interpret of the electronic properties of semiconductors, it is necessary to have a detailed picture of the energy band structure. An important parameter in the energy band structure is the effective mass m* which is different from the free-electron mass m_o due to interaction between the electron and the crystal lattice. Faraday rotation in the free-carrier region is one method of obtaining the value of effective mass m* for semiconductors, because it is approximately proportional to $1/(m^*)^2$. Analysis of the experimental data obtained from Faraday rotation enables the concentration and distribution of the carriers and the energy band parameters of a semiconductor to be determined. Magneto-optical dispresive effects thus complement cyclotron resonance measurements, especially at high temperatures and high carrier concentrations. These magneto-optical effects can be measured

under less stringent conditions than cyclotron resonance and magneto-absorption. The free-carrier Faraday rotation gives accurate values for the electron effective mass. The interpretation of experimental intraband rotation is somewhat restricted at short wavelengths by the fact that transitions between energy bands contribute to the rotation.

The Faraday effect is of particular interest in study of the conduction band of n-type InSb whose energy surfaces are spherical. Non-degenerate InSb crystals are also convenient because the rotation depends on $1/(m^*)^2$ and can be quite large due to the very small effective mass of free-electrons in indium antimonide. In this case, small magnetic fields are required when far-infrared radiation is used, e.g., $B = w_c m^*/e$, in order to measure Faraday rotation through the region of cyclotron resonance.

The experimental measurements and theoretical calculations for Faraday rotation and ellipticity through the cyclotron resonance region were done for n-type InSb samples at low temperatures as using a 0.337 mm pulsed HCN laser and a superconducting selenoid which could produced a magnetic field of up to 4 tesla (40 kG). As shown on the graphes which were drawn of the Faraday rotation versus magnetic field, at low magnetic fields (where $w_c < w$) the Faraday rotation increased with the magnetic field, but in the region where cyclotron resonance occurred, the rotation changed sign, and at high magnetic fields (where $w_c > w$) the rotation became inversely proportional to the magnetic field.

The conduction band edge effective mass ratio of free-electrons was determined by a least squares fit of the classical theoretical function (including an internal reflection correction) to

the data. It was assumed, that the effective mass was independent of the magnetic field. Because the magnetic field dependence of the effective mass was calculated from the eqs. (1.19) and (1.20) using the values $m^*=0.014m_o$, $k_z=0$, $E_g=0.235$ eV and $g=-50.3$. The results indicated that the effective mass is increased with the applied magnetic field about 2% up to $B_c=0.45$ tesla, which was within experimental error. Also all the sample used at liquid helium temperatures were non-degenerate in applied magnetic field. The average energy for free-electrons in these samples at 4.2K is $\frac{3}{2}k_BT \cong 0.54$ meV, therefore, all the free electrons are near the bottom of the conduction band which is parabolic as $k_z \to 0$. The quantum condition $\hbar w_c \gg E(k)$ is also satisfied (since $\hbar w_c \cong$ 3.69 meV and $E(k) \cong 0.54$ meV). In this case, non-parabolicity corrections for the energetic electrons which have higher effective mass was also negligible. All the band edge effective masses obtained from least squares fit to experimental data on the Faraday rotation and ellipticity for n-type InSb samples at low temperatures are tabulated in table 4.2.

These calculated band edge effective mass ratios are in good agreement with recent effective mass measurements. In order to compare these calculations with others and also to show the dependence of effective mass on the magnetic field, temperature and carrier concentration, the effective mass data obtained from various types of magneto-optical experiments by other workers for n-type InSb are collected in table 4.4 and displayed as a function of temperature and carrier concentration.

It should be noted that most of the effective mass measurements listed in table 4.4 were obtained with degenerate samples

TABLE 4.4

Effective masses of n-type InSb determined by magneto-optical experiments

m^*/m_o	N_D-N_A (cm^{-3})	T (K)	Experimental method	Wavelength used	Reference
0.015 ±0.0005	4.0×10^{13}	105	FR	FIR	(Shimura, et al., 1970)
0.0139 ±0.0001	1.0×10^{14}	4	CR	FIR	(Johnson & Dickey,1970)
0.0139 ±0.0002	1.0×10^{14}	4.2	CR	FIR	(Apel, et al., 1971)
0.0155 ±0.0005	2.0×10^{14}	4	CR	FIR	(Boyle, et al., 1957)
0.0134	$0.2\text{-}3\times10^{15}$	4	CR	MV	(Bemski, 1960)
0.013	3×10^{14}	77	FR	IR	(Smith, et al., 1959)
0.0148	3.8×10^{14}	77	FR	IR	(Pidgeon, 1962)
0.0131	2.6×10^{15}	77	FR	IR	(Smith, et al., 1959)
0.0145	$\times10^{15}$	77	CR	FIR	(Palik, et al., 1961)
0.0165	1.1×10^{16}	77	FR	IR	(Smith, et al., 1959)
0.0178	2.9×10^{16}	77	FR	IR	(Smith, et al., 1959)
0.019	4×10^{16}	77	FR,VE	IR	(Pidgeon,1962;Teitler,1961)
0.0185	4.3×10^{16}	77	FR	IR	(Pidgeon, 1962)
0.022	2.0×10^{17}	77	FR	IR	(Smith, et al., 1959)
0.023	2.0×10^{17}	77	FR,VE	IR	(Palik,1961a,Teitler,1961)
0.023	2.1×10^{17}	77	FR	IR	(Pidgeon, 1962)
0.029	6.4×10^{17}	77	FR	IR	(Smith, et al., 1959)
0.021	2.0×10^{16}	300	FR	IR	(Pidgeon, et al., 1964)
0.0225	4.5×10^{16}	300	FR	IR	(Pidgeon, 1962)
0.023	5.9×10^{16}	300	FR	IR	(Pidgeon, 1962)
0.035	7.8×10^{16}	300	FR	IR	(Pidgeon, 1962)
0.035	1.0×10^{18}	300	MPR	IR	(Pidgeon, 1962)
0.041	1.8×10^{18}	300	MPR	IR	(Wright & Lax, 1961)
0.038	2.4×10^{18}	300	MPR	IR	(Sniadower, et al., 1964)

FR = Faraday rotation; CR = Cyclotron resonance; VE = Voight effect; MPR = Magnetoplasma reflection or rotation; FIR = Far-infrared; IR = Infrared; MW = microwave.

at higher temperatures in which case more electrons are found at higher energy and momentum so that the effective mass of the electrons was increased. The dependence of the effective mass on the carrier density in n-InSb was studied by Smith et al. (1959) at liquid nitrogen temperatures using infrared radiation. At this temperature, all the samples investigated were degenerate and the corresponding average effective mass m_F^*, which is given by $1/m_F^* = \frac{1}{h^2 k_F}\left(\frac{dE(k)}{dk}\right)_F$ at the Fermi level was calculated from the data, taking into account the Fermi distribution of carriers in the non-parabolic band. By this technique the average effective mass value at $k = 0$ $m_o^* = (0.0143 \pm 0.0005)\, m_o$ was obtained from the k.p pertubation calculation for non-parabolic band by Kane (1957). The effective masses obtained in the experiments described in this thesis are in good agreement with this average effective mass within experimental error.

Most of the Faraday rotation measurements in table 4.4 have been observed in the near infrared region which means that the rotations were well away from cyclotron resonance and correspond to condition $w \gg w_c$. In this case, the Faraday rotation data were obtained from the rising part of the graph of rotation against magnetic field. A possible discrepancy between effective masses determined from Faraday rotation and cyclotron resonance arises from the non-parabolicity of the band. This condition was discussed in detail by Palik et al. (1961).

In earlier measurements of effective mass, an approximate theoretical expression eq. (1.16a) was used to calculate the effective mass of the free-electrons from the observed Faraday rotation when the conditions $w \gg w_p$ and $|w-w_c|\tau \gg 1$ were satisfied. One may

expect errors to arise from this approximation if the condition $w_c \ll w$ is not satisfied. In order to overcome this difficulty in the present work, the effective mass ratios tabulated in table 4.2 for non-degenerate n-InSb samples with different electron densities at low temperatures were calculated from the exact theoretical expression (including internal multiple reflection correction) through the cyclotron resonance region for both Faraday rotation and ellipticity by a least squares fit method using a computer program.

(ii) Scattering times

At low-temperatures, the conductivity and mobility of semiconductors, such as InSb, are governed by phonon scattering down to about 60K, while below this temperature ionized impurity scattering dominates. Hence the d.c. mobility, μ_{dc} exhibits a maximum near 60-70K. One normally expects these mechanisms to continue to function down to liquid helium temperatures at infrared and microwave frequencies, since previous Faraday rotation and ellipticity experiments in n-type InSb at 105K (Shimura et al., 1970) and cyclotron resonance experiments in n-type Ge at low temperatures (Bagguley et al., 1961 and 1963) have yielded approximately the same scattering times at far-infrared and microwave frequencies as those deduced from d.c. measurements.

More recently, however, cyclotron resonance linewidth data (which can be converted to scattering times by the equation $\tau = (\Delta w_{\frac{1}{2}})^{-1}$, where $\Delta w_{\frac{1}{2}}$ is the equivalent angular frequency half-width at half-maximum absorption) and Faraday rotation measurements made through the cyclotron resonance region (which are sensitive to scattering times) have shown that there is an anomalous increase

of scattering times in the far-infrared with respect to the field-dependent d.c. scattering times at liquid helium temperatures (Apel, 1970b; Apel et al., 1970a and 1971; Poehler, 1972; Poehler and Wang, 1972; Chamberlain, 1972 and Kaplan et al., 1973). Also, Potapov et al. (1973) have made measurements on the Faraday rotation in strongly compensated n-type InSb using microwave radiation (at 4 mm and 8 mm wavelengths) and also d.c. conductivity and mobility measurements at various temperatures from 4.5K to 50K. These Faraday rotation data were converted to the Hall mobility in order to compare with d.c. measurements. This comparison showed that the d.c. mobility did not agree with the Hall mobility deduced from the Faraday effect at liquid helium temperatures.

So far, however, very little experimental data have been obtained in the far-infrared at 4.2K in order to determine ionized impurity scattering times. In addition there are some theoretical calculations (Kawamura et al., 1964; Miyake, 1965 and 1973; Kawabata, 1967; Shin et al., 1972 and 1973; Lodder and Fujita, 1974 and Lodder, 1975) that have been considered scattering by ionized impurities in pure semiconductors under the experimental conditions appropriate to far-infrared experiments. Recent theoretical calculations and experimental works have shown that the scattering times τ determined from measurements of the cyclotron resonance width, may differ markedly from the zero-frequency values τ_{dc}, particularly for ionized impurity scattering in the quantum limit where $\hbar w_c \gg k_B T$ and $w_c \tau \gg 1$, (k_B is Boltzmann's constant and w_c is the angular cyclotron resonance frequency). However, for this case there is disagreement among the theoretical predictions, and comparison with experiments are uncertain (Shin et al., 1972 and 1973).

A recent calculation by Shin et al. (1972, 1973) has shown that the important parameter for the Coulomb field of the ionized impurities was the ratio of the magnetic length (radius of cyclotron orbit), $r = (\frac{\hbar c}{eB})^{\frac{1}{2}}$, to the screening length, $a = (\frac{\hbar}{4m^* w_p})^{\frac{1}{2}}$, where m^* is the carrier effective mass, and the plasma frequency w_p is given by $w_p = (4\pi Ne^2/m^* \epsilon_r)^{\frac{1}{2}}$. For a screened Coulomb scattering potential these authors find that when the magnetic length, r, is somewhat less than the screening length, a, of the impurities, the cyclotron resonance width in the quantum limit (all electrons in the lowest Landau level) should increase with increasing magnetic field or decreasing r/a. This is disagreement with the earlier results of Kawabata(1967) obtained for an unscreened Coulomb potential.

More recently, Kaplan et al.,(1973) have obtained cyclotron resonance data for various magnetic fields using thin samples of higher quality n-type InSb. These data were converted to scattering times and compared with the calculations of Shin et al. and Kawabata discussed above. The experimental data show a peak in scattering time near r/a = 0.5. For fields below this maximum, the scattering time increases with increasing field, in agreement with the theory of Kawabata for 'non-adiabatic' (inter-Landau level) scattering, but for fields above it, the scattering time decreases with increasing field, in agreement with the theory of Shin et al., for 'adiabatic' (intra-Landau level) scattering.

So it thus appears that some independent experimental measurements other than these of cyclotron linewidth are required to determine impurity scattering times for comparison with these experimental results. For this reason the free-carrier Faraday

effect in n-type InSb samples with different electron densities (and hence different screening lengths) was used in order to determine low-temperature scattering times; since only one wavelength (0.337 mm) was used in the experiments, so the magnetic length, r, was essentially constant in these experiments.

The electron-ion impurity scattering times were calculated from far-infrared Faraday rotation and ellipticity data and tabulated in table 4.1. These experimentally determined times which are in the range of 3 to 7×10^{-12} seconds are in sharp contrast to the d.c. scattering times measured at 4.2K and zero magnetic field (table 4.5).(The results of Apel et al. (1971) show that these d.c. scattering times are inversely proportional to the applied magnetic field). There is good agreement between the scattering times obtained from the Faraday rotation and ellipticity measurements and those derived from Faraday effect and cyclotron resonance linewidths using the same radiation frequencies (Poehler and Wang, 1972; Apel, 1970b and Apel et al., 1970a and 1971).

All the impurity scattering times measured recently in the far-infrared for n-type InSb (including those obtained by the others) are plotted as a function of the parameter r/a in Fig. 4.25. The comparison indicates that good agreement (within experimental error) exists between the experimental results obtained from the Faraday effect and the other results.

According to Shin et al's theory for $r/a < 1$, the dominant process is 'adiabatic' scattering. Their results for the half-linewidth at half-maximum, $\Delta w_{\frac{1}{2}}$, may be written in the form (Shin et al., 1972 and 1973)

TABLE 4.5

Sample properties at 4.2K

n-InSb sample	$N=N_D-N_A$ cm^{-3} at 77K	$N_i=N_D+N_A$ cm^{-3} at 4.2K	d.c conductivity measured at 4.2K and B=0 $(\Omega cm)^{-1}$	d.c. Hall mobility determined at 4.2K and B=0 $(cm^2/V\text{-}sec)$	d.c scattering time determined at 4.2K and B=0. (sec)
	$x10^{13}$	$x10^{15}$		$x10^{4}$	$x10^{-13}$
MCP-1	0.36	2.0	0.003	0.44	0.4
MEM-1	4.6	1.7	0.2	2.7	2.1
MEM-3	12.0	0.85	1.7	10.6	7.2
MEM-4	14.0	0.84	1.7	7.7	6.2
MCP-2	36.7	1.4	7.6	16.3	10.4

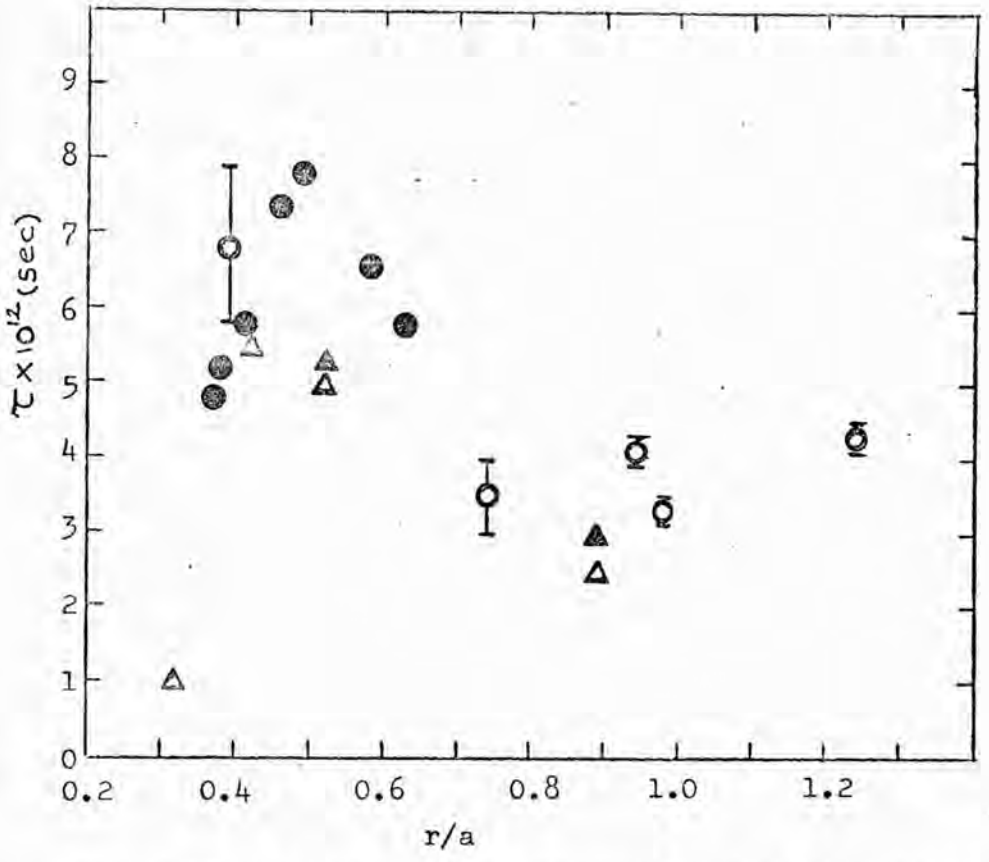

Fig. 4.25 Variation of the impurity scattering time observed by different methods as a function of the parameter r/a defined in the main text for n-InSb, plotted to compare the experimental results obtained in this investigation with earlier measurements at liquid helium temperature. Estimated total experimental error for our measurements is indicated by the bars on the data points. The symbols used in this figure represent following experimental works.

- The present work - Faraday effect
- Kaplan et al. (1973) - Cyclotron linewidth
- Poehler and Wang (1972) - Faraday effect
- Apel et al. (1971) - Cyclotron linewidth

$$\Delta w_{\frac{1}{2}} = \frac{(N_i \pi a)^{\frac{1}{2}} Ze^2}{\hbar\, \varepsilon_r} \left(1-0.86x \frac{r}{a}\right) \qquad (4.2)$$

where N_i is the concentration of ionized impurities of effective charge Ze, and ε_r is the lattice dielectric constant.

More recently, Lodder (1975) has combined the important features of the expressions given by Kawabata (1967) and Shin et al. (1972, 1973) for cyclotron resonance linewidth, taking into account 'gain and loss' factors which were neglected by Shin et al. and screening length a, which was not included in the Kawabata's expression. Lodder's result (1975) for the half-linewidth, $\Delta w_{\frac{1}{2}}$, for the screened Coulomb potential, which is valid for the experimental conditions $\Delta w_{\frac{1}{2}} \ll \frac{\hbar}{4m^*a}$, may be written in the form

$$\Delta w_{\frac{1}{2}} = \tfrac{1}{2} \frac{C_2^{4/3}\, r^{4/3}}{(\hbar/m^*)^{1/3}} \left(F\left(\frac{r^2}{2a^2}\right)\right)^{2/3} \qquad (4.3)$$

where $C_2 = (N_i \pi)^{\frac{1}{2}} (Ze^2/\hbar\varepsilon_r)$ and the function $F(r^2/2a^2) = F(p)$

$$F(p) = \int_0^\infty dt\, \frac{t^2 e^{-t}}{(t+p)^2} = p+1-(p^2+2p)\, \exp(p)\, E_1(p),$$

while $E_1(p) = \int_p^\infty \frac{e^{-t}}{t}\, dt$ is an exponential integral, and the other symbols have their usual meanings.

Under the present experimental conditions, the magnetic length, $r = (\hbar c/eB_c)^{\frac{1}{2}}$, where B_c is the field required for cyclotron resonance and the screening length, $a = (\hbar^2 \varepsilon_r/(64\pi m^* e^2 N))^{\frac{1}{4}}$, which is a function of the carrier concentration, N, of the sample used. The earlier theoretical work of Kawamura et al. (1964) and Kawabata (1967) for the adiabatic and non-adiabatic collision times arising from Coulomb interactios in the quantum limit are independent of the screening length a. For an unscreened Coulomb potential due to ionized impurities their results are

$$\tau_{na}(B) = \frac{\varepsilon_r^2}{2\pi e^4 N_i}(|\hbar k_z|\hbar w_c) \qquad (4.4)$$

$$\cong \frac{\varepsilon_r^2 \hbar w_c}{2\pi e^4 N_i}(2m^*k_BT) \quad \text{(non-adiabatic scattering term)}$$

$$\tau_a(B) = \left(\frac{15}{4\pi N_i}\right)^{\frac{1}{2}} \frac{\varepsilon_r}{e^2}(m^*\hbar^3 w_c)^{\frac{1}{4}} \quad \text{(adiabatic scattering term)} \qquad (4.5)$$

The final expression for the overall scattering in this approch is then given by Apel and Poehler (1970)

$$\frac{1}{\tau(B)} = \frac{1}{\tau_a(B)} + \frac{1}{\tau_{na}(B)} \qquad (4.6)$$

Apel et al. (1971) added the zero-field dc scattering time, τ_o, to this expression and obtained the equation below

$$\tau(B) = \tau_o + (\tau_a^{-1}(B) + \tau_{na}^{-1}(B))^{-1} \qquad (4.6a)$$

In order to calculate the impurity scattering times from these theoretical predictions by use of the equations (4.2), (4.3), (4.4), (4.5) and (4.6) the total impurity concentrations of the sample used, N_i, were estimated from the mobility which is product of the conductivity measured at 4.2K in zero magnetic field and the Hall coefficient determined at 77K by using the Brook-Herring equation (1951, 1955) which is given by (in Gaussian c.g.s. units)

$$\mu_I = \frac{2^{7/2}}{\pi^{3/2}} \frac{\varepsilon_r^2 (k_BT)^{3/2}}{(m^*)^{\frac{1}{2}} e^3 N_i} \frac{1}{\ln(1+b)-b/(1+b)} \qquad (4.7)$$

where $b = \frac{6}{\pi} \frac{\varepsilon_r (k_BT)^2 m^*}{N\hbar^2 e^2}$, and the symbols have their usual meanings.

All these measured and calculated quantities are listed in table 4.5 and 4.6.

TABLE 4.6

Impurity scattering time at 4.2K

n-InSb sample	parameter r/a	IMPURITY SCATTERING TIME AT 4.2K			
		observed	calculated from the theoretical exprs.		
			Kawabata (1967)	Shin et al (1972,1973)	Lodder (1975)
		(I N S E C O N D)			
			$x10^{-12}$	$x10^{-13}$	$x10^{-12}$	$x10^{-12}$
MCP-1	0.39	6.84±0.03	2.6	0.9	1.9
MEM-1	0.74	3.46±0.15	3.0	2.4	2.8
MEM-3	0.94	4.13±0.10	5.4	7.4	5.2
MEM-4	0.98	3.26±0.08	5.4	9.1	5.3
MCP-2	1.24	4.25±0.12	3.5	18.3	4.7

Comparison of the theoretical calculations and the experimental observatins listed in table 4.6 for the impurity scattering time in n-type InSb at 4.2K showed that the impurity scattering time depends effectively on the parameter r/a. Lodder's theoretical expression (i.e. eq. (4.3)) yields better agreement to the present experimental data except for the strongly compensated sample (MCP-1) which violates the condition $\Delta w_{\frac{1}{2}} \ll \frac{\hbar}{4m^*a}$. Therefore, this violation may be the reason for the scattering time calculated from the Lodder's expression (eq. (4.3)) being lower than the experimental values. The agreement between the experimental and calculated values for the impurity scattering times in the other samples used is reasonably good.

(iii) Hot electron effects

The non-linear behaviour of the resistivity of n-type InSb observed at liquid helium temperature in the presence of a magnetic field has been treated in many ways both theoretically (Kazarinov and Skobov, 1962) and experimentally (Sladek, 1958, 1959; Kobayashi and Otsuka, 1972, 1974; Kobayashi et al., 1973; and Murotani and Nisida, 1972). Some authors belive that impact ionization of frozen-out carriers cause the non-linear effect, while others assert that 'heating-up' of carriers within the conduction band can explain the main features of the phenomena. It is true that both processes may actually be taking place. According to Kobayashi and Otsuka's experimental results, in which they used n-type InSb with an electron density of 1.6×10^{13} cm^{-3} at 77K, a linear resistivity behaviour and a constant 'electron temperature' (4.2K) was observed up to an applied electron field of 1V/cm. Then, a drop in resistivity and an increasing

'electron temperature', T_e, up to 30K, was reported with applied electron fields between 1 and 2V/cm. After all the frozen-out carriers had been exhausted at about E = 2V/cm a further increase of the 'electron temperature' was explained by 'heating-up' of carriers within the conduction band. Still higher electric fields (up to 64V/cm) applied to the sample distributed the carrier over more than one Landau level transitions ($0_- \rightarrow 1_-$, $1_+ \rightarrow 2_+$, $1_- \rightarrow 2_-$) were also observed experimentally. Similar experimental results in n-type InSb with an electron density of $2.5 \times 10^{13} cm^{-3}$ were reported at liquid helium temperatures by Murotani and Nisida (1972) using a CW 0.337 mm wavelength HCN laser.

The Faraday rotation due to hot electrons in strongly compensated n-InSb samples with different electron densities (from 1.4×10^{13} to $9.8 \times 10^{13} cm^{-3}$) was investigated in the millimetre wavelength range at liquid ^{4}He temperatures by Potapov et al. (1973). According to their experimental results if the incident laser power on the sample was less than 10^{-5} watts/cm^2, the relative value of the correction to the Faraday rotation angle due to 'electron heating' will be negligible.

The maximum power incident on the samples used in the present investigation was estimated to be about 10^{-5} watts/cm^2. In the case of electron 'heating' by the e.m. wave field, we have $E^2 = 2p(\mu_o/\varepsilon_o \varepsilon_r)^{\frac{1}{2}} = 2p/(\varepsilon_o c \varepsilon_r^{\frac{1}{2}})$ using $\mu_o \varepsilon_o c^2 = 1$, where p is the power of the incident wave in watts/m^2 and ε_r, ε_o are the permittivities of n-type InSb and vacuum. If these values are substituted in the above equation, the maximum value of the electric field produced by the pulsed HCN laser will be E = 0.05 V/cm. D.c. electric fields were applied

to the Hall bars at 4.2K, which were cut as near to the corresponding samples used as possible, up to this calculated a.c. electric field, during d.c. conductivity measurements of these samples in zero magnetic field. Current and potential measurements showed that the Ohm's law held for fields up to this a.c. value (= 0.05 V/cm) for the samples used. So,a.c. electric field produced by incident laser power on the samples was so small and 'hot electron' effects were also negligible under the experimental conditions used in the experiments described in this thesis.

(iv) Faraday effect for other semiconductors

Values of Faraday rotation for n-type InAs and n-type GaAs with electron densities of $1.7X10^{16}$ and $1.45X10^{16}$ cm^{-3} at 77 K respectively were calculated from eqs.(1.16) and (1.17) as a function of magnetic field for the 0.337 mm pulsed HCN laser radiation;(lower carrier concentrations of these samples than we have got were not commercially available). The calculated results showed that the absorption coefficient for these materials was very high and the 'plasma frequency' $w_p = (Ne^2/(m^*\varepsilon_0\varepsilon_r))^{\frac{1}{2}}$ calculated was larger than the laser frequency w. These properties of these materials indicated that the plasma would be opaque for some values of the magnetic field, (see Fig. 4.25A, (after Wright, 1964)).

The theoretical calculation of the Faraday rotation was continued for the high purity epitaxial films of n-type GaAs as used by Chamberlain (1972) and n-type HgTe as used by Tuchendler et al. (1973). The calculated Faraday rotation for these materials and one of the n-type InSb samples used is shown in Fig. 4.26, (the properties of the materials used in the calculations are given on this figure). It can be seen that the calculated Faraday rotation

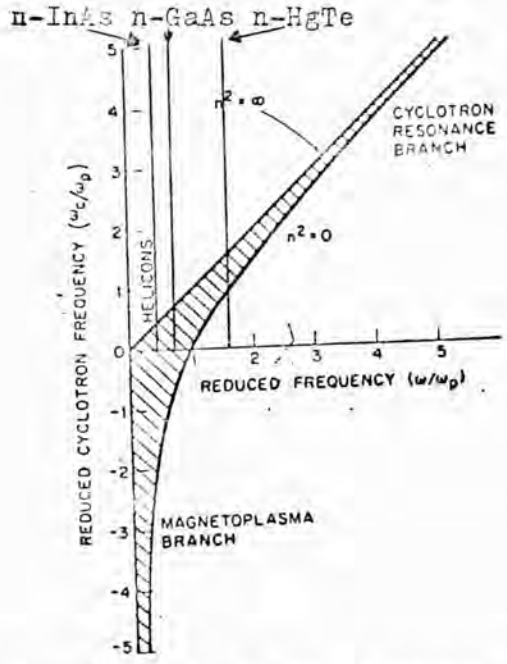

Fig. 4.25A Poles and zeros of the index of refraction for a lossless plasma (k=0) in a longitudinal ($\underline{q} \parallel \underline{B}$) magnetic field, ($w_c=\frac{eB}{m^*}$, $w_p^2= Ne^2/(m^* \varepsilon_o \varepsilon_r)$. The plasma is opaque in the cross-hatched region, in which $n^2<0$: and hence the radiation does not propagate through the sample (reflectivity R is 1). Under the present experimental conditions, the reduced frequency (w/w_p) is kept fixed and the reduced cyclotron frequency (w_c/w_p) is proportional to the applied magnetic field. Transparent and opaque regions of the samples whose properties are given below can be seen in this figure. (After G.B. Wright, 1964).

n-InAs	n-GaAs	n-HgTe
$N=1.7X10^{16} cm^{-3}$	$N=1.45X10^{16} cm^{-3}$	$N = 2X10^{15} cm^{-3}$
d= 0.5 mm.	d= 0.5 mm.	d = 0.010 mm.
$m^*=0.023m_o$	$m^*= 0.068m_o$	$m^* = 0.026m_o$
$\varepsilon_r=14.55$	$\varepsilon_r=11.1$	$\varepsilon_r = 20.0$
$\tau=4.0x10^{-11}$ sec.	$\tau=2.8X10^{-11}$ sec.	$\tau = 8.87X10^{-12}$ sec.
$w/w_p= 0.44$	$w/w_p= 0.72$	$w/w_p= 1.6$

(Tuchendler et al's data (1973))

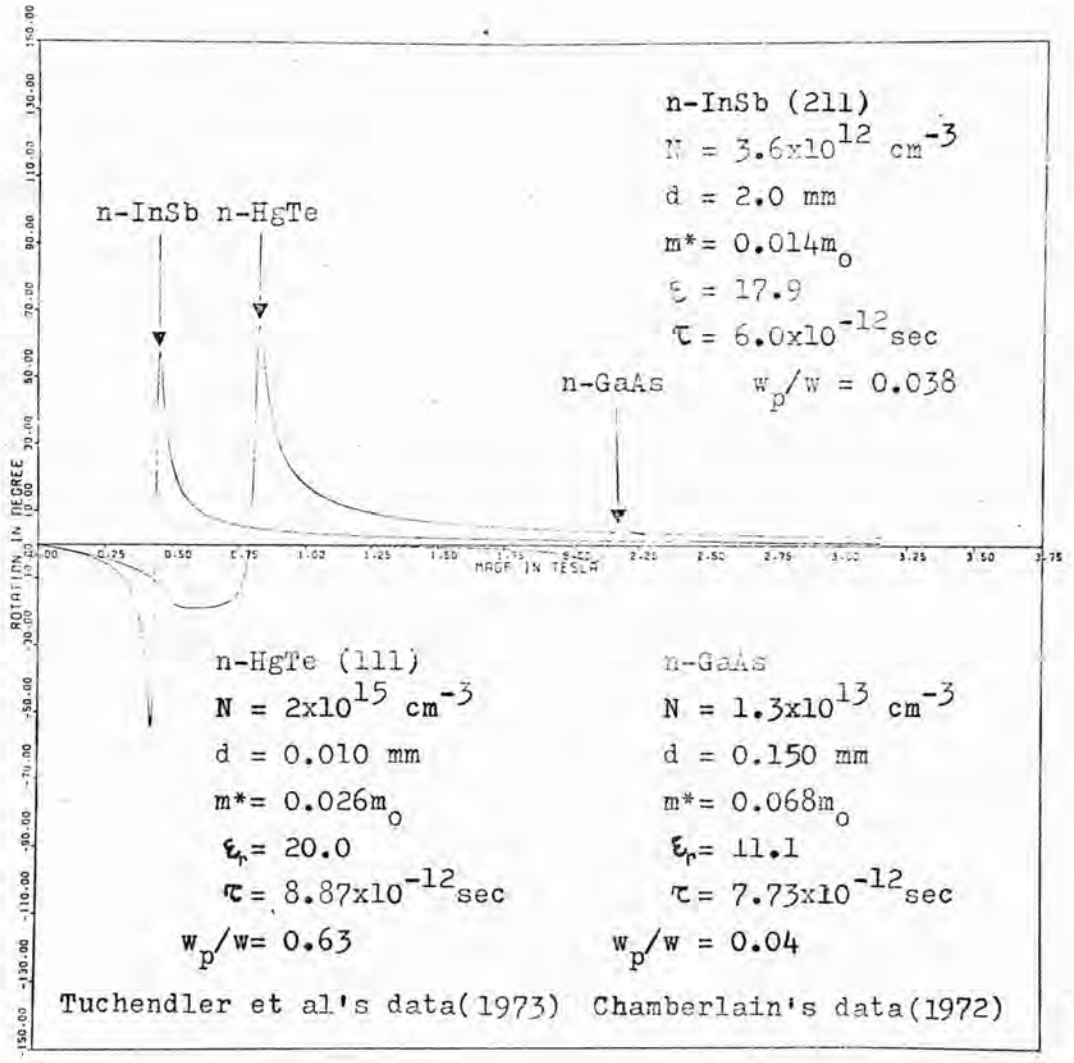

Fig. 4.26 Calculated Faraday rotation curves through cyclotron resonance for n-type InSb, HgTe and GaAs versus magnetic field with 0.337 mm incident pulsed HCN laser radiation. These curves are computed from eq.(1.16) with indicated parameters.

through cyclotron resonance for n-type GaAs would be too small to measure with any degree of accuracy using the techniques described in this thesis and for n-type HgTe was affected by magneto-plasma reflection phenomena, just before the cyclotron resonance field was reached.

In order to demostrate the magneto-plasma effect of these materials the reflectivity R given by eq. (1.26) was calculated and is shown in Fig. 4.27 as a function of the magnetic field applied (for left-hand circularly polarized radiation only) using the parameters given in Fig. 4.26. Similar theoretical calculations of the reflectivity R for different values of $(w_p/w)^2$ as a function of (w_c/w) (which varies with the applied magnetic field) have also been published by Zeiger and Hilsentrath (1957).

Note that the calculated reflectivity R for n-type GaAs and n-type InSb shown in Fig. 4.27 is nearly constant: slight changes of the reflectivity occur at cyclotron resonance. However, the reflectivity R for n-type HgTe exhibits a drastic change just before the cyclotron resonance field, the refractive index of n-type HgTe, which is function of the applied magnetic field, tends towards unity at about 0.5 tesla and the reflectivity R, becomes nearly equal to zero, which makes the material more transparent. The refractive index of this material at higher magnetic fields, increases and at about 0.75 tesla, the reflectivity R, reaches a maximum nearly equal to unity and the material becomes almost opaque. This phenomenon is usually called the magneto-plasma effect. At still higher magnetic fields, the reflectivity R falls again.

The reflectivity minimum is shifted by amount $\pm w_c/2$ by the application of the magnetic field as the frequency of incident

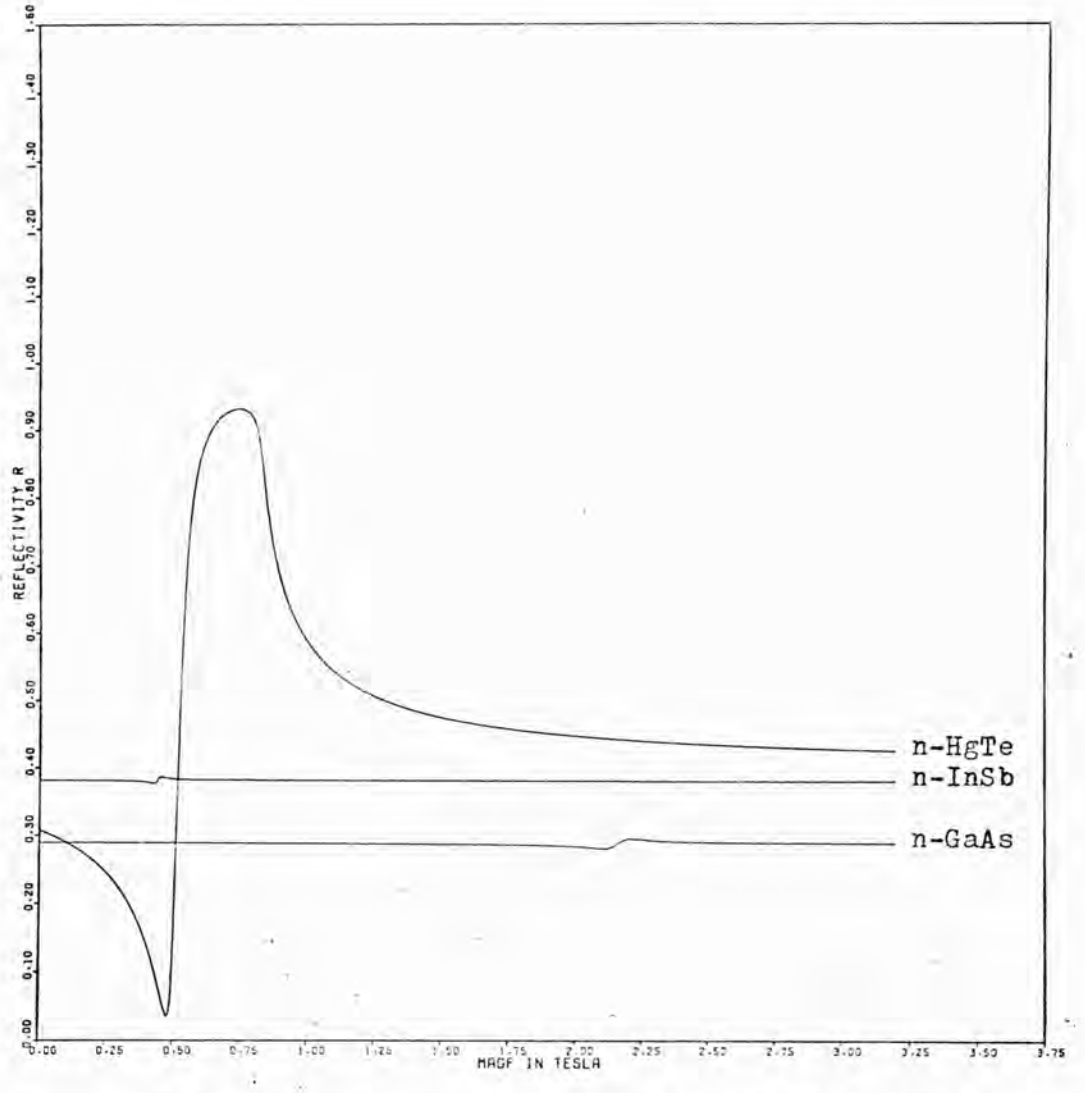

Fig. 4.27 Theoretical curves of the reflectivity R for the magnetoplasma effects of the same semiconductors with properties given in fig. 4.26 versus magnetic field with indicated parameters in fig. 4.26 for 0.337 mm left hand circularly polarized radiation only.

radiation is varied. This has been observed experimentally in many semiconductors (Spitzer and Fan, 1957; Lipson et al., 1958; Palik et al., 1962). The measurement of magneto-plasma shifts allows an another independent determination of cyclotron frequency w_c, and thereby effective mass m*, of the charge carriers in the semiconductors.

CHAPTER 5

5.1 SUMMARY AND CONCLUSION

A satisfactory experimental system, signal processing and recording technique for an experimental investigation of magneto-optical effects including free-carrier Faraday rotation, ellipticity and cyclotron resonance in n-type InSb samples with different electron densities has been developed and applied to the study of electron-ionized-impurity scatterings in the presence of magnetic fields at cryogenic temperatures. A pulsed far-infrared (HCN) laser has been made to operate as a source of a stable monochromatic signal having a wavelength of 0.337 mm with an average power of 1 mW. It should be noted that this laser can be made to produce radiation at other discrete wavelengths (0.028 mm, 0.119 mm, etc.) in the far-infrared by simply changing the gas in the tube, if required.

The theoretical formulation chosen was a classical theory based on the Drude free-electron model and Maxwell's equations for a conducting medium, taking into account multiple internal reflections in the specimens. A quantum mechanical calculation for Faraday effect has been used by Poehler and Wang (1972). Comparison indicated that the present classical calculation with the same parameters used in Poehler and Wang's data for the Faraday rotation was higher than the quantum mechanical calculation by about 5-6 % in the range 0-0.4 tesla and 35-40 % in the range 0.4-1.2 tesla magnetic field range; (see appendix D).

The experimental results on n-type InSb with different electron densities were in good agreement with the classical

theory in most respects. With the measurements over a wide range of magnetic field through the cyclotron resonance, it was possible to determine the effective mass, impurity scattering time and density of conduction-band electrons for the sample used from both the Faraday rotation and ellipticity by using a cur-fitting method. Near the cyclotron resonance field, however, the measured ellipticity was found to be much lower than the calculated one. A similar discrepancy has been observed by other experiments in measurements at 77 K with classical calculation (Shimura et al., 1970) and in measurements at 4.2 K with quantum mechanical calculation (Poehler and Wang, 1972).

Analyses of the experimental data obtained from both the Faraday rotation and ellipticity measurements through cyclotron resonance by using a least squares method gave a mean value of 0.0139 $\pm$ 0.0001 for the fundamental effective mass ratio of the conduction-band electrons in n-type InSb specimens at 4.2K. This effective mass ratio was in good agreement with earlier measurements at low temperatures obtained by several other different experimental methods.

The electron-ion impurity scattering times measured by the present experiments yielded values of the order of 10^{-12} seconds at liquid helium temperatures for several different samples. These measurements were in sharp contrast to the field dependent d.c. scattering times (of the order of 10^{-13} seconds) measured at 4.2K in zero magnetic field. However, there was good agreement between these impurity scattering times observed from the present Faraday effect measurements and those derived from the cyclotron resonance linewidth measurements using the same radiation frequencies and temperatures (Apel et al., 1970c and 1971).

Comparison of the data with theories of linewidth, recently given by Shin et al. (1972, 1973) and Lodder (1975), in the quantum limit (where $w_c\tau \gg 1$ and $E_F \ll k_BT \ll \hbar w_c$, — E_F is the Fermi energy, k_B is Boltzmann's constant and w_c is the angular cyclotron frequency) showed that the impurity scattering times depend effectively on the size of the parameter r/a, where r is the magnetic length and a is the screening length. Values of the impurity scattering times obtained by different methods were plotted as a function of the parameter r/a and compared with the present experimental results (Fig. 4.25).

The comparison of the impurity scattering times observed with the values calculated from the theories of linewidth given by Kawamura et al. (1964), Kawabata (1967), Shin et al. (1972 and 1973) and Lodder (1975) indicates that a disagreement exists between these theoretical values. Better agreement with experimental results was obtained from Lodder's linewidth expression (1975), which was derived using an approximation to a screened Coulomb potential.

From the present experimental work on n-type InSb samples with different electron densities, one can conclude that there are still considerable discrepancies between the experimental data and the values calculated from theretical expressions even the effect of internal multiple reflections in the specimens is taken into account.

Several investigations of the free-carrier Faraday effects in n-type InSb at 4.2K at 0.337 mm wavelength have been made, but less work has been done on these effects at other far-infrared wavelengths (0.028 mm, 0.119 mm, etc.). Therefore, there is

a need for more experimental data on the Faraday effect in n-type InSb at these far-infrared frequencies for comparison with the results of cyclotron linewidth measurements.

Also additional work, both on cyclotron resonance linewidth measurements and Faraday effects in other semiconductors at far-infrared frequencies, is required to make clear the results obtained from both the experimental investigations and the theoretical predictions and also to support the Lodder's linewidth expressions (1975).

A P P E N D I X A

A typical computer program output for one of the n-InSb samples used in the present investigations was shown on the next page. The symbols used in this program output have following meanings:

N-MINUS and N-PLUS are refractive indices; K-MINUS and K-PLUS are extinction coefficients; IMP-MINUS and IMP-PLUS are imaginary part, REP-MINUS and REP-PLUS are real part of the propagation constant (in per meter), which defines as $p_{\pm} = \frac{w}{c} (n_{\pm} - ik_{\pm})$, for left- and right-hand circularly polarized radiation respectively; THETA is the Faraday rotation angle (in degree) and T is the relaxation time (in second).

InSb EFFECTIVE MASS RATIO= .0140 DIELECTRIC CONSTANT= 17.90

WAVELENGTH= .00337METER OMEGA= .55935E+13/SECOND

CYCLOTRON RESONANCE FIELD= .44534E+00TESLA CYCLOTRON FREQUENCY= .55930E+13/SECOND

RELAXATION TIME= .30000E-11SECOND OMEGA*T= .16780E+02 ($\omega\tau$)

PLASMA FREQ.= .76386E+12/SEC. OMEGA*T= .22916E+01 ($\omega_p\tau$)

N-MINUS= .42811E+01 N-PLUS= .42111E+01 K-MINUS= .65424E+00 K-PLUS= .59009E-03

IMP-MINUS= .12198E+05 IMP-PLUS= .11000E+02 REP-MINUS= .79821E+05

REP-PLUS= .78515E+05 THETA= .18656E+02DEGREE THICKNESS= .5000E-03METER CARRIER DENSITY= .4600E+20/METER CUBE

N-MINUS AND N-PLUS ARE REFRACTIVE INDICES; K-MINUS AND K-PLUS ARE EXTINCTION COEFFICIENTS;

IMP-MINUS AND IMP-PLUS ARE IMAGINARY PART, REP-MINUS AND REP-PLUS ARE REAL PART OF THE PROPAGATION CONSTANT;

FOR LEFT AND RIGHT CIRCULARLY POLARIZED RADIATION

FIELD IN TESLA	N-MINUS	N-PLUS	K-MINUS	K-PLUS	IMP-MINUS	IMP-PLUS	REP-MINUS	REP-PLUS	THETA	ELLIPTICITY
0	.41913E+01	.41913E+01	.23448E-02	.23448E-02	.44092E+02	.44092E+02	.78147E+05	.78147E+05	0	0
.22222E-01	.41895E+01	.41930E+01	.25927E-02	.21657E-02	.48348E+02	.40379E+02	.78113E+05	.78179E+05	-.94436E+00	.39532E-05
.44444E-01	.41875E+01	.41946E+01	.28551E-02	.19007E-02	.53233E+02	.37116E+02	.78075E+05	.78208E+05	-.19091E+01	.16761E-04
.66667E-01	.41852E+01	.41960E+01	.31594E-02	.16360E-02	.58906E+02	.34233E+02	.78034E+05	.78234E+05	-.28789E+01	.38317E-04
.88889E-01	.41827E+01	.41973E+01	.35149E-02	.16987E-02	.65535E+02	.31472E+02	.77987E+05	.78259E+05	-.39935E+01	.71048E-04
.11111E+00	.41797E+01	.41986E+01	.39339E-02	.15762E-02	.73348E+02	.29389E+02	.77935E+05	.78282E+05	-.49503E+01	.12057E-03
.13333E+00	.41769E+01	.41997E+01	.44324E-02	.14465E-02	.82642E+02	.27394E+02	.77877E+05	.78303E+05	-.60956E+01	.19758E-03
.15556E+00	.41733E+01	.42008E+01	.50317E-02	.13479E-02	.93916E+02	.25580E+02	.77812E+05	.78323E+05	-.73609E+01	.29137E-03
.17778E+00	.41694E+01	.42018E+01	.57619E-02	.12789E-02	.10741E+03	.23845E+02	.77737E+05	.78342E+05	-.86344E+01	.40307E-03
.18727E+00	.41648E+01	.42027E+01	.66404E-02	.11983E-02	.12418E+03	.22342E+02	.77652E+05	.78359E+05	-.10162E+02	.44747E-03
.22222E+00	.41595E+01	.42036E+01	.77872E-02	.11259E-02	.14519E+03	.20974E+02	.77553E+05	.78375E+05	-.11748E+02	.58796E-03
.24444E+00	.41532E+01	.42044E+01	.92247E-02	.10583E-02	.17199E+03	.19732E+02	.77437E+05	.78390E+05	-.13624E+02	.74E-03E-02
.24727E+00	.41459E+01	.42052E+01	.11098E-01	.99737E-03	.20691E+03	.18594E+02	.77299E+05	.78405E+05	-.15798E+02	.92115E-02
.26667E+00	.41369E+01	.42059E+01	.13607E-01	.94157E-03	.25357E+03	.17555E+02	.77133E+05	.78418E+05	-.18386E+02	.11[illegible]E-02
.28889E+00	.41263E+01	.42066E+01	.17044E-01	.89025E-03	.31781E+03	.16599E+02	.76936E+05	.78431E+05	-.21466E+02	.5[illegible]
.31111E+00	.41123E+01	.42072E+01	.21969E-01	.84304E-03	.42962E+03	.15718E+02	.76673E+05	.78443E+05	-.25093E+02	.8[illegible]
.33333E+00	.40944E+01	.42078E+01	.29339E-01	.79949E-03	.54702E+03	.14903E+02	.76340E+05	.78455E+05	-.29[illegible]	.11[illegible]
.35556E+00	.40712E+01	.42084E+01	.41036E-01	.75923E-03	.76517E+03	.14150E+02	.75918E+05	.78466E+05	-.33[illegible]	.[illegible]
.36727E+00	.40393E+01	.42092E+01	.61124E-01	.72194E-03	.11393E+04	.13452E+02	.75312E+05	.78476E+05	-.38[illegible]	.[illegible]
.37778E+00	.39947E+01	.42095E+01	.99203E-01	.68732E-03	.18049E+04	.12815E+02	.74481E+05	.78486E+05	-.57222E+02	.1[illegible]
.40000E+00	.39359E+01	.42100E+01	.18139E+00	.65510E-03	.33918E+04	.12215E+02	.73385E+05	.78495E+05	-.73[illegible]	.[illegible]
.42222E+00	.39041E+01	.42105E+01	.37475E+00	.62517E-03	.69971E+04	.11654E+02	.72792E+05	.78504E+05	-.81[illegible]	.[illegible]
.44444E+00	.41508E+01	.42110E+01	.64814E+00	.59727E-03	.12085E+05	.11135E+02	.77392E+05	.78513E+05	-.16017E+02	.[illegible]
.46667E+00	.45209E+01	.42114E+01	.47477E+00	.57107E-03	.88507E+04	.10648E+02	.84023E+05	.78521E+05	.84[illegible]	.85[illegible]
.48889E+00	.45457E+01	.42118E+01	.22613E+00	.54662E-03	.42535E+04	.10192E+02	.84781E+05	.78529E+05	.84[illegible]	.41[illegible]
.51111E+00	.44851E+01	.42122E+01	.11929E+00	.52370E-03	.22942E+04	.97644E+01	.83625E+05	.78537E+05	.76[illegible]	.20[illegible]
.52000E+00	.44355E+01	.42126E+01	.72919E-01	.51422E-03	.13923E+04	.95859E+01	.82730E+05	.78544E+05	.59[illegible]	.14[illegible]
.54000E+00	.43999E+01	.42130E+01	.46036E-01	.48199E-03	.86579E+03	.89867E+01	.82035E+05	.78551E+05	.49[illegible]	.44[illegible]
.55000E+00	.43748E+01	.42133E+01	.32589E-01	.46294E-03	.60761E+03	.86322E+01	.81590E+05	.78557E+05	.42[illegible]	.29[illegible]
.58000E+00	.43547E+01	.42137E+01	.24066E-01	.44507E-03	.44871E+03	.82983E+01	.81194E+05	.78564E+05	.37[illegible]	.12216E-01
.60000E+00	.43399E+01	.42140E+01	.18473E-01	.42818E-03	.34442E+03	.79838E+01	.80916E+05	.78570E+05	.33522E+02	.70[illegible]
.62000E+00	.43281E+01	.42143E+01	.14613E-01	.41223E-03	.27244E+03	.76861E+01	.80697E+05	.78576E+05	.30[illegible]	.83[illegible]
.64000E+00	.43186E+01	.42146E+01	.11842E-01	.39716E-03	.22080E+03	.74051E+01	.80520E+05	.78581E+05	.27688E+02	.20[illegible]
.66000E+00	.43127E+01	.42149E+01	.97874E-02	.38290E-03	.18249E+03	.71392E+01	.80373E+05	.78587E+05	.25527E+02	.19177E-02
.68000E+00	.43042E+01	.42152E+01	.82226E-02	.36940E-03	.15331E+03	.68874E+01	.80251E+05	.78592E+05	.23693E+02	.15377E-02
.70000E+00	.42986E+01	.42155E+01	.70041E-02	.35659E-03	.13059E+03	.66486E+01	.80146E+05	.78597E+05	.22132E+02	.95471E-03
.72000E+00	.42938E+01	.42157E+01	.60309E-02	.34444E-03	.11256E+03	.64221E+01	.80057E+05	.78602E+05	.20782E+02	.70314E-03
.74000E+00	.42896E+01	.42160E+01	.52565E-02	.33290E-03	.98088E+02	.62069E+01	.79979E+05	.78607E+05	.19603E+02	.52611E-03
.76000E+00	.42859E+01	.42162E+01	.46187E-02	.32193E-03	.86102E+02	.60024E+01	.79911E+05	.78611E+05	.18563E+02	.40[illegible]
.78000E+00	.42827E+01	.42165E+01	.40889E-02	.31150E-03	.76237E+02	.58079E+01	.79851E+05	.78616E+05	.17639E+02	.3[illegible]

A P P E N D I X B

The list of experimental apparatus used in this investigation

a) Power supplies for the 0.337 mm pulsed HCN laser

1. EHT unit (Bedford College, 1967)
2. Control unit (variac), (Bedford College, 1968)
3. Thyratron triggering unit with variable frequency (Bedford, College, 1968)
4. Triggered spark gap (Bedford College, 1968)
5. Power supplies for the thyratron unit (A.P.T. Electronic Indistries Ltd, model 512)

b) The cryomagnetic system (as supplied by the Oxford Instriment Company Ltd.)

1. Transverse-access optical cryostat (model, G452)
2. 0-60 amp, stabilised air cooled single phase magnet power supply (type, 60A, Ø, serial number 6/3131)
3. Vacuum insulated helium transfer tube
4. Vibrating diaphragm helium level indicator

c) Pumping system

1. Pumping unit for the optical cryostat (Genevac, PL66)
2. Pirani (M7B) and Penning (M6) gauge heads with control unit Pirani 10 and Penning 8 (Edwards)
3. 1-stage rotary vacuum pump for the laser system (Metrovac, type, DR1H)

d) Signal processing and recording system

1. Golay cell detector (Unicam Instr. Ltd, type, SP 50)
2. Electric motor (Erwin Halstrup/Rayleigh Instr., type, RSM 50)

3. Double pulse generator with variable delay (Farnell, model, PG 5222)
4. Two-linear gates (Brookdeal model, 9415)
5. Double pen XY/Yt recorder with chart drive unit (Yokogawa, type, 3078)
6. Dual-beam oscilloscope (Tektronix, type, 551 + type H and L plug-in unit with maximum sensitivity 5 mV/cm, 12 MHz)
7. Stabilised power supply for the Golay cell (Farnell, type, SSA)
8. Electronic circuits produced pulses for triggering the pulse generator and oscilloscope:

   Light activated switch, which produces pulses from flashing light during discharging laser tube, (Radio-spares, 5V, Las) + Monostable multivibrator (TTL, SN 74121) + Transistor amplifier and Emitter follower (Bedford College, 1974)

e) General purpose

1. Keithley digital-multimeter with 1 μV voltage sensitivity (type, 160B)
2. Keithley autoranging DMMM (type, 168)
3. Avometer (Avo. Ltd, model 8)

APPENDIX C

LIST OF SYMBOLS

Only those symbols that are used throughout this thesis are included in this list. Other, less frequently used symbols are defined as they appear.

$\underline{A}$	vector potential
a	screening length
a_n	Bohr radius
α	absorption coefficient
B	magnetic induction
B_c	cyclotron resonance field
c	speed of light
d	sample thickness
Δ	ellipticity or spin-orbit splitting of valence band
$E(z,t)$	electric field
$E(n,k,s)$	conduction band, Landau energy levels
$E_i(n,M,\lambda)$	impurity energy levels
E_c	lower edge of the conduction band
E_F	Fermi energy
E_g	width of the forbidden energy gap
E_v	upper edge of the valence band
e	electronic charge (absolute value)
ϵ_r	dielectric constant
ϵ_o	permittivity of free space
$f_o(n,k,s)$	Fermi distribution function
$G(E)$	density of state functions
g	effective g-factor

H Hamiltonian operator

h Planck's constant

J current density

k extinction coefficient or wave number ($1/\lambda$)

k_B Boltzmann's constant

λ wavelength

M_B Bohr magneton

μ_H Hall mobility

μ_D drift mobility

μ_{dc} d.c. mobility

μ_{ac} a.c. mobility

m_o electron rest mass

m^* effective mass of electrons

m_F^* effective mass at Fermi energy

N electron concentration

N_i total ionized impurity concentration

N_D donor concentration

N_A acceptor concentration

n refractive index or Landau quantum number (0,1,2,...)

n^* complex refractive index

$\underline{p}$ momentum operator

p propagation constant (wm^*/c)

ψ wavefunction

ϕ harmonic oscillator wavefunction

$\underline{q}$ propagation wave vector ($\underline{\hat{n}}/\lambda$), $\underline{\hat{n}}$ is the unit vector in direction of propagation.

R reflectivity

R_H Hall's constant

r magnetic length

s spin quantum number ($\frac{1}{2}$)

σ conductivity

T transmission coefficient or temperature

τ impurity scattering time

τ_o d.c. scattering time at zero field

τ_{dc} d.c. scattering time

θ Faraday rotation angle

θ_c correction term due to internal multiple reflection

$\underline{v}$ velocity of charged particles

w angular frequency

w_c cyclotron resonance frequency

w_p plasma frequency

A P P E N D I X D

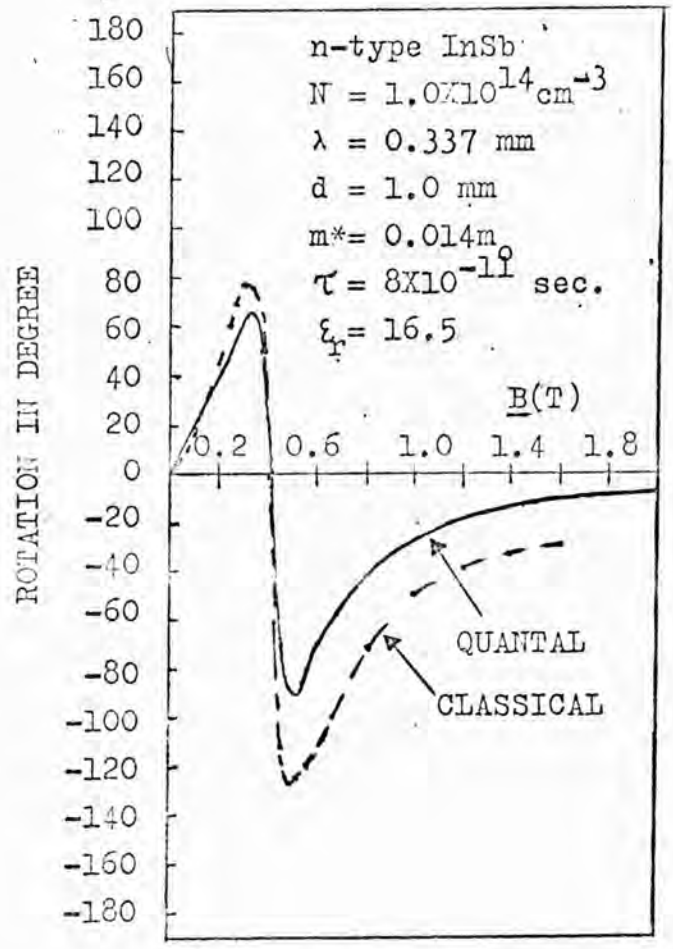

Fig. 1 Comparison of classsical and quantum mechanical calculation of Faraday rotation angle using indicated parameters. Solid line is computed from eqs. (1.18), (1.19), (1.20), (1.23) and (1.14) (quantum mechanical case) by Poehler and Wang (1972); dashed line is calculated from eq. (1.16) (classical case) using the same parameters.

ACKNOWLEDGEMENTS

I should like to express my sincere gratitude to Professor E.R. Dobbs, Head of the Department of Physics at Bedford College, for providing the facilities for my work in this department.

I wish to express my sincere appreciation to my supervisor, Mr. T.B. Taylor, for his patience and guidance throughout this research, and also for his advice and help on the problems of language during the writing of this thesis.

I also wish to express my thanks to Dr. R. Mansfield, Dr. M.J. Lea and Mr. R.N. Thomas for their help and interest.

Thanks are due to Dr. P. Pal, Dr. T. Lake and the other staff of the Computer Unit at Bedford College for their assistance with data analysis.

In particular, I should like to thank the following:

Mr. F.A. Grimes (Chief Technician, Workshop), Mr. A.W. King, Mr. J. Kavanagh (Technician, Workshop) for the construction of the laser system and associated equipment.

Mr. A.K. Betts (Technician) for the construction of the laser power supplies and making the leads on the samples for Hall measurements.

Mr. W.A.G. Baldock (Chief Technician, Laboratories) and Mr. A.O.T. Le Mottee (Technician) for their technical assistance and Mr. B. Pashley (Technician) for taking the photographs of the experimental apparatus illustrating in this thesis.

My particular gratitude is due to the University Central Research Fund (C.R.F) and Science Research Council (S.R.C) for providing a grant to purchase the following apparatus:

Unicam Golay cell and power supply (C.R.F)

Tranverse-access optical cryostat (C.R.F)

2 linear gates (Brookdeal model) (C.R.F)

Tektronix Type 551 Oscilloscope with plug-in units and accessories (S.R.C)

2 Unicam Golay cells (3mm windows) (S.R.C)

I also wish to express my sincere gratitude to the Ministry of Education of the Turkish Government for the award of a scholarship, and the British Council for an Overseas Students Fees Award.

Finally, my thanks also go to my wife for her forbearance.

REFERENCES

1. Apel, J.R., and Poehler, T.O., 1969, Appl. Phys. Lett. 14, 161.
2. Apel, J.R., and Poehler, T.O., 1970a, Sol. St. Comm. 8, 1275.
3. Apel, J.R., 1970b, Ph.D. thesis, The John Hopkins University, Maryland, Baltimore, U.S.A.
4. Apel, J.R., Poehler, T.O., and Westgate, C.R., 1970c, Sol. St. Commun. 8, 1693.
5. Apel, J.R., Poehler, T.O., and Joseph, R.I., 1971, Phys. Rev. B 4, 436.
6. Appleton, B.V., 1925, Proc. Phys. Soc. 37, 160.
7. Baggulay, D.M.S., Stradling, R.A., and Whiting, J.S.S., 1961, Roy. Soc. Proc. 262, 340.
8. Baggulay, D.M.S., Robinson, M.L.A.,and Stradling, R.A., 1963, Phys. Lett. 6, 143.
9. Beer, A.C., 1963, Sol. St. Phys. Supplement 4, 92.
10. Bemski, G., 1960, Phys. Rev. Lett. 4, 62.
11. Blakemore, J.S., 1962, Semiconductor Statistics, (Pergamon Press, Oxford).
12. Bovers, R.,and Yafet, Y., 1959, Phys. Rev. 115, 1165.
13. Boyle, W.S.,and Brailsford, A.D., 1957, Phys. Rev. 107, 903.
14. Broida, H.P., Evanson, K.M.,and Kikuchi, T.T., 1965, J. Appl. Phys. 36, 3335.
15. Brooks, H., 1951, Phys. Rev. 83, 879.
16. Brooks, H.,and Herring, C., 1955, In Advances in Electronics and Electron Phys. 8.

17. Brown, R.N., 1958, M.S. thesis, M.I.T.

18. Brown, R.N.,and Lax, B., 1959, Bull. Am. Phys. Soc. 4,133.

19. Chamberlain, J.M.,and Stradling, R.A., 1969, Sol. St. Comn. 7, 1275.

20. Chamberlain, J.M., 1972, Ph.D. thesis, University of Oxford.

21. Champlin, K.S., 1962, Physica, 28, 1143.

22. Chantry, G.W., Gebbie, H.A.,and Chamberlain, J.E., 1965, Nature, 205, 377.

23. Chantry, G.W., Evans,M.M., Fleming, J.W.,and Gebbie, H.A., Infrared Phys. 9, 3 (1969).

24. Chantry, G.W., 1971, Submillimetre Spectroscopy, (Academic Press, London and New York).

25. Clark, D., and Grainger, J.F., 1971, Polarised light and Optical Measurements, 80, (Pergamon Press).

26. Dingle, R.B., 1952, Proc. Roy. Soc. A 211, 500 and A 212, 38.

27. Donovan, B.,and Webster, J., 1961 and 1962, Proc. Phys. Soc. 78, 120 and 79, 46; 81, 90.

28. Donovan, B.,and Medcalf, T., 1964, Brit. J. Appl. Phys. 15, 1139.

29. Dresselhaus, G., Kip, A.F.,and Kittel, C., 1953, Phys. Rev. 92, 827.

30. Faraday, M., 1846, Phil. Trans. Roy. Soc. p.1

31. Furdyna, J.K.,and Brodwin, M.E., 1961, Phys. Rev. 124,740.

32. Gabriel, C.J.,and Piller, H., 1967, Appl. Opt. 6, 661.

33. Gebbie, H.A.,Stone, N.W.B.,and Findlay, F.D., 1964, Nature, 202, 685.

34. Gibbons, D.F., 1958, Phys. Rev. 112, 136.

35. Harris, R.E.,Cappelletti, R.E.,and Ginsberg, D.M., 1966, Appl. Opt. 5, 1083.

36. Herzberg, G., 1945, Infrared and Raman Spectra, D. Van.

37. Hocker, L.O., Javan, A.,and Rao, D.R., 1967a, Appl. Phys. Lett. 10, 147.

38. Hocker, L.O., and Javan, A., 1967b, Phys. Rev. Lett. 25 A, 489.

39. Jassby, D.L., Marhic, M.E., and Regan, D.E., 1973, Appl. Opt. 12, 1403.

40. Johnson, E.J.,and Dickey, D.H., 1970, Phys. Rev. B 1, 2676.

41. Kane, E.O., 1957, J. Phys. Chem. Solids, 1, 249.

42. Kaplan, R., 1969, Phys. Rev. 181, 1154.

43. Kaplan, R., McCombe, B.D.,and Wagner, R.J., 1973, Sol. St. Commun. 12, 967.

44. Kawabata, A., 1967, J. Phys. Soc. Japan, 23, 999.

45. Kawamura,H., Saji, H., Fukai, M., Sekido, K., and Imai, I., 1964, J. Phys. Soc. Japan, 19, 288.

46. Kazarinov, R.F.,and Skobov, V.G., 1962, Zh. Exsp. Teo. Fiz. 42, 1047; Sov. Phys. JETP 15, 726 (1962).

47. Kobayashi, K.L.I.,and Otsuka, E., 1972, Sol. St. Commun. 11, 815; and 1974, J. Phys. Chem. Solids, 35, 839.

48. Kobayashi, K.L.I., Komatsubara, K.F.,and Otsuka, E., 1973, Phys. Rev. Lett., 30, 702.

49. Kone, S.,Yamanaka, M., Yamamoto,J.,and Yoshinaga, H., 1967, J. Appl. Phys. Japan, 6, 612.

50. Koteles, E.S.,and Datars, W.R., 1974, Phys. Rev. B9, 568.

51. Kotthaus, J.P., 1968, Appl. Opt. 7, 2422.

52. Larsen, D.M., 1968, J. Phys. Chem. Solids, 29, 271.

53. Lax, B., Zeiger, H.J., Dexter, R.N., and Rosenblum, E.S., 1954a, Phys. Rev. 93, 1418.

54. Lax, B., Zeiger, H.J., and Dexter, R.N., 1954b, Physica, 20, 818.

55. Lax, B., Zeiger, H.J., Mavroides, J.G., and Keyes, R.J., 1960, Phys. Rev. Lett. 5, 241.

56. Lax, B., Mavroides, J.G., Zeiger, H.J., and Keyes, R.J., 1961, Phys. Rev. 122, 31.

57. Lax, B., and Halpern, J., 1962, Cyclotron Resonance and Magneto-optical effects in semiconductor, Technical Rep. No: 249.

58. Lide, D.R., and Maki, A.G., 1967, Appl. Phys. Lett. 11, 2.

59. Lipson, H.G., Zewerdling, S, and Lax, B., 1958, Bull. Am. Phys. Soc. (2), 3, 218.

60. Lodder, A., and Fujita, S., 1974, Phys. Lett. 46A, 381.

61. Lodder, A., 1975, Sol. St. Commun. 16, 117.

62. Loewenstein, E.V., and Newell, D.C., 1969, J. Opt. Am. 59, 407.

63. Lorentz, H.A., 1906, Theory of Electrons, (Teubner, Leipziq).

64. Luttinger, J.M., and Kohn, W., 1955, Phys. Rev. 97, 869.

65. Maki, A.G., 1970, IEEE, J. Quant. Elect. QE6, 178.

66. Mansfield, R., and Borst, M.R., 1965, Brit. J. Appl. Phys. 16, 570.

67. Mansfield, R., 1967, Contemp. Phys. 8, 197.

68. Mathias, L.E., Crocker, A., and Wills, M.S., 1965, Electronics Lett. 2, 44.

69. McCoul, B.W., 1970, Appl. Opt. 9, 653.

70. Mears, A.L.,and Stradling, R.A., 1969, Sol. St. Commun. 7, 1267.

71. Mitchell, E.W.J., 1955, Proc. Phys. Soc. A68, 973(London).

72. Miyake, S.J., 1965 and 1973, J. Phys. Soc. Japan, 20, 412 and 35, 551.

73. Moss, T.S., Smith, S.D.,and Taylor, K.M., 1959, J. Phys. Chem. Solids, 8, 323.

74. Moss, T.S.,and Ellis, B., 1964, Proc. Phys. Soc. 83, 217.

75. Moss, T.S., Burrell, G.J.,and Ellis, B., 1973, Semiconductor Opto-electronics (Butterworths, London).

76. Muller, R.H.,and Fletcher, G.T., 1967, Appl. Phys. Lett. 10, 93.

77. Murotani, T.,and Nisida, Y., 1972, J. Phys. Soc. Japan, 32, 986.

78. Ohlmann, R.C., Richards, P.L.,and Tinkham, M., 1968, J. Opt. Soc. Am. 48, 531.

79. Palik, E.D., Picus, G.S., Teitler, S.,and Wallis, R.F., 1961, Phys. Rev. 122, 475.

80. Palik, E.D., Teitler, S.,and Wallis, R.F., 1961a, J. Appl. Phys. Suppl. 32, 2132.

81. Palik, E.D., Teitler, S., Henvis, B.W., and Wallis, R.F., 1962, Proc. Int. Conf. Phys. Semicond. 288. (Exeter); 1962, Inst. Phys. and Phys. Soc. (London).

82. Palik, E.D., 1963, Appl. Opt. 2, 527.

83. Palik, E.D., Stevenson, J.R.,and Webster, J., 1966, J. Appl. Phys. 37, 1982.

84. Palik, E.D., and Wright, G.B., 1967, Semiconductors and Semimetals, 3, Chap. 10, Willardson, R.K.,and Beer, A.C, Eds. (Academic Press, New York, London).

85. Palik, E.D., and Furdyna, J.K., 1970, Rep. Prog. Phys. 33, 1193.

86. Palmetshofer, L.,and Kranzer, D., 1974, Phys. Stat. Solidi (b), 62, 491.

87. Pidgeon, C.R., 1962, Ph.D. dissertation, University of Reading, Reading, England.

88. Pidgeon, C.R.,and Smith, S.D., 1964, Infrared Phys. 4, 13.

89. Pidgeon, C.R.,and Brown, R.N., 1966, Phys. Rev. 97, 575.

90. Piller, H., 1966, J. Appl. Phys. 37, 763.

91. Poehler, T.O.,and Turner, R., 1970, Appl. Opt. 9, 971.

92. Poehler, T.O., 1972, Appl. Phys. Lett. 20, 69.

93. Poehler, T.O.,and Wang, C.H., 1972, Phys. Rev. B5, 1483.

94. Potapov, V.T., Trifonov, V.I., Chusov, I.I., and Yaremenko, N.G., 1973, Sov. Phys. Semiconductors,6, 1076, (Trans. from Fz. Tek. Pol., 6, 1227, (1972)).

95. Potapov, V.T., Sokolovskii, A.V., Trifonov, V.I., and Yaremenko, N.G., 1973, Sov. Phys. Semiconductors,6, 1081, (Trans. from Fz. Tek. Pol., 6, 1234, (1972)).

96. Rau, R.R.,and Caspari, M.E., 1955, Phys. Rev. 100, 632.

97. Robinson, L.C.,and Whitbourn, L.B., 1971, Proc. IREE Australia, 32, 355.

98. Rosenbaum, R.L., 1968, Rev. Scient. Inst. 39, 890.

99. Sanders, J.H., 1959, Phys. Lett. 3, 86.

100. Sharp, L.E.,and Wetherell, A.T., 1972, Appl. Opt. 11, 1737.

101. Shimura, M., Takeuchi, N., Yajima, T., 1970, J. Appl. Phys. Japan, 9, 1334.

102. Shin, E.E.H., Argyres, P.N.,and Lax, B., 1972, Phys. Rev. Lett. 28, 1634.

103. Shin, E.E.H., Argyres, P.N.,and Lax. B., 1973, Phys. Rev. B7, 3572.

104. Shin, E.E.H., Argyres, P.N., Morgenstern Horing, N.J.,and Lax, B., 1973, Phys. Rev. B7, 5408.

105. Sladek, R.J., 1953 and 1959, J. Phys. Chem. Solids, 5, 157 and 8, 515.

106. Smith, S.D., Moss, T.S.,and Taylor, K.W., 1959, J. Phys. Chem. Solids, 11, 131.

107. Smith, S.D., and Moss, T.S., 1960, Proc. Intern. Conf. Sol. Stat. Phys. (Brussels), 1958, 2, part,2, Eds. Desirand, M.,and Michiel, J.L. (Academic Press, New York), p. 671.

108. Smith, H.A., 1963, Proc. Ital. Phys. Soc. Cours, 22, (Academic Press, New York).

109. Sniadower, L., Rauluszkiewicz, J.,and Galazka, R.R., 1964, Phys. Stat. Solidi, 6, 549.

110. Spitzer, W.G.,and Fan, H.Y., 1957, Phys. Rev. 106, 882.

111. Stafsudd, Q.M., Haak, F.A.,and Radisavljevic, K., 1967, IEEE, J. Quant. Elects. QE3, 618.

112. Stair, R., Scheider, W.E.,and Fussell, W.B., 1967, Appl. Opt. 6, 101.

113. Steffen, H., Steffen, J., Moser, J.F., and Kneubuhl, F.K., 1966, Phys. Lett. 21, 425.

114. Steffen, H., Schwaller, P., Moser, J.F.,and Kneubuhl, F.K. 1966, Phys. Lett. 23, 313.

115. Stephen, M.J.,and Lidiard, A.B., 1959, J. Phys. Chem. Sol. 9, 43.

116. Sugden, T.M.,and Kenney, C.N., Microwave Spectroscopy of Gases, (D. Van Nostrand Company Ltd.), London.

117. Teitler, S., Palik, E.D.,and Wallis, R.F., 1961, Phys. Rev. 123, 1631.

118. Tuchendler, J., Grynberg, M., Couder, Y., Thome, H.,and Le Toullec, R., 1973, Phys. Rev. B8, 3884.

119. Ukhanov, Yu.I.,and Maltsev, Yuv., 1963, Sov. Phys. Sol. Stat. 4, 2354.

120. Von Kimmel, H., 1957, Z. Naturf. 12A, 1016.

121. Wallis, R.F.,and Bowlden, H.J., 1958, J. Phys. Chem. Solids , 7, 78.

122. Walton, A.K.,and Moss, T.S., 1961, Proc. Phys. Soc. 78, 1393.

123. Williamson, E.D., 1952, J. Opt. Soc. Am. 42, 712.

124. Wilson, E.B., Jr. Decius, J.C.,and Cross, P.C., 1955, Molecular Vibrations, The Theory of Infrared and Raman Vibrational Spectra, (Mcgraw Hill, New York).

125. Wright, G.B.,and Lax, B., 1961, J. Appl. Phys. Suppl. 32, 2113.

126. Wright, G.B., 1964, Sol. St. Res. Rep. Lincoln Laboratory, (M.I.T), part, 1, p. 42.

127. Yafet, Y., Keyes, R.W.,and Adams, E.N., 1956, J. Phys. Chem. Solids, 1, 137.

128. Zeiger, H.J.,and Hilsenrath, S., 1957, Lincoln Laboratory, QPR, group 35, p.54.